

©2010

WANTINEE VIRATYAPORN

ALL RIGHTS RESERVED

**EFFECT OF DOMAIN SIZE AND INTERFACE CHARACTERISTICS ON THE  
IMPACT RESISTANCE OF SELECTED POLYMER COMPOSITES**

by

WANTINEE VIRATYAPORN

A Dissertation submitted to the

Graduate School-New Brunswick

Rutgers, The State University of New Jersey

in partial fulfillment of the requirements

for the degree of

Doctor of Philosophy

Graduate Program in Materials Science and Engineering

written under the direction of

Professor Richard L. Lehman

and approved by

---

---

---

---

---

New Brunswick, New Jersey

January, 2010

## ABSTRACT OF THE DISSERTATION

# **EFFECT OF DOMAIN SIZE AND INTERFACE CHARACTERISTICS ON THE IMPACT RESISTANCE OF SELECTED POLYMER COMPOSITES**

By WANTINEE VIRATYAPORN

Dissertation Director:  
Professor Richard L. Lehman, PhD

Nanocomposite technology has advanced considerably in recent years and excellent engineering properties have been achieved in numerous systems. In multiphase materials the enhancement of properties relies heavily on the nature at the interphase region between polymer domains and nanoparticle reinforcements. Strong adhesion between the phases provides excellent load-transfer and good mechanical elastic modulus and strength, whereas weak interaction contributes to crack deflection mechanisms and toughness. Polymer molecules are large and the presence of comparably sized filler particles affects chain gyration, which in turn influences the conformation of the polymer and the properties of the composite.

Nanoparticles were incorporated into a poly(methyl methacrylate) matrix by means of *in situ* free radical (bulk) polymerization. Aluminum oxide and zinc oxide nanoparticles were added to study the effects of particle chemistry and shape on selected

mechanical properties such as impact resistance, which showed significant improvement at a certain loading of zinc oxide. The elongated shape of zinc oxide particles appears to promote crack deflection processes and to introduce a pull-out mechanism similar to that observed in fiber composite systems. Moreover, the thermal stability of PMMA was improved with the addition of nanoparticles, apparently by steric hindrance of polymer chain motion and a second mechanism related to the dipole inducing effect of the oxide particles. The sensitivity of infrared spectroscopy to changes in molecular dipoles was used to study the nature of the polymer/particle interface. The results revealed some interesting aspects of the secondary bonds between polymers and oxides. Raman spectroscopy was used to investigate the extent of polymerization and changes in polymer conformation. A degree of polymerization of 93% was achieved in neat PMMA, and even when 5.0 v/o of PGMEA was introduced into the system no monomer was detected. However, when nanoparticles were included in the system, the ability of these surfaces to absorb active species reduced the degree of polymerization to about 87%. Furthermore, the syndiotactic sequence increases with the addition of nanoparticles as a consequence of enhanced accessibility to both the metal oxide surface and the dispersing solvent within the system.



## **Preface**

I first worked on polymer composites as senior project for my undergraduate degree. A broad array of material combinations to create new type of composite materials has attracted my interest since. The motivation for this study was the exceptional property enhancement obtained when at least one phase of composites has a dimension in nano scale. The content of this dissertation was based on the experiment conducted in the Department of Materials Science and Engineering at Rutgers, The State University of New Jersey within the Advanced Materials via Immiscible Polymer Processing Center (AMIPP). The guidance of this work was contributed by AMIPP center and NEI Corporation.

## **Dedication**

To my family

for their lovingly support

## **Acknowledgements**

I am very grateful to my advisor, Professor Richard Lehman, for his guidance and support during my years here at Rutgers. He not only helps me build my confidence in public but also keeps me focus in my work. His creativity and experience helps me improve and achieve all the works. Thank you so much. Lots of thanks go to Professor Dunbar Birnie, Professor Manish Chhowalla, Professor Adrian Mann and Dr. Ganesh Skandan for not only being my committee but also suggestion and ideas contributed in my work.

Many thanks go to Professor Gene Hall from Chemistry and Chemical Engineering department for his assistance on spectroscopy both ATR-FTIR and Raman spectroscopy. I also would like to thank Professor Lisa Klein for her assistance and help in all academic matters. I also would like to acknowledge Professor Victor Greenhut for his help and suggestions in SEM.

I would like to thank Professor James Idol for all the helpful discussions. I would also like to thank AMIPP members both past and present, Professor Thomas Nosker, Dr. Jennifer Lynch, Dr. Kim-Phuong Le, Dr. Jayant Joshi, Dr. Vivek Thirtha, Zeena Cherian, and Giorgiana Giancola, for their technical helps and guidance in the laboratory.

Many thanks go to all the staff members and colleagues in the department to help make things go smoothly. To Claudia Kuchinow, John Yaniero, Phyllis Cassell, and

Philip Grill, thank you for their help and kindness. To Dr. Steve Miller and Dan Maiorano, thank you for helping me in FESEM and EDS. To Varun Gupta and Milca Aponte-Roman, thank you for their assistance in Raman spectroscopy. To Piyaluk (Note), Chiraporn (Tum), and other Thai friends in Rutgers, thank you for everything.

Special thanks go to all teachers in Wat.Plubplachai School, Benjamarachalai School, and Silpakorn University, Thailand. Without strong basic knowledge they have given me, I would not have come this far.

No word is enough to express thank my dad, Mr. Vichai Viratyaporn, and my mom, Mrs. Laddawan Viratyaporn, to all the things they have done for me and also to my brothers and sister, Watchara Viratyaporn (M.D.), Siriphen Viratyaporn, and Ronnakorn Viratyaporn, for the strength and the support they have given me.

Last but not least, I am thankfully to Sutapat Thiprungsri for all encouragement and support she has for me.

THANK YOU.

## Table of Contents

<b>ABSTRACT OF THE DISSERTATION.....</b>	<b>ii</b>
<b>Preface .....</b>	<b>iv</b>
<b>Dedication .....</b>	<b>v</b>
<b>Acknowledgements .....</b>	<b>vi</b>
<b>Table of Contents .....</b>	<b>viii</b>
<b>Lists of tables .....</b>	<b>xii</b>
<b>List of illustrations .....</b>	<b>xiii</b>
<b>Chapter 1 Introduction.....</b>	<b>1</b>
1.1 Objectives .....	1
1.2 Dissertation Outline .....	2
<b>Chapter 2 Polymer composites: Nanocomposites and Immiscible Polymer Blends (IMPBs).....</b>	<b>4</b>
2.1 Polymer nanocomposites: Literature review .....	4
2.1.1 Nanoparticles .....	7
2.1.1.1 Carbon nanotubes .....	8
2.1.1.2 Montmorillonite.....	10

2.1.1.3	Aluminum oxide.....	11
2.1.2	Thermal degradation of PMMA.....	16
2.1.3	Interphase/interface of Polymer/particulate nanocomposites .....	19
2.1.3.1	Surface chemistry of metal oxide.....	19
2.1.3.2	Interfacial interaction: Polymer/particulate nanocomposites .....	22
2.1.3.3	Interfacial interaction of PMMA and metal oxide particles.....	25
2.2	Immiscible polymer blends: Literature review .....	28
2.3	Objectives of thesis .....	30
	References.....	32
<b>Chapter 3 Polymer nanocomposites: Processing .....</b>		<b>39</b>
3.1	Materials .....	39
3.2	In-situ Polymerization of PMMA/nanocomposites .....	40
3.2.1	Polymerization mechanism of poly(methyl methacrylate).....	42
3.3	Testing and characterization .....	44
3.3.1	Mechanical testing .....	44
3.3.1.1	Tensile testing.....	44
3.3.1.2	Impact testing .....	44
3.3.2	Thermal analysis .....	45
3.3.2.1	Differential Scanning Calorimetry (DSC).....	45
3.3.2.2	Thermal Gravimetric Analysis (TGA) .....	45
3.3.3	Characterization techniques .....	46

3.3.3.1	Image analysis .....	46
3.3.3.2	Infrared spectroscopy .....	46
3.3.3.3	Raman spectroscopy .....	46
<b>Chapter 4 Mechanical behavior of polymer nanocomposites.....</b>		<b>48</b>
4.1	Tensile properties of PMMA/metal oxide nanocomposites.....	49
4.2	Impact resistance.....	57
4.3	Image analysis.....	60
4.3.1	Nanoparticle dispersion .....	60
4.3.2	Fractured surface of polymer nanocomposites .....	65
4.3.3	Material responses: time-temperature dependence .....	67
Summary .....		70
References.....		71
<b>Chapter 5 Thermal behavior of polymer/particulate nanocomposites.....</b>		<b>72</b>
5.1	Thermal Gravimetric Analysis (TGA).....	72
5.1.1	Pre-dispersed nanoparticles .....	72
5.1.2	Polymer-inorganic nanocomposites.....	76
Summary .....		85
References.....		86
<b>Chapter 6 PMMA/particulate nanocomposites: Spectroscopic analysis .....</b>		<b>87</b>
6.1	Interfacial interactions .....	87

6.2	Extent of polymerization.....	98
6.3	Effect of polymer microstructure.....	103
	Summary .....	107
	References.....	109
<b>Chapter 7 Summary and Conclusion.....</b>		<b>111</b>
<b>Chapter 8 Future work.....</b>		<b>113</b>
<b>Appendix A - Raman spectroscopic analysis.....</b>		<b>115</b>
A.1	Raman assignment .....	115
A.2	Statistical analysis.....	117
<b>Curriculum Vita.....</b>		<b>119</b>



## **Lists of tables**

Table 2.1 Structure and parameters of PMMA (Data taken from Vacatello). <sup>[67]</sup> .....	27
Table 3.1 Purchased Nanoparticles Information.....	39
Table 3.2 Polymer Nanocomposites Compositions. ....	41
Table 5.1 Weight Percent of PGMEA on Nanoparticle Surface (Region II).....	74
Table 6.1 Vibrational frequency of carboxylate complex. <sup>[4]</sup> .....	93

## List of illustrations

Figure 2.1 Schematic of nanoscale fillers (redraw from ref.[15]) .....	7
Figure 2.2 Plot of the function describing the ratio of surface area to volume ( $A/V$ ) vs. aspect ratio for cylindrical particles with a given volume. <sup>[34]</sup> .....	8
Figure 2.3 Chiral vector on single graphene sheet. <sup>[39]</sup> .....	9
Figure 2.4 Structures of SWNTs. <sup>[40]</sup> .....	10
Figure 2.5 Chemical structure of montmorillonite nanoclays. <sup>[30]</sup> .....	11
Figure 2.6 Thermal transformation sequence of the aluminum hydroxides. <sup>[41]</sup> .....	12
Figure 2.7 The corundum structure of aluminum oxide .....	13
Figure 2.8 Cubic $\gamma$ - $Al_2O_3$ spinel-type unit cell. <sup>[43]</sup> .....	14
Figure 2.9 Semi-cell of ideal structure in $\beta$ - $Al_2O_3$ ; Large spheres: alkaline or alkaline earth metal; medium sphere: oxygen ions; small spheres: aluminum ions; m: mirror plane; s: spinel block. <sup>[45]</sup> .....	15
Figure 2.10 Surface charge at various pH. <sup>[57]</sup> .....	20
Figure 2.11 Ionic potential of various ions (left) and the interactions between ions at difference ionic potential value (right). <sup>[57]</sup> .....	21
Figure 2.12 Ionic potential and surface charged of various types of metal oxide. <sup>[57]</sup> .....	22
Figure 2.13 Interparticle distance for spherical particles that are ideally dispersed. <sup>[15]</sup> .	23
Figure 2.14 Interphase region between the particulate filler and polymer matrix. <sup>[33]</sup> .....	24
Figure 2.15 Conformation of adsorbed polymer molecules (redraw from ref. [60]).....	25

Figure 2.16 Schematic representation of the acid-base interaction (a) and the ionic bonding (b) which take place at the PMMA/aluminum interface. <sup>[63]</sup> .....	27
Figure 4.1 Tensile modulus and impact resistance of PMMA/PGMEA at various volume fractions of PGMEA. ....	50
Figure 4.2 Tensile modulus of PMMA/aluminum oxide nanocomposites at various particle size, shape, and volume fractions. ....	52
Figure 4.3 Tensile modulus of PMMA/zinc oxide nanocomposites at various particle size, shape, and volume fractions.....	53
Figure 4.4 Comparison of tensile modulus in PMMA/PGMEA composites (red dot) and PMMA/Al <sub>2</sub> O <sub>3</sub> (20 nm) nanocomposites (black dot).....	54
Figure 4.5 Load-displacement curve comparison: PMMA (red) and PMMA/FG-Al <sub>2</sub> O <sub>3</sub> (0.5 vol%, 20 nm) (grey).....	55
Figure 4.6 Work of fracture of PMMA/Al <sub>2</sub> O <sub>3</sub> nanocomposites at various particle size, shape, and volume fractions.....	56
Figure 4.7 Work of fracture of PMMA/ZnO nanocomposites at various particle size, shape, and volume fractions.....	57
Figure 4.8 Impact resistance of PMMA/Al <sub>2</sub> O <sub>3</sub> nanocomposites at various particle size, shape, and volume fractions.....	59
Figure 4.9 Impact resistance of PMMA/ZnO nanocomposites at various particle size, shape, and volume fractions.....	60
Figure 4.10 Dispersion of dry-Al <sub>2</sub> O <sub>3</sub> (1 v/o) in PMMA by Ultra-sonication technique..	62

Figure 4.11 Pre-dispersed zinc oxide nanoparticle in PGMEA.....	63
Figure 4.12 Nanoparticle dispersion as a function of particle volume fraction.....	64
Figure 4.13 Fracture surface of Impact testing at 1 v/o of nanoparticles. ....	66
Figure 4.14 Debonding and cavitation around nanoparticles under tension.....	67
Figure 4.15 Fracture surfaces of PMMA and PMMA nanocomposites. ....	69
Figure 5.1 TGA curve of various nanoparticles: I is the reduction of the excess PGMEA and II is the decomposition of the chemisorb molecules.....	74
Figure 5.2 DTG curve of chemisorb molecules (region II) of various nanoparticles and the area under region II (inserted).....	76
Figure 5.3 DTG and TGA curves of neat PMMA. ....	78
Figure 5.4 DTG curve on the effect of aluminum oxide nanoparticles and small molecules of PGMEA on the thermal stability of PMMA. ....	80
Figure 5.5 DTG curve on the effect of zinc oxide nanoparticles on the thermal stability of PMMA.....	81
Figure 5.6 Glass transition temperature of PMMA/FG-ZnO nanocomposites and PMMA/PGMEA at various PGMEA volume fractions.....	84
Figure 6.1 ATR-FTIR spectra of PGMEA, bound PGMEA, and aluminum oxide.....	91
Figure 6.2 ATR-FTIR spectra of PGMEA, bound PGMEA, and zinc oxide. ....	92
Figure 6.3 Interfacial interactions between PGMEA and aluminum oxide.....	95
Figure 6.4 Effect of nanoparticles on hydrolysis reaction of PMMA. The extent of hydrolysis reaction in the absense of nanoparticles shown as inserted. ....	97

Figure 6.5 Interfacial interactions between PMMA and aluminum oxide nanoparticles.	98
Figure 6.6 Conversion vs. time curves of MMA polymerization (1 mass% AIBN). <sup>[9]</sup> ...	99
Figure 6.7 Raman intensity ratio and Raman spectra (inserted) as a function of polymerization time. ....	100
Figure 6.8 Effect of PGMEA additions on the C=C to C=O Raman intensity ratio in bulk PMMA in the absence of nanoparticles. ....	101
Figure 6.9 Effect of dry nanoparticle and FG-nanoparticle additions on the C=C to C=O Raman intensity ratio in bulk PMMA. ....	103
Figure 6.10 Effect of nanoparticle additions on polymer tacticity determined by the ratio of rocking vibration of $\alpha$ -CH <sub>3</sub> for syndiotactic to isotactic PMMA. The effect of PGMEA on the polymer tacticity shown as inserted. ....	106

## **Chapter 1 Introduction**

### **1.1 Objectives**

Polymers are macromolecules composed of a large number of repeating units generally connected by covalent bonds and classified as either natural or synthetic. Natural rubber, cellulose, and proteins are examples of natural polymers that have been known and used since antiquity. Synthetic polymers, on the other hand, are human-made materials such as polyamide, silicone, and polyurethane. Lightweight, low cost, and ease of processing are the main reasons that motivate the use of these materials, especially in today's market where low energy consumption becomes a highly significant factor in the consideration of materials. Heavy glass windows are being replaced with lightweight alternative of acrylic sheet made from poly(methyl methacrylate) such as Plexiglas®. Many segments and components in airplanes are also being replaced with various types of polymeric materials generally in the form of composite materials to reduce fuel consumption during flight. Neat polymers do not usually attain all the property requirements in certain applications and thus a composite approach is required. One of the most economical ways to improve properties of polymeric materials is via the fabrication of multi-component materials, or polymer composites. Subsequent to the commercialization of nanosize oxide particles, polymer nanocomposites have been the subject of intense research and development in academia and industry. High surface-to-volume ratio and the small size of nanoparticles results in favorable property improvements in many systems. However, the most significant difference between these

new nanocomposites and the more traditional microcomposites is the small size of the composite morphology and the very large amount of polymer/particle interface that exists when the particles become very small, i.e. in the nano scale range.

The thesis under which this dissertation was written is that the interfacial region between the polymer and the inorganic nanoparticles in a polymer/particulate nanocomposite, i.e. the bound region of polymer that can be considered permanently associated with the nanoparticle, has chemical and conformational differences from the bulk matrix polymer that influence the resultant properties. Although it has long been accepted that small nanoparticles, which are of approximately the same scale as the polymer chains, disrupt the bonding of the polymer as evidenced by changes in  $T_g$  and  $T_m$ , the molecular nature of these effects, particularly at the particle interface, has never been fully elucidated. In this dissertation I have sought to contribute to the understanding of this important element of polymer nanocomposites.

## **1.2 Dissertation Outline**

**Chapter 2 – Literature Review.** In this section, up to date work from the literature on polymer nanocomposites is summarized and evaluated. Improvements in both mechanical and thermal behaviors of polymer have been reported. The significance of interfacial interaction toward properties of composites is demonstrated. Aside from polymer nanocomposites, research on immiscible polymer blends is also summarized.

**Chapter 3 – Polymer nanocomposites: Processing.** This section reviews material selections and synthesis techniques used in this work. The detail of mechanical testing and characterization procedures are also discussed.

**Chapter 4 – Mechanical behavior of polymer nanocomposites.** The effect of nanoparticles on mechanical behavior of polymeric nanocomposites, especially tensile modulus and impact resistance are discussed. The improvements of these properties have been reported with the addition of nanoparticles. In this Chapter, the effect of particle size, chemistry, shape, and volume fraction are studied.

**Chapter 5 – Thermal behavior of polymer/particulate nanocomposites.** The influence of nanoparticle on thermal stability of PMMA is studied. The degradation of PMMA was shifted to higher temperature with the nanoparticle addition. Additionally, the mobility of polymer chains is enhanced with the presence of nanoparticles.

**Chapter 6 – PMMA/particulate nanocomposites: Spectroscopic analysis.** The interactions at the interface in polymer nanocomposites are proposed along with the conformation and configuration of PMMA. The extent of polymerization of PMMA is also analyzed.

**Chapter 7 – Conclusion.** This section summarizes all the results discussed in this dissertation.

**Chapter 8 – Future work.** The ideas toward future work are proposed in this section.



## **Chapter 2 Polymer composites: Nanocomposites and Immiscible Polymer Blends (IMPBs)**

### **2.1 Polymer nanocomposites: Literature review**

Polymeric materials have become an alternative choice for a large number of applications ranging from household goods to sophisticated materials used in aerospace and electronic devices. Most applications require multi-functionality in a single material which is not usually found in a typical polymer. Polystyrene and poly(methyl methacrylate) are two examples of high modulus materials that have limited impact resistance, whereas polyethylene and polypropylene are two high strain-to-failure, i.e. tough, materials that have poor stiffness. Exceptions exist, of course, such as polycarbonate which possesses good stiffness and toughness. An economical way to fabricate multi-functional materials is to mix polymer with other materials (fillers), such as glass fiber, metal and wood, known as polymer composite. For instance, high stiffness glass fibers are introduced to various polymer matrices to increase Young's modulus of materials.<sup>[1, 2]</sup> In the traditional composite systems where the fillers typically have micrometer-scale dimensions, the property improvement in such systems normally comes with trade-offs. As one example, the optical clarity of composites is sacrificed when domain sizes are near the wavelength of light or larger. Furthermore, stress concentration created by large particle in the composite leads to material failure which consequently reduces the ductility of the composite materials.

The incorporation of nanoparticles into polymer systems to form functionalized nanocomposites has become increasingly popular in recent years and this class of composites has become a significant category among all polymer composites.<sup>[3, 4, 5, 6, 7, 8, 9, 10, 11]</sup> In fact, nanoparticles have been used in the rubber industry for a long time<sup>[12]</sup>, however, extensive attention to polymer nanocomposites was not until the early 1990's when the study from Toyota Laboratories showed significant improvement in yield and tensile strengths of nylon 6 when mica was incorporated into the polymer matrix.<sup>[13, 14]</sup> The motivation for polymer nanocomposites is the exceptional engineering properties that can be generated when particulate additives are of the same dimensional order of magnitude as the molecular structure of the polymer.<sup>[7]</sup> Moreover, nano-scale particles do not generate large stress concentration; therefore, ductility is not significantly compromised. Another advantage is the low light scattering of nanoparticles which make it possible to maintain optical clarity in the final composites.<sup>[15]</sup> Last but not least, the large amount of interfacial area that results provides a medium for various functionalities that can range from crack deflection and elongation for structural composites to conductivity and capacitance for electrical materials. Much has been said and written about the particle shape and size in such composites.<sup>[8, 9, 10]</sup> For example, at a given volume fraction, the smaller particle size of aluminum oxide resulted in enhancement of fractural toughness compared to the neat polyester resin.<sup>[8]</sup>

Thermal stability of polymer can be enhanced by the addition of nanoparticles.<sup>[16, 17, 18, 19, 20, 21, 22, 23, 24]</sup> A study of radical polymerization of the ZnO/PMMA system reported that the ZnO surface induced chain termination, thus leading to less defect linkage

elements (e.g. Head-to-Head linkage) that would be created during polymerization of the neat PMMA.<sup>[23]</sup> The effect of nanoparticles on increasing the thermal stability of polymeric materials was proposed through several mechanisms. The first mechanism is the barrier effect in which nanoparticles retard heat and mass transport necessary for the degradation process.<sup>[17, 18]</sup> Additionally, the paramagnetic iron presents in clay particles is key to a proposed radical trapping mechanism which enhances the thermal stability of the clay/polymer composites.<sup>[19]</sup> Furthermore, the thermal stability was also reported to be enhanced by the restriction of the polymer chain mobility in particle/polymer composites.<sup>[21, 22]</sup>

In particulate/polymer composite systems, the polymer-particle surface interaction is a critical factor that influences the final properties of the polymer composite systems.<sup>[25, 26, 27]</sup> The quality of the interaction determines to a significant extent the load-transfer efficiency and hence the mechanical properties.<sup>[28, 29]</sup> Naturally, this factor increases in significance as the size of the particles decreases, and the effect becomes dominant when the particles are at the nanometer scale. Nanoparticles have special effects on polymers since the particle size is of the same order as the polymer chain gyration which is typically about 40 nm.<sup>[7, 30]</sup> Consequently, the nanoparticles can have a strong affect on the configuration and conformation of the surrounding polymer which leads to alterations in the bulk properties of the composite.<sup>[31, 32, 33]</sup>

### 2.1.1 Nanoparticles

Nanoparticles are generally categorized into three geometries i.e. equi-axial, rod (fiber-like), and sheet, as shown in Figure 2.1. A significant advantage of small-sized particle is the high surface-to-volume ratio which is varied by the particle geometry. At a given volume particles with high aspect ratios, such as sheet-like clay materials, possess the highest surface area followed by rod-like and equi-axial particles, respectively (Figure 2.2).<sup>[34]</sup>

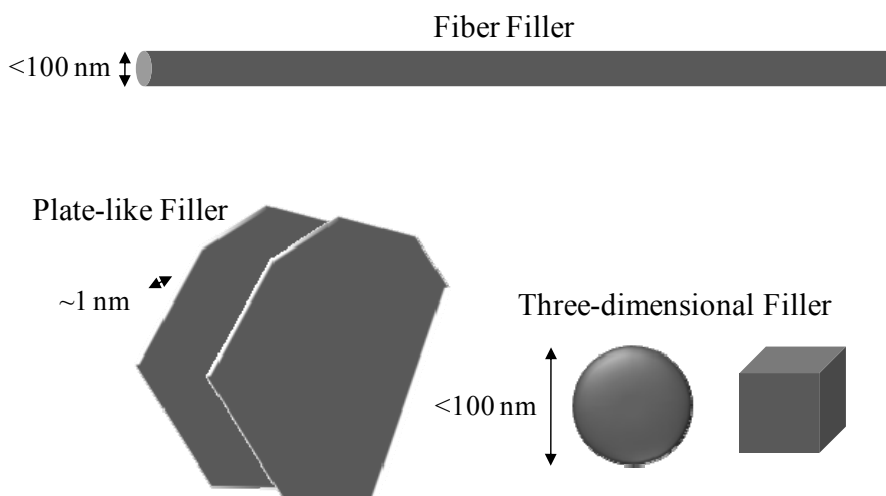


**Figure 2.1** Schematic of nanoscale fillers (redraw from ref.[15])

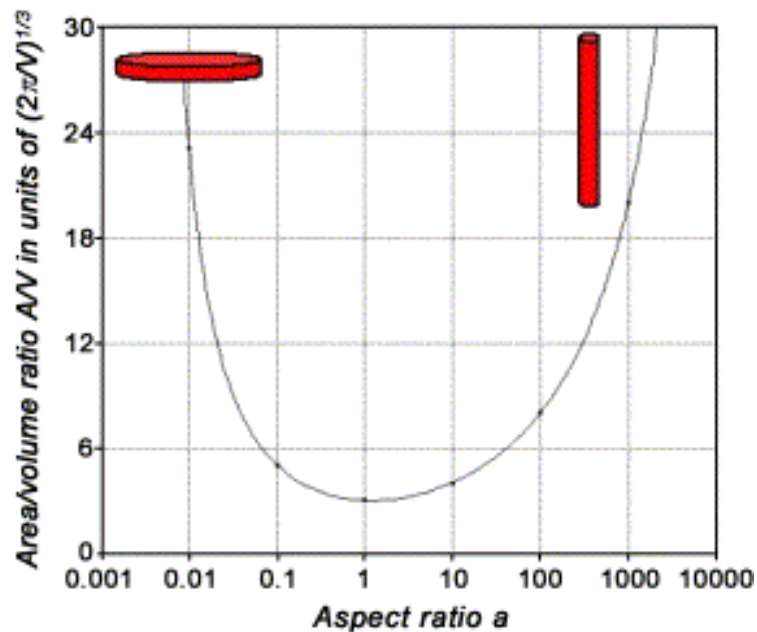


**Figure 2.2** Plot of the function describing the ratio of surface area to volume ( $A/V$ ) vs. aspect ratio for cylindrical particles with a given volume.<sup>[34]</sup>

Properties of polymer composites can be tailored by type of nano-scale fillers used in the system. Many types of nanoparticles are commercially available today. Montmorillonite (MMT) is one of the most studied in polymer nanocomposites. Other fillers include carbon nanotubes, aluminum oxide, and silica. The following sub-sections describe examples of filler in each type of geometry.

#### 2.1.1.1 Carbon nanotubes

The nanosize tube of carbon was first discovered by Radushkevich and Lukyanovich in 1952. However, the majority of the research did not start until the work by Iijima which was published in 1991.<sup>[35]</sup> The first nanotubes discovered were multi-walled nanotubes (MWNTs) consisting two or more layers of concentric sheets of

graphite with the interlayer distance of 0.34 nm.<sup>[36]</sup> Later, with the failed experiment in synthesizing MWNTs, single-walled nanotubes (SWNTs), single roll of graphite sheet with diameter 1-2 nm (Figure 2.4), were discovered simultaneously by two teams, one by Iijima and Ichihashi from NEC<sup>[37]</sup> and another by Bethune et al. from IBM<sup>[38]</sup>. The structure of SWNTs depends on the wrapping direction of the graphene sheet. According to Figure 2.3, the vector direction (m, n), known as chiral vector, is the index for each structure. The direction of  $m=0$ , the nanotube structure is called “zigzag”, whereas if  $m=n$ , it is referred to “armchair”. In other conditions, the structure is considered as “chiral”. Figure 2.4 illustrates all three structures of SWNTs.

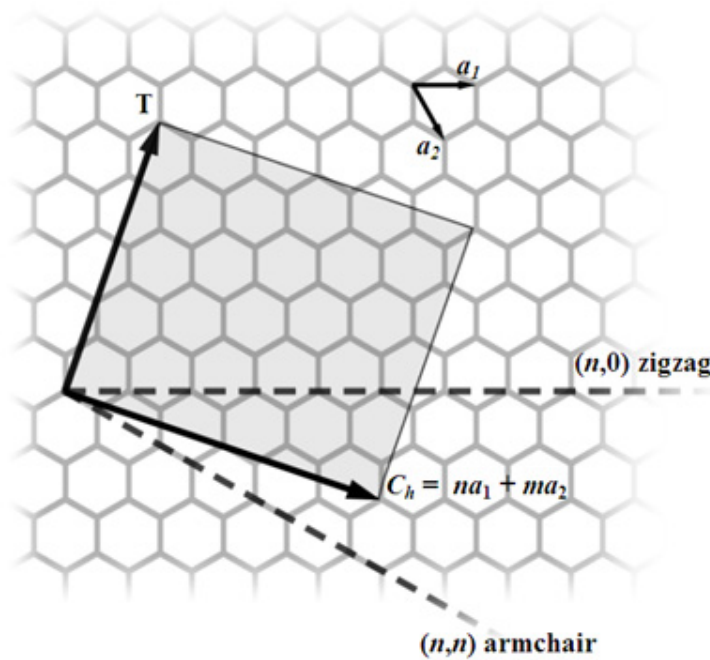


**Figure 2.3** Chiral vector on single graphene sheet.<sup>[39]</sup>

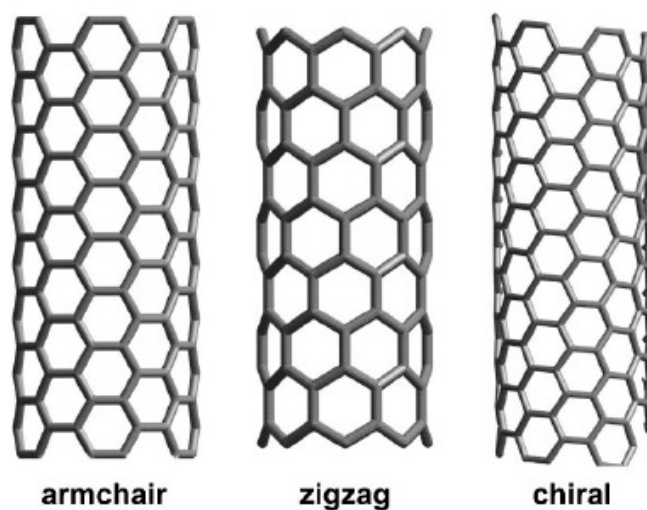


**Figure 2.4** Structures of SWNTs.<sup>[40]</sup>

One attractive property of CNTs is its high mechanical property. Carbon nanotubes possess high Young's modulus ( $\sim 1$  TPa for SWNTs and  $\sim 0.3$ -1 TPa for MWNTs) and tensile strength (50-500 GPa for SWNTs and 10-60 GPa for MWNTs) as a result of the covalent  $sp^2$  hybridization between each carbon atom. CNTs is a semi-conducting material resulted from the curvature structure of the graphene sheet that varies the electronic structure along the tube.<sup>[15]</sup>

#### 2.1.1.2 Montmorillonite

Clay is known as layered silicate where the bonding between each layer can be strong or weak. Mica, talc, and kaolin are examples of strong bonding and categorized as non-expanding clay. Phyllosilicates, smectite, and montmorillonite are, on the contrary, have weak bonding between each layer, thus referred as expanding clay. Each layer,  $\sim 1$  nm thick, consists of two sheets of silica tetrahedral with one alumina octahedral sheets

in the center. Every one-eighth of octahedral sheet located between two sheets of silica tetrahedral, the aluminum ion ( $\text{Al}^{3+}$ ) is substituted with manganese ion ( $\text{Mg}^{2+}$ ) resulting in negative charge which is normally neutralized by sodium ion ( $\text{Na}^+$ ). The structure of montmorillonite clay is shown in Figure 2.5.<sup>[30]</sup> Montmorillonite clay platelets possess high aspect ratios, and these thin layers of aluminosilicate are capable of carrying high loads – an ideal configuration for reinforcement. Additionally, the layered structure of montmorillonite provides outstanding barrier to gas and water.<sup>[15]</sup>

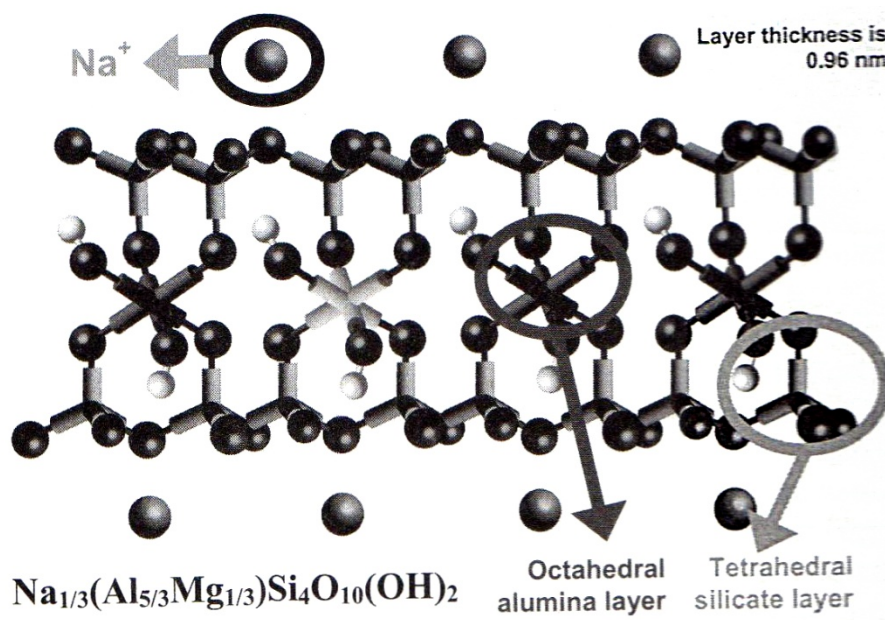


**Figure 2.5** Chemical structure of montmorillonite.<sup>[30]</sup>

### 2.1.1.3 Aluminum oxide

Aluminum oxide, or alumina ( $\text{Al}_2\text{O}_3$ ), is a widely used ceramic material. The outstanding physical properties, such as high stiffness, good thermal properties, and excellent dielectric properties, make aluminum oxide suitable for various applications.



Several crystalline phases of alumina exist which are formed along the dehydration temperature profile as demonstrated in Figure 2.6.<sup>[41]</sup> The general crystalline form of aluminum oxide is corundum, also known as  $\alpha$ - $\text{Al}_2\text{O}_3$  with rhombohedral unit cell where oxygen atoms form hexagonal close-packed structure and aluminum atoms are situated in about two-third of the octahedral interstices (Figure 2.7).<sup>[42]</sup>

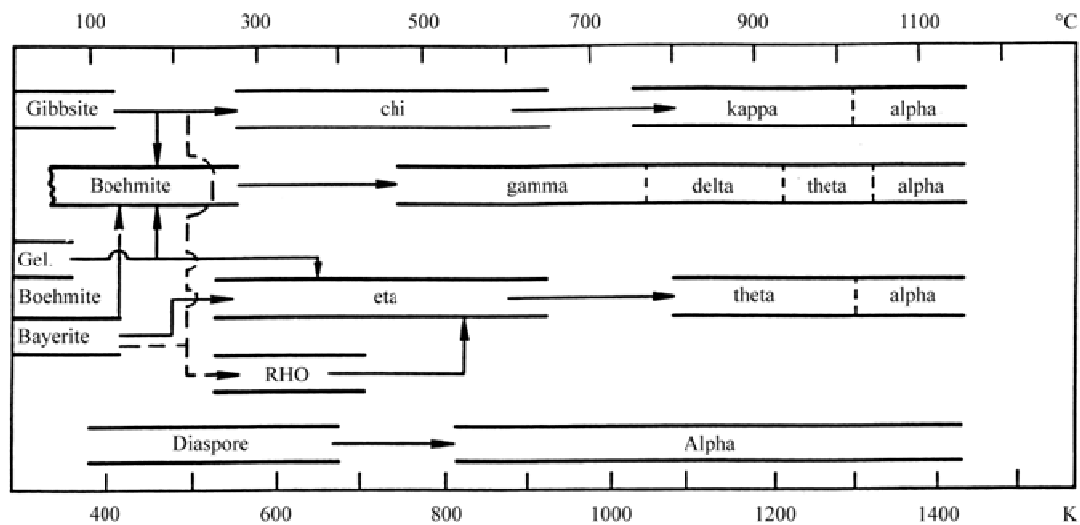


**Figure 2.6** Thermal transformation sequence of the aluminum hydroxides.<sup>[41]</sup>

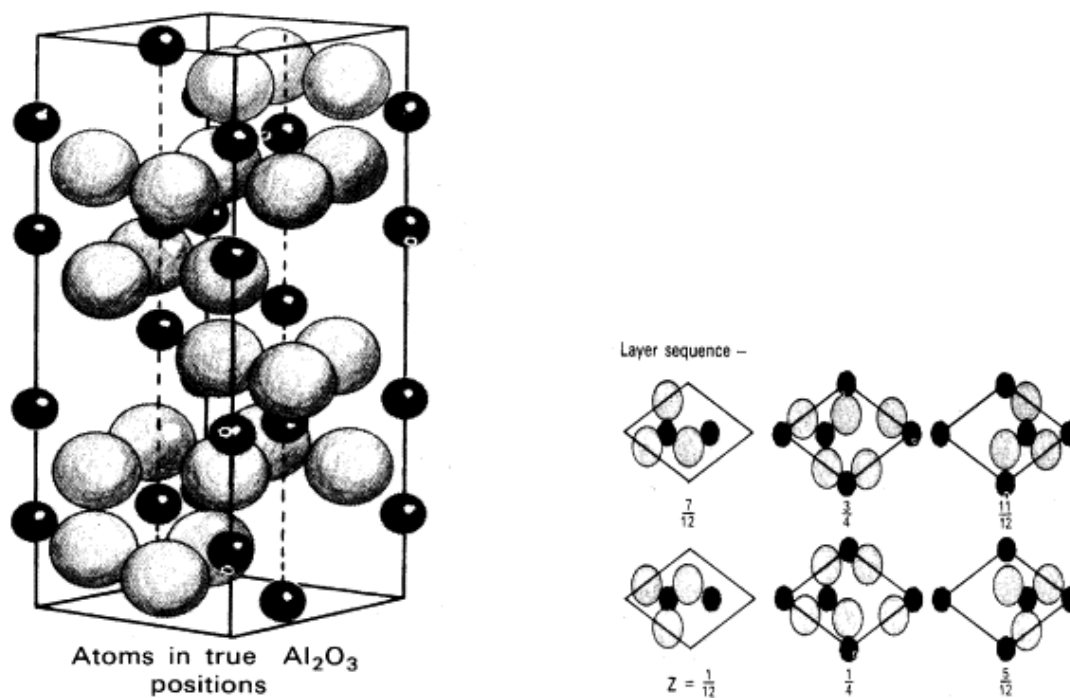
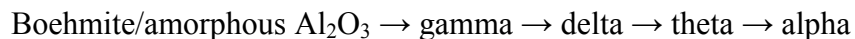


**Figure 2.7** The corundum structure of aluminum oxide

(Al, small sphere; O, large sphere).<sup>[42]</sup>

During calcination process of aluminum hydroxides and oxyhydroxides, many metastable transition phases are formed.  $\gamma$ -alumina is one of the metastable phases achieved during the calcination process.<sup>[43]</sup>



Structure of  $\gamma\text{-Al}_2\text{O}_3$  is categorized into defect spinel cubic as expressed in Figure 2.8.<sup>[43]</sup> The oxygen atom is formed as cubic close-packed having aluminum atoms situated in octahedral and tetrahedral sites. Some positions are unoccupied to satisfy the stoichiometry of alumina which distributed between octahedral and tetrahedral site. Under high temperature, hydroxyl groups are eliminated from the  $\gamma\text{-Al}_2\text{O}_3$  surface.

The advantage of nanotechnology in the property enhancement of materials is the driving force for the development of nano-size particles. Considering the exceptional properties, it is no surprise that aluminum oxide is one of the interesting materials. High surface energy of  $\alpha\text{-Al}_2\text{O}_3$  makes it unstable when the particle size in the nano-scale range. Nano-scale aluminum oxide is more stable in gamma-phase ( $\gamma\text{-Al}_2\text{O}_3$ ) rather than the traditional alpha phase ( $\alpha\text{-Al}_2\text{O}_3$ ) as a result of higher entropy of  $\gamma\text{-Al}_2\text{O}_3$  which results from random distribution of aluminum atoms and vacancies.<sup>[44]</sup>

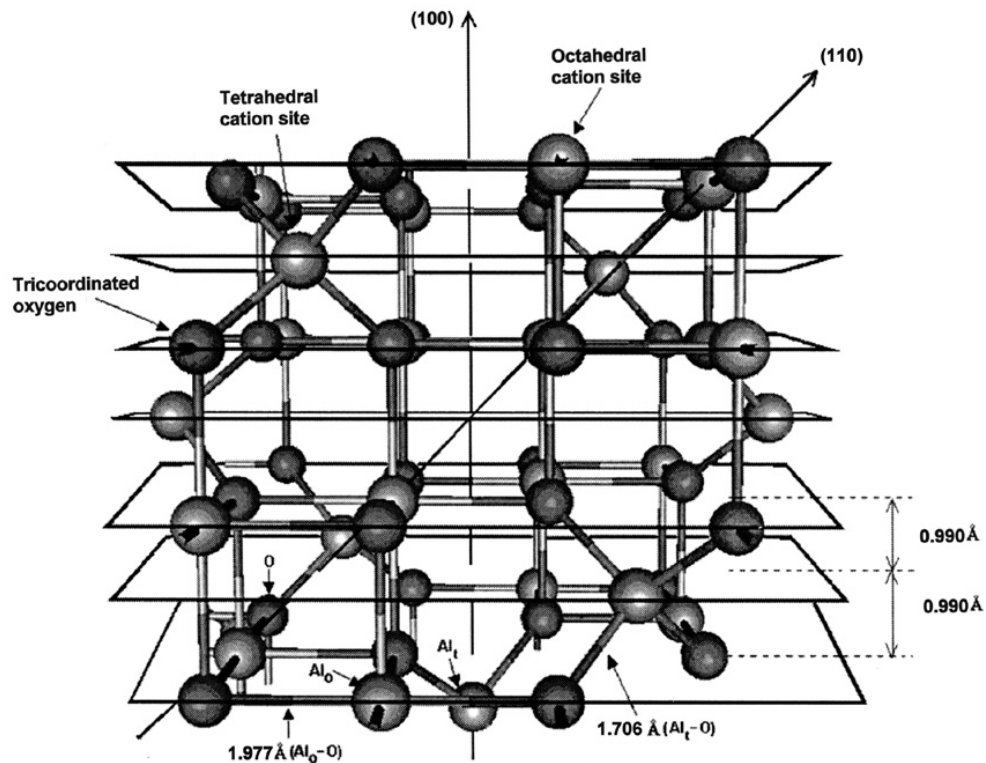


**Figure 2.8** Cubic  $\gamma\text{-Al}_2\text{O}_3$  spinel-type unit cell.<sup>[43]</sup>

Beta-alumina,  $\beta\text{-Al}_2\text{O}_3$ , has the formula of  $\text{Na}_2\text{O} \cdot x\text{Al}_2\text{O}_3$ ,  $x = 11$ . The structure of  $\beta\text{-Al}_2\text{O}_3$  shown in Figure 2.9 is categorized by hexagonal symmetry with Na-O planes,

mirror planes, in between blocks of spinel-like Al-O.<sup>[45]</sup> Two types of beta-alumina are available differing by the sodium content. Low sodium content, having a formula  $\text{NaAl}_{11}\text{O}_{17}$ , is more thermodynamically stable than the higher content one ( $\beta''\text{-Al}_2\text{O}_3$ :  $\text{NaAl}_5\text{O}_8$ ).<sup>[46]</sup>

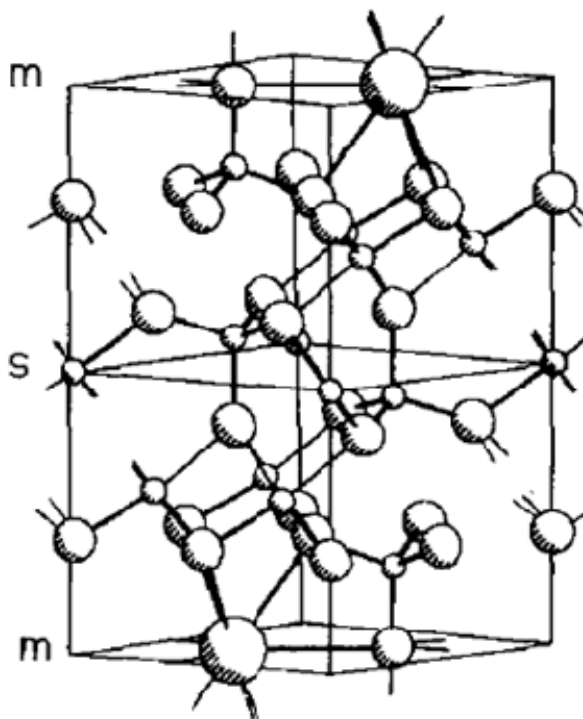
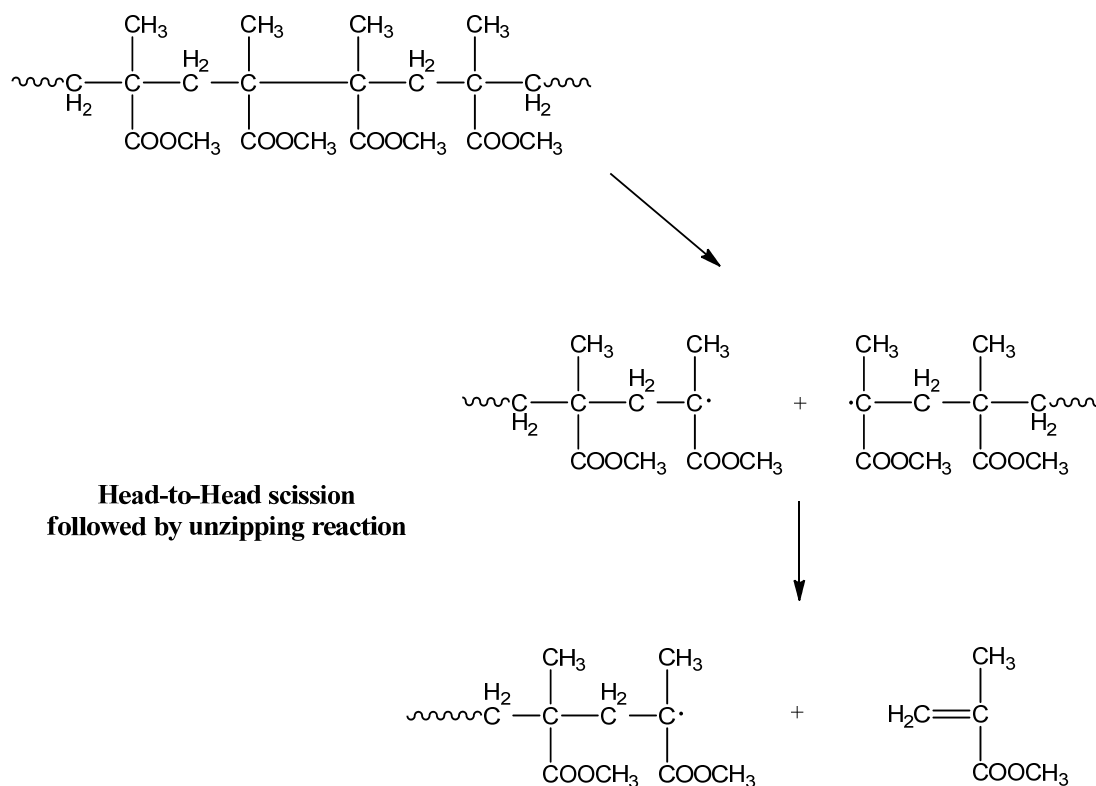


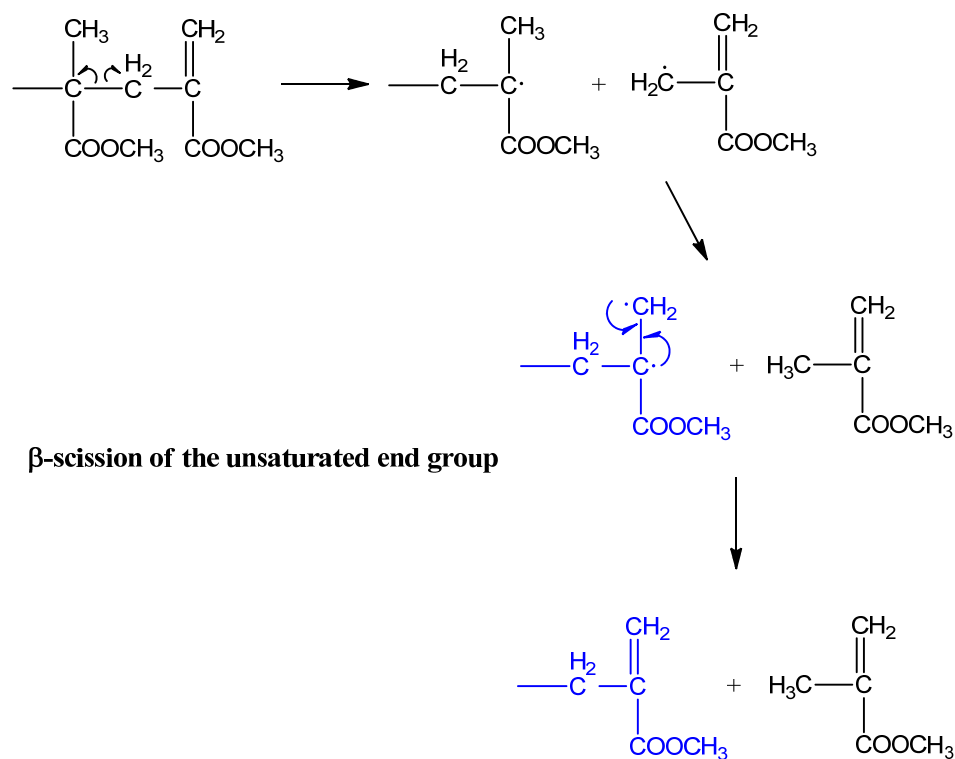
**Figure 2.9** Semi-cell of ideal structure in  $\beta\text{-Al}_2\text{O}_3$ ; Large spheres: alkaline or alkaline earth metal; medium sphere: oxygen ions; small spheres: aluminum ions; m: mirror plane; s: spinel block.<sup>[45]</sup>

### 2.1.2 Thermal degradation of PMMA

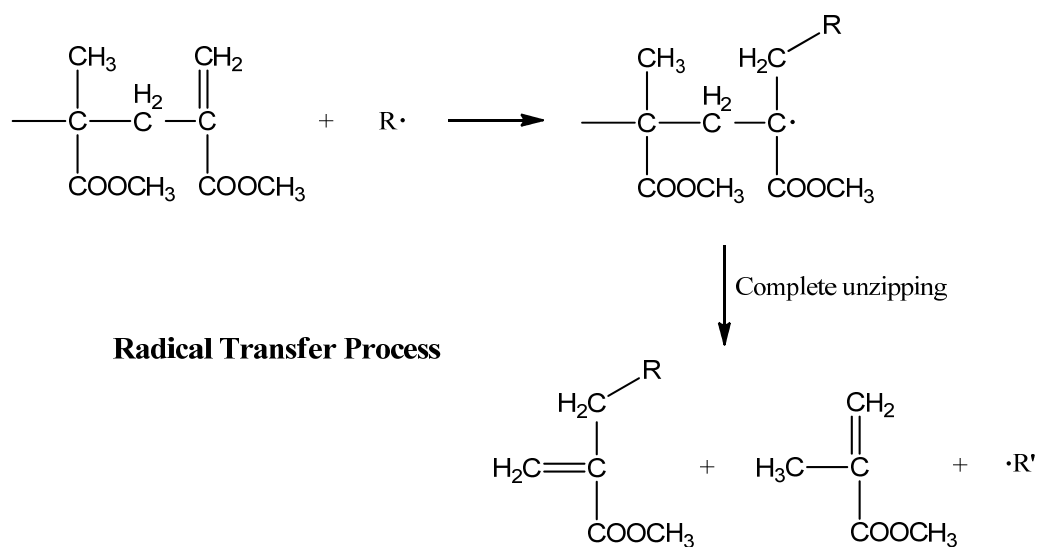
Poly(methyl methacrylate), or PMMA, is an important thermoplastic for numerous uses and particularly for optical applications due to excellent transparency in the visible region. Nevertheless, PMMA has limiting properties, particularly its low toughness and poor thermal stability. One of the reasons is the defects (unsaturated end group and H-H linkage) in the polymer chain that occur during polymerization process (discussed in Chapter 3). Thermal degradation of PMMA has been studied by many authors. In the case of radical polymerized PMMA, three chain scission steps were observed in the thermal degradation process.<sup>[47, 48, 49, 50]</sup> From thermal gravimetric analysis (TGA), each step of the degradation temperature of PMMA has been reported to be around 165, 270, and 360°C, respectively, with 2°C/min heating rate under N<sub>2</sub> atmosphere. The lowest degradation temperature of the three is due to the scission of head-to-head (H-H) linkages as shown below. The instability of the H-H linkage is attributable to the close proximity of the bulky pendent groups creating higher localized free energy via steric hindrance as well as the inductive effect of the ester groups with respect to electron extraction. Consequently, the bond dissociation energy of this H-H linkage was found to be about 84 kJ/mol less than that of C-C backbone bond.<sup>[47]</sup> The mechanism of the scission of H-H linkage is in the illustration below.<sup>[49]</sup>



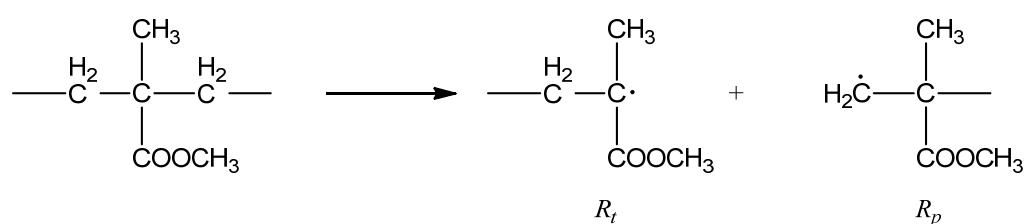
The second weakest point is at the unsaturated vinylidene end group. One study reported that the scission at this point occurred at the C-C bond in the  $\beta$  position to the unsaturated vinylidene end group since the dissociation energy of the C-C bond in this position is approximately 42-50 kJ/mol lower than the adjacent saturated C-C bond. This is known as the  $\beta$ -scission and the dissociation mechanism is expressed as follows.<sup>[47]</sup>



Another suggested mechanism of the scission at this unsaturated vinylidene end group was due to the radical transfer process. Such reaction is illustrated as follows: <sup>[50]</sup>



Both H-H linkage and unsaturated vinylidene end group are considered as defects in the polymer chain which consequently influence the properties of the polymer, especially the thermal stability.<sup>[47]</sup> The last and the most stable bond is the C-C main chain bond which decomposes at the highest temperature. The breaking of the main chain results in one primary radical ( $R_p$ ) and one tertiary radical ( $R_t$ ) which eventually depolymerize to MMA.<sup>[51]</sup> The reaction is given below:



Besides the main chain decomposition, random scission of the side-groups in anionic polymerized PMMA was proposed by Manring due to the cage effect of the radical.<sup>[52]</sup> This effect may cause the radicals to be trapped and recombined as part of the disproportionation reaction. Such a recombination leaves them inactive while the side-group, on the other hand, has the better ability to migrate and participate in subsequent decomposition processes.

### 2.1.3 Interphase/interface of Polymer/particulate nanocomposites

#### 2.1.3.1 Surface chemistry of metal oxide

Isoelectric point (or zero point of charge, zpc) is associated with the pH at which the surface is neutralized. Surface is positively and negatively charged when the pH is above and below the zpc value, respectively (Figure 2.10). Due to different chemistries,



each metal oxide has its own isoelectric point, for instance, zpc of aluminum oxide is 7.0-7.9<sup>[53, 54]</sup> whereas it is 9.0-9.3 for zinc oxide<sup>[55, 56]</sup>.

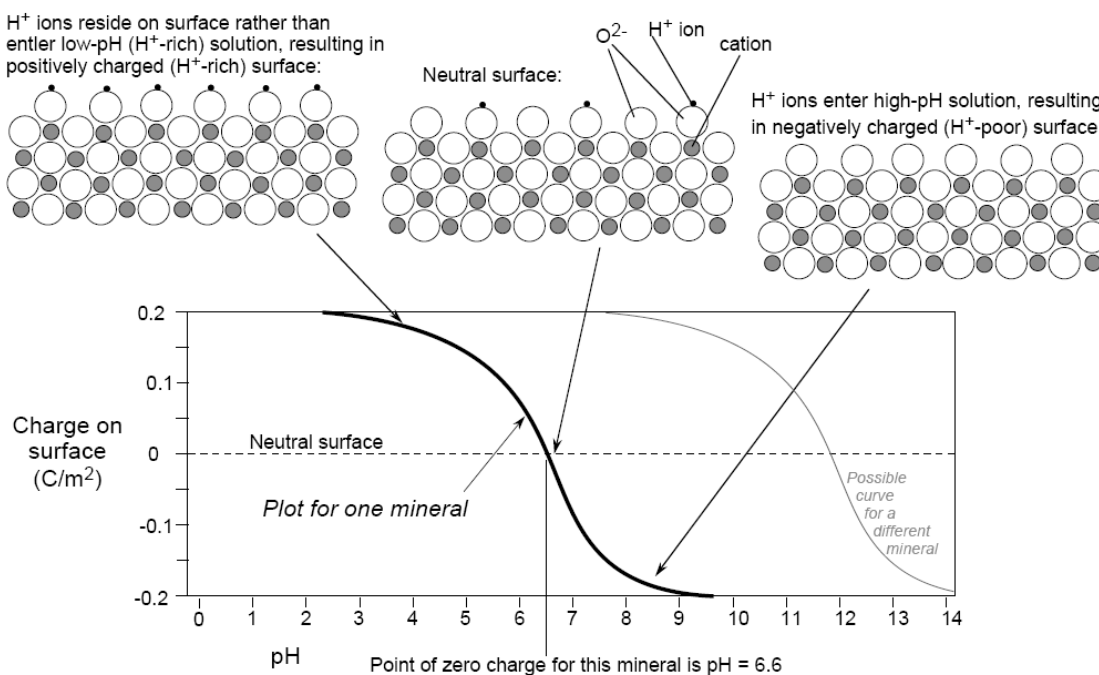


**Figure 2.10** Surface charge at various pH.<sup>[57]</sup>

Ionic potential determines charge density of an ion and can be determined by the charge/ radius (ionic) ratio,  $q/r$ . High ionic potential implies that an ion will strongly attach to the opposite charge and at the same time repel the ion of like charge. Figure 2.11 gives an idea of ionic potential of various ions.<sup>[57]</sup> For instant, high ionic potential of  $S^{6+}$  strongly attach with  $O^{2-}$ , however, the repulsive force between  $S^{6+}$  is very high results in unstable solid. Unlike, ions with moderate ionic potential values, such as  $Ti^{4+}$ ,  $Mg^{2+}$ , and  $Al^{3+}$ , the systems are stable enough to form stable solid.

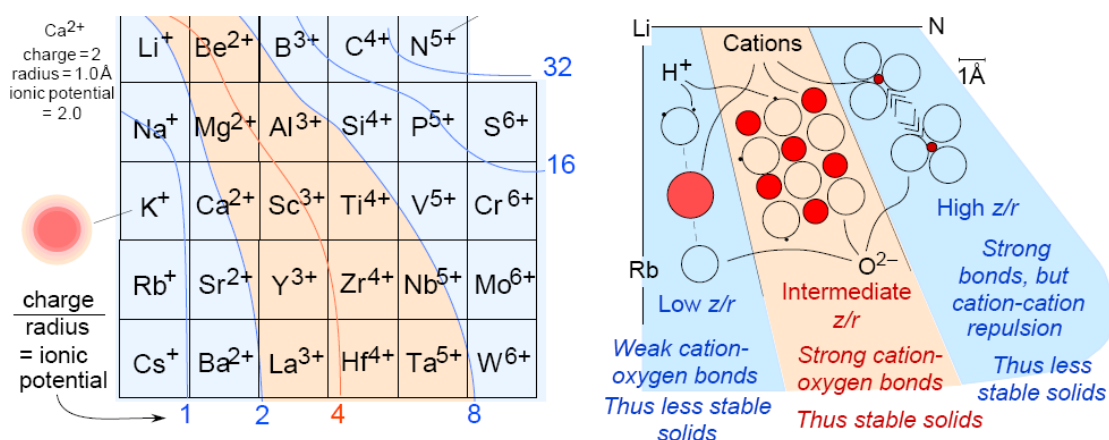


**Figure 2.11** Ionic potential of various ions (left) and the interactions between ions at difference ionic potential value (right).<sup>[57]</sup>

Ionic potential and zpc relate to one another in such a way that the lower the ionic potential of the cation, the lower is the ability to repel like charge, which consequently leave positive charge on the surface. Therefore, to neutralize this high proton surface, higher pH is required which results in higher zpc. For instance, at a given pH, the lower ionic potential and higher zpc of  $\text{Zn}^{2+}$  ( $q/r = 2.7$ ) as compared to  $\text{Al}^{3+}$  ( $q/r = 5.6$ ) provide higher positive charge on the surface. Figure 2.12 illustrates the effect of ionic potential of cation on the surface charge.

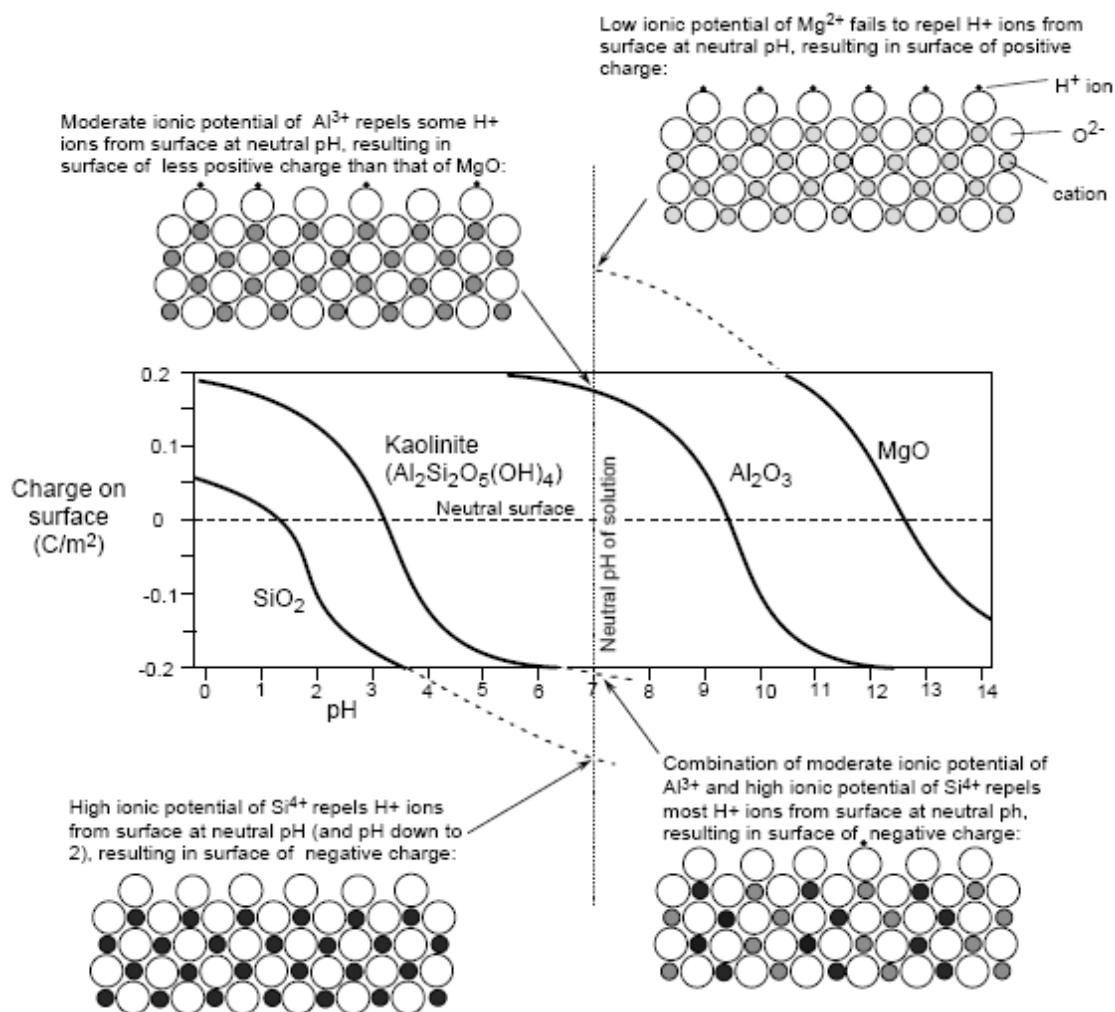


**Figure 2.12** Ionic potential and surface charged of various types of metal oxide.<sup>[57]</sup>

### 2.1.3.2 Interfacial interaction: Polymer/particulate nanocomposites

The degree of improvement in particulate/polymer composites relies heavily on how they interrelate with one another. Besides property of individual component, such as mechanical behavior, property of particulate/polymer composites depends strongly on both quality as well as quantity of interactions at this interfacial area where the surface chemistry plays significant role. For instance, to improve tensile modulus of polymeric

material, excellent load transfer between high modulus filler and polymer matrix is required. The outer surface of each phase is generally responsible for the interactions. These interfacial interactions are very significant particularly in polymer nanocomposite systems due to very high interfacial area provided. In the ideal dispersed system of nanoparticles, the interparticle distance of the smaller particles is shorter as compared to the larger one leading to a large amount of interfacial region throughout the composites (Figure 2.13). At the interfacial region, both physical and chemical interactions occur which result in perturbed and constrained polymer chains.

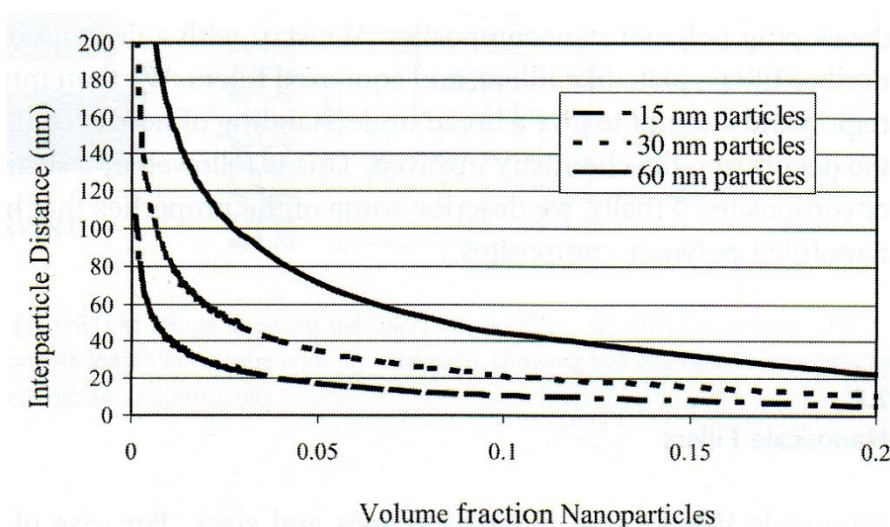


**Figure 2.13** Interparticle distance for spherical particles that are ideally dispersed. <sup>[15]</sup>

Due to the length and flexibility of polymer chains, not all functional groups along the chain will contribute to the interaction. Only few points along the chain will interact with the filler surface which are referred as anchoring points which leave unreacted parts of the polymer chain to entangle to other chains as shown in Figure 2.14.<sup>[33]</sup> The

unreacted chain segment can extend away from the surface; therefore, the interaction affects not only the chain segment at the interface but also in vicinity areas and this perturbed area can be referred as “interphase region”. The thickness of such region varies by the strength of the interaction which differs from one system to another.<sup>[58]</sup> Free volume in polymer nanocomposites is varied by how polymer chain interact with nanoparticles. Therefore, strength of interfacial interaction between polymer chain and nanoparticles can be determined by glass transition temperature ( $T_g$ ).<sup>[15, 59]</sup> According to work carried out by Ash, the  $T_g$  of PMMA/ $\text{Al}_2\text{O}_3$  decreased in the case of non-wetted interface whereas the  $T_g$  was stabilized or raised in wetted system.<sup>[59]</sup>

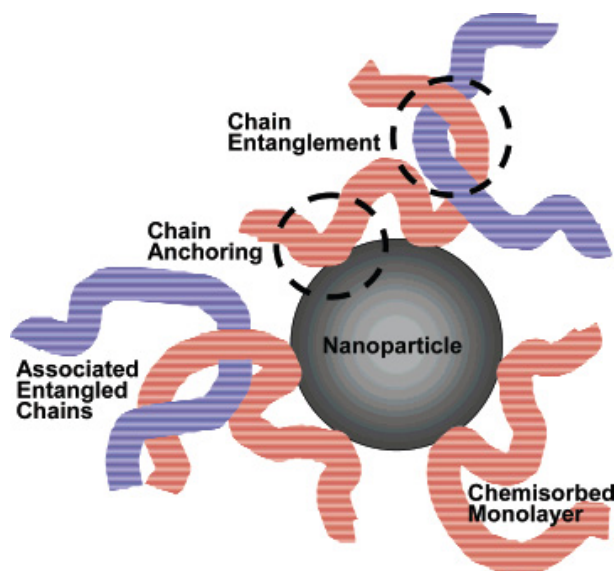


**Figure 2.14** Interphase region between the particulate filler and polymer matrix.<sup>[33]</sup>

Upon interaction with particle surface, a variety of polymer chain configurations at the interface can be achieved (Figure 2.15) depending on the number and the position of the active sites on both the particle surface and along the polymer chain.<sup>[60]</sup> The adsorbed

chain configuration becomes more complex as small molecular species are introduced into the system because the absorptivity of polymer chain competes with small molecular absorption. Although the bonding mechanisms in both cases are similar, the long nature and flexibility of polymer chains makes them different. Multiple sites, but not all, on a polymer chain can contribute to the adsorption mechanism. Chain configuration at the particle surface relates to the number of anchoring segments; higher anchoring point per polymer chain is equivalent to the more extended (flatten) configuration.<sup>[61]</sup>

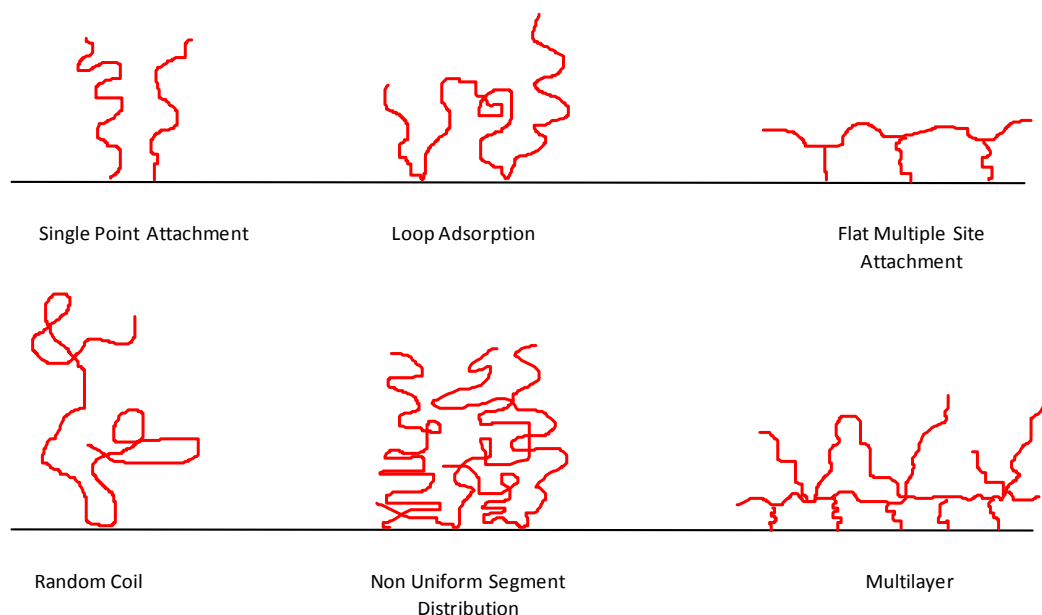


**Figure 2.15** Conformation of adsorbed polymer molecules (redraw from ref. [60]).

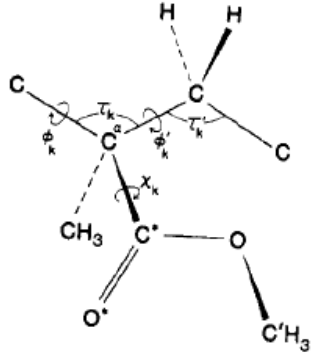
### 2.1.3.3 Interfacial interaction of PMMA and metal oxide particles

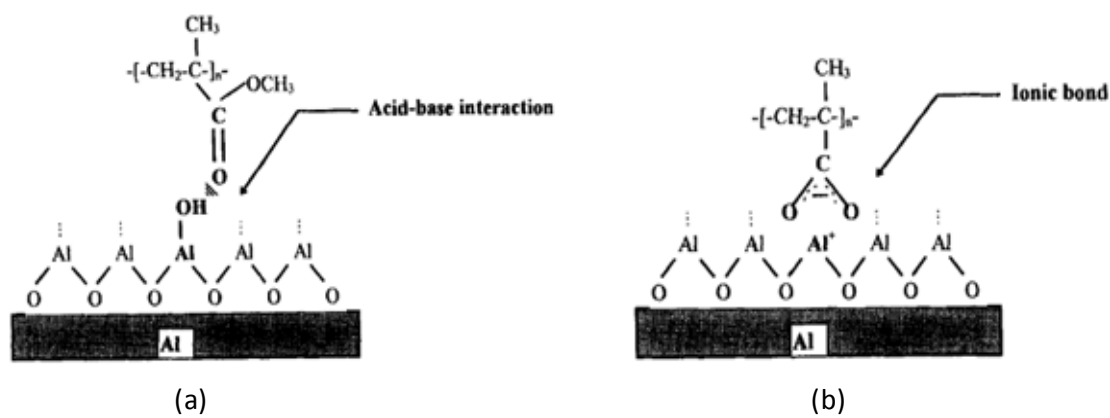
Metal oxide, for instance alumina, silica, and zinc oxide, under normal conditions reacts with surrounding moieties and forms considerable amount of hydroxyl group (-OH) on the surface. These hydroxyl groups are responsible for the interaction with another

substance via secondary bonding such as hydrogen bond. Polarity of metal oxide surface enables it to interact with polar polymers, for instance nylon, poly(ethylene glycol, and poly(methyl methacrylate), PMMA.<sup>[62]</sup>

Many studies have reported the interaction between PMMA and metal oxide particularly aluminum oxide particles.<sup>[61, 63, 64]</sup> The common interaction is acid-base interaction (Figure 2.17a) where the partial negative of carbonyl oxygen (as seen in Table 2.1) behaves as electron donating group and interacts with electron accepting species on the metal oxide surface via hydrogen bonding. Another proposed interaction was ionic interaction between carboxylate anion ( $\text{COO}^-$ ) and aluminum ion ( $\text{Al}^{3+}$ ) on the surface (Figure 2.17b). As the ester group approaches the surface hydroxyl group, the hydrolysis reaction (also known as de-esterification) takes place which generates the carboxylate anion and vacancy on aluminum ion ( $\text{Al}^{3+}$ ) at the particle surface.<sup>[61, 63]</sup> As a consequence of the interaction, the polymer chain in particular at the interfacial region is more preferably in trans-trans (*tt*) conformation to obtain more flatten chain fashion.<sup>[61, 63]</sup> The strong dipole moment of carbonyl group ( $\text{C}=\text{O}$ ) shows strong absorption in infrared spectroscopy. The vibration of free carbonyl (un-bound) peak for PMMA is normally observed near  $1730\text{ cm}^{-1}$ . When carbonyl group is bound to another molecule or self aggregation in neat polymer, the peak is shifted toward lower frequency.<sup>[65, 66]</sup> The bound species donate electron to the anti-orbital of carbonyl which weaken the carbonyl bond and lower the stretching frequency.<sup>[65]</sup>

**Table 2.1** Structure and parameters of PMMA (Data taken from Vacatello).<sup>[67]</sup>

Structure	Bond	Length (Å)	Atom	Partial Charge (esu)
	C-C	1.53	C*	0.517
	C-C*	1.52	O*	-0.417
	C-H	1.10	O	-0.202
	C*-O	1.36	C'	0.102
	C*=O*	1.22		
	O-C'	1.45		

**Figure 2.16** Schematic representation of the acid-base interaction (a) and the ionic bonding (b) which take place at the PMMA/aluminum interface.<sup>[63]</sup>



## 2.2 Immiscible polymer blends: Literature review

Polymer blends is an economical way to create a new material by combination of the properties of different polymers together. However, high molecular weight and entropy constrained of polymer molecules make most polymers immiscible to one another. Consequently, the coarse morphology and lack of interfacial adhesion are usually observed. Nevertheless, the non-bonded interphase of immiscible polymer blends possesses both positive and negative ramifications. Such interfaces are excellent crack deflection sites that can arrest or deflect fast propagating cracks in brittle polymers such as polystyrene. Deflection generates a more tortuous crack path through the composite, increasing the work of fracture and the toughness. On the contrary, non-bonded interfaces prevent load transfer across the interface, thus weakening the material in some context. In poorly engineering immiscible blends, the interfaces and morphology are gross, thus greatly reducing the strength and toughness of such blends.

To achieve miscibility of the blends, a compatibilizer is often used.<sup>[68, 69, 70]</sup> In such compatibilized blends, the phase bonding substantially improves the impact toughness but in many cases the modulus and time-dependent properties (e.g. creep) are sacrificed. Yet, in some prominent cases the impact strength of the materials enhanced without losing tensile and flexural strength.<sup>[71]</sup> In uncompatibilized immiscible polymer blends, however, with the proper processing conditions and compositions, the synergistic properties of the blends can be achieved.<sup>[72, 73, 74, 75]</sup> Leclair and Favis observed impact

strength improvement in uncompatibilized PC/HDPE when PC was the dispersed phase in a HDPE matrix.<sup>[74]</sup>

### 2.3 Objectives of thesis

Polymer nanocomposites have attracted the majority of interest in recent years. However, optimization of the properties in these classes of materials requires considerable understanding about interaction between phases. The ability of nanoparticles to interact with polymers at the molecular level makes each combination unique from one another.

A guiding premise of this dissertation is that the behavior of nanocomposites is influenced critically by the bound interfacial volume between phases. As such, the heart of this dissertation addresses the characterization of the interfacial region of a certain class of polymer nanocomposites. The influence of nanoparticles on mechanical and thermal behaviors of polymer is also investigated.

Bulk polymerization was selected as a synthesis technique to show that a simple polymerization process generally used in mass production can be applied to efficiently produce this class of materials. Poly(methyl methacrylate) was chosen as a polymer matrix. Two types of nanoparticles, aluminum oxide and zinc oxide, were selected to manifest the effect of surface chemistry and shape differences. Three particle volume fractions were used to determine the effect of percent loading. Additionally, two particle sizes of aluminum oxide and three particle sizes of zinc oxide were chosen to study to effect of particle size on the properties of polymer nanocomposites.

Another portion of this thesis contributes to the study of immiscible polymer blends. The microstructure of such blends has effect on the final properties of the composites.

The results of mechanical behavior, particularly impact resistance and tensile modulus of uncompatibilized immiscible polymer blends of this part are summarized and the complete detail about this system is attached.

## References

1. J. L. Thomason and M. A. Vlugs, Influence of fibre length and concentration on the properties of glass fibre-reinforced polypropylene: 1. Tensile and flexural modulus, *Composites: Part A* 27A (1996), 477-484.
2. W. Viratyaporn, N. Twu and R. Lehman, Fiber reinforced multiphase polymer composites by in situ fiber alignment, *Mater. Res. Soc. Symp. Proc.*, 2008.
3. R. W. Siegel, S. K. Chang, B. J. Ash, J. Stone, P. M. Ajayan, R. W. Doremus and L. S. Schadler, Mechanical behavior of polymer and ceramic matrix nanocomposites, *Scripta materialia* 44 (2001), 2061–2064.
4. E. T. Thostenson, C. Li and T.-W. Chou, Nanocomposites in context, *Composites Science and Technology* 65 (2005), 491–516.
5. A. Choudhury, A. K. Bhowmick and C. Ong, Novel role of polymer–solvent and clay–solvent interaction parameters on the thermal, mechanical and optical properties of polymer nanocomposites, *Polymer* 50 (2009), 201-210.
6. J.-Y. Lee, Q. Zhang, T. Emrick and A. J. Crosby, Nanoparticle alignment and repulsion during failure of glassy polymer nanocomposites, *Macromolecules* 39 (2006), 7392-7396.
7. A. J. Crosby and J.-Y. Lee, Polymer nanocomposites: The “nano” effect on mechanical properties, *Polymer Reviews* 47 (2007), 217-229.
8. R. P. Singh, M. Zhang and D. Chan, Toughening of a brittle thermosetting polymer: Effects of reinforcement particle size and volume fraction, *J. Mater. Sci.* 37 (2002), 781-788.
9. X. L. Ji, J. K. Jing, W. Jiang and B. Z. Jiang, Tensile modulus of polymer nanocomposites, *Polymer Engineering and Science* 42 (2002), 983-993.
10. W.-J. Boo, L. Sun, G. L. Warren, E. Moghbelli, H. Pham, A. Clearfield and H.-J. Sue, Effect of nanoplatelet aspect ratio on mechanical properties of epoxy nanocomposites, *Polymer* 48 (2007), 1075-1082.
11. W. Viratyaporn and R. L. Lehman, Impact resistance and raman characterization of Al<sub>2</sub>O<sub>3</sub>/ZnO poly(methyl methacrylate) nanocomposites, *ANTEC* 2009, 2009.
12. A. C. Balazs, T. Emrick and T. P. Russell, Nanoparticle polymer composites: Where two small worlds meet, *Science* 314 (2006), 1107-1110.

13. A. Usuki, Y. Kojima, M. Kawasumi, A. Okada, Y. Fukushima, T. Kurauchi and O. Kamigaito, Synthesis of nylon 6-clay hybrid, *J. Mater. Res.* 8 (1993), 1179-1184.
14. Y. Kojima, A. Usuki, M. Kawasumi, A. Okada, Y. Fukushima, T. Kurauchi and O. Kamigaito, Mechanical properties of nylon 6-clay hybrid, *J. Mater. Res.* 8 (1993), 1185-1189.
15. L. Schadler, "Polymer-based and polymer-filled nanocomposites," *Nanocomposite science and technology*, Wiley, 2003, pp. 77-153.
16. E. Tang, G. Cheng and X. Ma, Preparation of nano-ZnO/PMMA composite particles via grafting of the copolymer onto the surface of zinc oxide nanoparticles, *Powder Technology* 161 (2006), 209-214.
17. J. W. Gilman, C. L. Jackson, A. B. Morgan and J. Richard Harris, Flammability properties of polymer-layered-silicate nanocomposites. Polypropylene and polystyrene nanocomposites, *Chemistry of Materials* 12 (2000), 1866-1873.
18. J. Wang, J. Du, J. Zhu and C. A. Wilkie, An XPS study of the thermal degradation and flame retardant mechanism of polystyrene-clay nanocomposites, *Polymer Degradation and Stability* 77 (2002), 249-252.
19. J. Zhu, F. M. Uhl, A. B. Morgan and C. A. Wilkie, Studies on the mechanism by which the formation of nanocomposites enhances thermal stability, *Chemistry of Materials* 13 (2001), 4649-4654.
20. H. Wang, S. Meng, P. Xu, W. Zhong and Q. Du, Effect of traces of inorganic content on thermal stability of poly(methyl methacrylate) nanocomposites, *Polymer Engineering and Science* 47 (2007), 302-307.
21. Y. Li, B. Zhao, S. Xie and S. Zhang, Synthesis and properties of poly(methyl methacrylate)/montmorillonite (PMMA/MMT) nanocomposites, *Polymer International* 52 (2003), 892-898.
22. A. Laachachia, M. Cochez, M. Ferriola, J. M. Lopez-Cuestab and E. Leroy, Influence of  $\text{TiO}_2$  and  $\text{Fe}_2\text{O}_3$  fillers on the thermal properties of poly(methyl methacrylate) (pmma), *Materials Letters* 59 (2005), 36-39.
23. M. M. Demir, M. Memesa, P. Castignolles and G. Wegner, PMMA/zinc oxide nanocomposites prepared by in-situ bulk polymerization, *Macromol. Rapid Commun.* 27 (2006), 763-770.
24. C. Dong and X. Ni, The photopolymerization and characterization of methyl methacrylate initiated by nanosized titanium dioxide, *Journal of Macromolecular Science Part A—Pure and Applied Chemistry* A41 (2004), 547-563.

25. K. Liao and S. Li, Interfacial characteristics of a carbon nanotube–polystyrene composite system, *APPLIED PHYSICS LETTERS* 79 (2001), 4225-4227.
26. M. Du, B. Guo, Y. Lei, M. Liu and D. Jia, Carboxylated butadiene–styrene rubber/halloysite nanotube nanocomposites: Interfacial interaction and performance, *Polymer* 49 (2008), 4871-4876.
27. W. Zhou, B. Wang, Y. Zheng, Y. Zhu, J. Wang and N. Qi, Effect of surface decoration of CNTs on the interfacial interaction and microstructure of epoxy/MWNT nanocomposites, *ChemPhysChem* 9 (2008), 1046 – 1052.
28. A. Durmus, A. Kasgoz and C. W. Macosko, Mechanical properties of linear low-density polyethylene (LLDPE)/clay nanocomposites: Estimation of aspect ratio and interfacial strength by composite models, *Journal of Macromolecular Science, Part B: Physics* 47 (2008), 608–619.
29. G. Sui, W. H. Zhongb, X. P. Yang and Y. H. Yu, Curing kinetics and mechanical behavior of natural rubber reinforced with pretreated carbon nanotubes, *Materials Science and Engineering A* 485 (2008), 524–531.
30. J. H. Koo, *Polymer nanocomposites: Processing, characterization, and applications*, McGraw-Hill, New York, 2006.
31. Y. Grohens, M. Brogly, C. Labbe and J. Schultz, Interfacial conformation energies of stereoregular poly(methyl methacrylate) by infra-red reflection absorption spectroscopy, *Polymer* 38 (1997), 5913-5920.
32. P. Carriere, Y. Grohens, J. Spevacek and J. Schultz, Stereospecificity in the adsorption of tactic PMMA on silica, *Langmuir* 16 (2000), 5051-5053.
33. D. Ciprari, K. Jacob and R. Tannenbaum, Characterization of polymer nanocomposite interphase and its impact on mechanical properties, *Macromolecules* 39 (2006), 6565-6573.
34. H. Fischer, *Polymer nanocomposites: From fundamental research to specific applications*, *Mater. Sci. Eng. C* 23 (2003), 763–772.
35. W. Bacsa, "Who discovered carbon nanotubes? - all you need to know about the discovery of carbon nanotubes.," 2006.
36. P. M. Ajayan and T. W. Ebbesen, Nanometre-size tubes of carbon, *Rep. Prog. Phys.* 60 (1997), 1025-1062.
37. S. Iijima and T. Ichihashi, Singlw-shell carbon nanotubes of 1-nm diameter, *Nature* 363 (1993), 603-605.

38. D. S. Bethune, C. H. Klang, M. S. d. Vries, G. Gorman, R. Savoy, J. Vazquez and R. Beyers, Cobalt-catalysed growth of carbon nanotubes with single-atomic-layer walls, *Nature* 363 (1993), 605-607.
39. "[Http://www.Absoluteastronomy.Com/topics/carbon\\_nanotube](http://www.Absoluteastronomy.Com/topics/carbon_nanotube)."
40. "[Http://coecs.Ou.Edu/brian.P.Grady/nanotube.Html](http://coecs.Ou.Edu/brian.P.Grady/nanotube.Html)."
41. P. S. Santos, H. S. Santos and S. P. Toledo, Standard transition aluminas. Electron microscopy studies, *Materials Research* 3 (2000), 104-114.
42. F. R. Feret, D. Roy and C. Boulanger, Determination of alpha and beta alumina in ceramic alumina by x-ray diffraction, *Spectrochimica Acta Part B* 55 (2000), 1051-1061.
43. M. Trueba and S. P. Trasatti, G-alumina as a support for catalysts: A review of fundamental aspects, *Eur. J. Inorg. Chem.* 2005 (2005), 3393-3403.
44. J. M. McHale, A. Auroux, A. J. Perrotta and A. Navrotsky, Surface energies and thermodynamic phase stability in nanocrystalline aluminas, *Science* 277 (1997), 788-791.
45. G. Groppi, F. Assandri, M. Bellotto, C. Cristiani and P. Foraztti, The crystal structure of Ba- $\beta$ -alumina materials for high-temperature catalytic combustion, *J. Solid State Chemistry* 114 (1995), 326-336.
46. A. C. Sutorik, S. S. Neo, D. R. Treadwell and R. M. Laine, Synthesis of ultrafine  $\beta$ "-alumina powders via flame spray pyrolysis of polymeric precursors, *J. Am. Ceram. Soc.* 81 (1998), 1477-1486.
47. T. Kashiwagi, A. Inaba, J. E. Brown, K. Hatada, T. Kitayama and E. Masuda, Effects of weak linkages on the thermal and oxidative degradation of poly(methyl methacrylates), *Macromolecules* 19 (1986), 2160-2168.
48. L. E. Manring, Thermal degradation of saturated poly(methyl methacrylate), *Macromolecules* 21 (1988), 528-530.
49. L. E. Manring, D. Y. Sogah and G. M. Cohen, Thermal degradation of poly(methyl methacrylate). 3. Polymer with head-to-head linkages, *Macromolecules* 22 (1989), 4652-4654.
50. L. E. Manring, Thermal degradation of poly(methyl methacrylate). 2. Vinyl-terminated polymer, *Macromolecules* 22 (1989), 2673-2677.



51. T. Kashiwagi, A. Inabil and A. Hamins, Behavior of primary radicals during thermal degradation of poly(methyl methacrylate), *Polymer Degradation and Stability* 26 (1989), 161-184.
52. L. E. Manring, Thermal degradation of poly(methyl methacrylate). 4. Random side-group scission, *Macromolecules* 24 (1991), 3304-3309.
53. J. M. Dominguez, J. L. Hernandez and G. Sandoval, Surface and catalytic properties of  $\text{Al}_2\text{O}_3\text{-ZrO}_2$  solid solutions prepared by sol-gel methods, *Applied Catalysis A: General* 197 (2000), 119-130.
54. B. Xing, Natural organic material characteristics affect the environmental behavior of manufactured nanoparticles, *Assessment of the Biological Effects of Nanomaterials Symposium*, 2009.
55. O. A. Fouad, A. A. Ismail, Z. I. Zaki and R. M. Mohamed, Zinc oxide thin films prepared by thermal evaporation deposition and its photocatalytic activity, *Applied Catalysis B: Environmental* 62 (2006), 144-149.
56. M. Mrowetz and E. Selli, Photocatalytic degradation of formic and benzoic acids and hydrogen peroxide evolution in  $\text{TiO}_2$  and  $\text{ZnO}$  water suspensions, *Journal of Photochemistry and Photobiology A: Chemistry* 180 (2006).
57. B. Railsback, "Some fundamentals of mineralogy and geochemistry."
58. B. J. Fontana, The configuration of an adsorbed polymeric dispersant by infrared studies, *J. Phys. Chem.* 67 (1963), 2360-2362.
59. B. J. Ash, J. Stone, D. F. Rogers, L. S. Schadler, R. W. Siegel, B. C. Benicewicz and T. Apple, Investigation into the thermal and mechanical behavior of PMMA/alumina nanocomposites, *Mat. Res. Soc. Symp. Proc.* 661 (2001), KK2.10.11.
60. T. Sato and R. Ruch, *Stabilization of colloidal dispersions by polymer adsorption*, vol. 9, Marcel Dekker, New York, 1980.
61. K. Konstadinidis, B. Thakkar, A. Chakraborty, L. W. Potts, R. Tannenbaum and M. Tirrell, Segment level chemistry and chain conformation in the reactive adsorption of poly(methyl methacrylate) on aluminum oxide surfaces, *Langmuir* 8 (1992), 1307-1317.
62. R. F. Colletti, H. S. Gold and C. Dybowski, Characterization of the adsorption of poly(acrylamide), poly(4-methoxystyrene), and poly(acrylic acid) on aluminum oxide by inelastic tunneling spectroscopy, *Appl. Spectrosc.* 41 (1987).

63. Y. Grohens, J. Schultz and R. E. Prud'homme, PMMA conformational changes on  $\gamma$ -alumina powder: Influence of the polymer tacticity on the configuration of the adsorbed layer, *Int. J. Adhesion and Adhesives* 17 (1997), 163-167.
64. N. Cinausero, N. Azema, M. Cochez, M. Ferriol, M. Essahli, F. o. Ganachaud and J.-M. Lopez-Cuesta, Influence of the surface modification of alumina nanoparticles on the thermal stability and fire reaction of PMMA composites, *POLYMERS FOR ADVANCED TECHNOLOGIES* 19 (2008), 701–709.
65. S. Kulkeratiyut, S. Kulkeratiyut and F. D. Blum, Bound carbonyls in PMMA adsorbed on silica using transmission FTIR, *Journal of Polymer Science Part B: Polymer Physics* 44 (2006), no. 15, 2071-2078.
66. J. Wang and X. Ni, Interfacial structure of poly(methyl methacrylate)/TiO<sub>2</sub> nanocomposites prepared through photocatalytic polymerization, *J. Appl. Polym. Sci.* 108 (2008), 3552–3558.
67. M. Vacatello and P. J. Flory, Conformational statistics of poly(methyl methacrylate), *Macromolecules* 19 (1986), 405-415.
68. S. N. Sathe, S. Devi, G. S. S. Rao and K. V. Rao, Relationship between morphology and mechanical properties of binary and compatibilized ternary blends of polypropylene and nylon 6, *Journal of Applied Polymer Science* 61 (1996), no. 1, 97-107.
69. S. C. Tjong and S. A. Xu, Impact and tensile properties of SEBS copolymer compatibilized PS/HDPE blends, *Journal of Applied Polymer Science* 68 (1998), no. 7, 1099-1108.
70. M. A. Debolt and R. E. Robertson, Impact strength and elongation-to-break of compatibilized ternary blends of polypropylene, nylon 66, and polystyrene, *Polym. Eng. Sci.* 44 (2004), 1800–1809.
71. T.-K. Kang, Y. Kim, W.-K. Lee, H.-D. Park, W.-J. Cho and C.-S. Ha, Properties of uncompatibilized and compatibilized poly(butylene terephthalate)-LLDPE blends, *Journal of Applied Polymer Science* 72 (1999), no. 8, 989-997.
72. J. Joshi, R. L. Lehman and T. J. Nosker, Mechanical grafting and morphology characterization in immiscible polymer blends, *MRS*, 2004.
73. J. Joshi, R. Lehman and T. Nosker, Selected physical characteristics of polystyrene/high density polyethylene composites prepared from virgin and recycled materials, *Journal of Applied Polymer Science* 99 (2006), no. 5, 2044-2051.

74. A. Leclair and B. D. Favis, The role of interfacial contact in immiscible binary polymer blends and its influence on mechanical properties, *Polymer* (1996), 4723-4728.
75. W. Viratyaporn, R. L. Lehman and J. Joshi, Impact resistance of selected immiscible polymer blends, *ANTEC*, 2007, 1854-1858.

## Chapter 3 Polymer nanocomposites: Processing

### 3.1 Materials

Poly(methyl methacrylate), PMMA, was purchased from Polysciences, Inc. (Warrington, PA) as micro bead having the dimension of 200 micrometer with the molecular weight ( $M_w$ ) of 75000. The stabilized methyl methacrylate, MMA, was purchased from Acros Organics (Morris Plains, NJ). The density for both PMMA and MMA are  $1.19 \text{ g/cm}^3$  and  $0.93 \text{ g/cm}^3$  respectively. Azobis isobutyronitrile (AIBN) was chosen as the initiator in this work. Nanoparticles were purchased from Nanophase Technologies (Romeoville, IL) as pre-dispersed and dry powder forms. The dispersing solvent was propylene glycol monomethyl ether acetate (PGMEA or PMA). Two types of nanoparticles were chosen and further details are listed in the Table 3.1.

**Table 3.1** Purchased Nanoparticles Information.

Trade Name	Type	v/o in PGMEA	d*	Morphology
NanoTek® Aluminum oxide (dry powder)	$\text{Al}_2\text{O}_3$	-	45	Sphere
NanoArc® R1130PMA	$\text{Al}_2\text{O}_3$	10.35	20	Sphere
NanoDur® X1130PMA	$\text{Al}_2\text{O}_3$	21.23	45	Sphere
NanoArc® Q1102PMA	ZnO	10.35	20	Elongated
NanoTek® ZH1102PMA	ZnO	10.35	35	Elongated
NanoTek® Z1102PMA	ZnO	14.76	70	Elongated

\*Mean particle size

Since the PGMEA is bonded to the nanoparticles, albeit via weak secondary bonds, the particles are subsequently referred as functionalized and use the nomenclature FG-nanoparticles henceforth.

### **3.2 In-situ Polymerization of PMMA/nanocomposites**

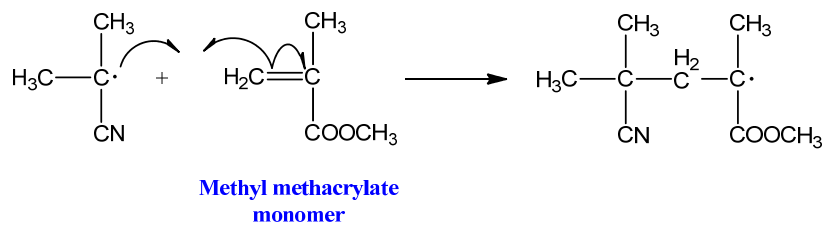
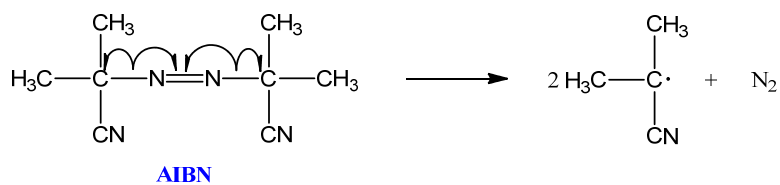
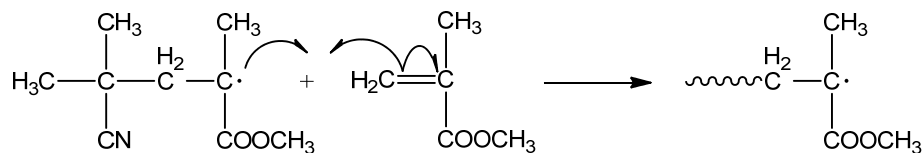
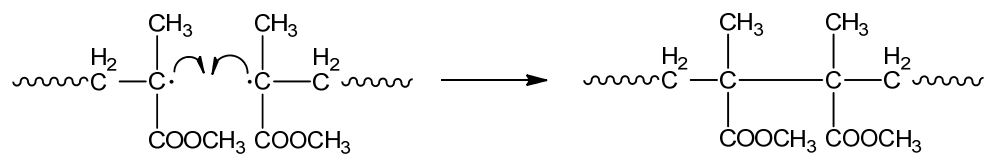
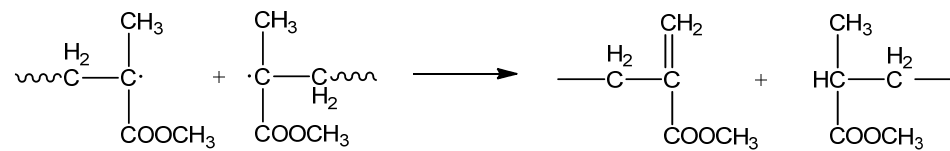
First MMA monomer was purified by passing through a column packed with aluminum oxide to remove the inhibitor by adsorption. A PMMA syrup was prepared by combining PMMA beads (15 vol%) with purified MMA (85 vol%) and stirring for 24 h at room temperature. The oxide nanoparticles were dispersed in the syrup by ultrasonication (420 kJ, 20 min at 350 Watts) followed by the addition of AIBN (1 wt%) with magnetic stirrer for 5 minutes. Subsequently, the mixture was degassed under mechanical vacuum for 5 minutes. Sheet molds, prepared from two glass plates sealed with window spacing tape was filled with the degassed mixture and placed into an isothermal water bath at 50 °C for 24 h to polymerize the composite and to develop initial strength. A final stage of polymerization was conducted at 95 °C for 1 h. Each type of nanoparticles was varied with three concentrations. Detailed quantities of the polymer nanocomposites are listed in Table 3.2.

**Table 3.2** Polymer Nanocomposites Compositions.

<b>Systems</b>	<b>Compositions</b>		
	<b>Particle (v/o)</b>	<b>PMMA (v/o)</b>	<b>PGMEA (v/o)</b>
<b>PMMA</b>	0	100	0
<b>PMMA/PGMEA</b>	0	99	1
	0	97	3
	0	95	5
	0	93	7
<b>PMMA/Al<sub>2</sub>O<sub>3</sub> (Dry powder, 45 nm)</b>	1	99	0
<b>PMMA/FG-Al<sub>2</sub>O<sub>3</sub> (20 nm)</b>	0.49	95.25	4.26
	0.94	90.90	8.16
	1.36	86.88	11.76
<b>PMMA/FG-Al<sub>2</sub>O<sub>3</sub> (45 nm)</b>	0.50	97.63	1.87
	0.99	95.34	3.67
	1.46	93.14	5.40
<b>PMMA/FG-ZnO (20 nm)</b>	0.48	95.37	4.15
	0.92	91.11	7.97
	1.33	87.17	11.50
<b>PMMA/FG-ZnO (35 nm)</b>	0.48	95.37	4.15
	0.92	91.11	7.97
	1.33	87.17	11.50
<b>PMMA/FG-ZnO (70 nm)</b>	0.49	96.70	2.81
	0.95	93.59	5.46
	1.38	90.65	7.97

### 3.2.1 Polymerization mechanism of poly(methyl methacrylate)

Polymerization is a process used to connect monomer molecules to form long polymer chains. The polymerization process of a polymer consists of three steps: initiation, propagation, and termination. First, initiator decomposes in half and reacts with a monomer molecule to create an active species. Then, the activated monomer reacts with another monomer to generate the propagating species. With the continuous addition of monomer, the process results in long polymer chains with the active species at the propagating end. When the active site is neutralized, the propagating chain will stop growing. This last step is known as termination step which may result from one of two different mechanisms depending on the stability of the propagating radicals. In the case of well stabilized radicals, termination by the combination process is preferred where two propagating chains combine to create one long chain with Head-to-Head (H-H) configuration at the linkage. Another is terminated by proton transfer known as the disproportionation process, which results in two polymer chains: saturated and unsaturated chain end. Both H-H linkage and vinylidene end groups are considered as defects in the polymer chain and have an influence on the properties of polymer. The mechanism of free radical polymerization of poly(methyl methacrylate) is shown below.

**Initiation step:****Propagation step:****Termination step:****Combination:****Disproportionation:**



### **3.3 Testing and characterization**

#### **3.3.1 Mechanical testing**

##### **3.3.1.1 Tensile testing**

Tensile testing was performed according to ASTM D638-03 with Universal Testing Machine (QTest/25) from MTS. Due to the limited size of the fabricated composite sheets, type V dumbbell specimens were selected for this test. However, the small gage length of type V specimens did not permit use of the extensometer available in our laboratory. Therefore, for tensile modulus, the specimens were machined into rectangular bars with the dimension 63 x 12.5 x 3.1 mm, which enabled the extensometer to be used in the tensile modulus measurement. The test was performed with speed of 1 mm/min at room temperature.

##### **3.3.1.2 Impact testing**

Impact testing was performed according to the Izod impact procedure (ASTM D-256A) with an instrumented pendulum impact machine (Instron POE2000). The impact specimens were machine cut to the dimension of the Izod specimens, 63 x 12.5 x 3.1 mm. Six specimens were tested for each composition. All specimens were notched at a 45 degree angle notch tip to eliminate crack initiation energy. The test was performed at room temperature with the test speed of 3.5 m/s.

### **3.3.2 Thermal analysis**

#### **3.3.2.1 Differential Scanning Calorimetry (DSC)**

The glass transition of PMMA/particulate nanocomposites was characterized by modulated DSC (Q1000 from TA Instrument, Delaware). Samples of approximately 10 mg were cut from the polymerized sheet and sealed in aluminum pans. DSC runs, heat-cool-modulated heat, were conducted over the temperature range of 30-180°C with the modulated heat of  $\pm 1.300$  °C every 40 seconds. The system was purged with nitrogen gas at flow rate of 50 ml/min.

#### **3.3.2.2 Thermal Gravimetric Analysis (TGA)**

Thermal stability of the composites was determined by thermal gravimetric analysis (TGA) under flowing N<sub>2</sub> atmosphere (20 ml/min) and a heating rate of 10 °C/min. The test was performed on the TGA 7 from Perkin-Elmer. The PGMEA-stabilized nanoparticles were measured as-is without any previous drying process to avoid errors from the volatilization of PGMEA. The temperature range was 20-700 °C. For the polymer-inorganic nanocomposites, the sample was cut from the sheet and run at the temperature range of 25-600 °C.

### **3.3.3 Characterization techniques**

#### **3.3.3.1 Image analysis**

Field emission scanning electron microscopy (Leo-Zeiss Gemini 982 and Sigma-Zeiss) was used to observe the fractured surface (cold fractured, tensile fractured, and impact fractured surfaces) of samples as well as nanoparticles themselves. The fractured samples were mounted on an SEM stud and vacuum degassed overnight followed by either gold or chromium coated (Gatan model 681-High resolution ion beam coater) prior to performing on the FESEM to eliminate out-gassing materials. In the case of nanoparticles, a drop of pre-dispersed nanoparticles was put on a stud and vacuum dry overnight before perform gold coating.

#### **3.3.3.2 Infrared spectroscopy**

Infrared spectra were collected by diamond crystal ATR-FTIR from Bruker. Each spectrum was scanned on average of 100 scans with scan resolution of 4  $\text{cm}^{-1}$ . All spectra were analyzed with KnowItAll software from BioRad. For analysis of pre-dispersed nanoparticles, the excess PGMEA was first eliminated. The pre-dispersed particles were weight into aluminum pan and dried under isothermal vacuum at 50 °C for at least 19 h.

#### **3.3.3.3 Raman spectroscopy**

In this study, Raman shift spectra were collected with inVia Raman microscope in the 200-3200  $\text{cm}^{-1}$ . The excitation wavelength was 785 nm and magnification was 50x

resulting approximately 1  $\mu\text{m}$  of beam diameter on the sample surface. A grating beam path of 1200 l/mm was used. Each spectrum accumulation was replicated 16 times and averaged to enhance accuracy and increase signal-to-noise ratio. Subsequently, data were analyzed with Wire2 (SP9), software supplied by Renishaw. Due to the constant in peak intensity and position, the symmetric stretching of CC4 (813  $\text{cm}^{-1}$ ) was chosen to perform in normalization process. Peak deconvolution was performed by Wire 2 software provided by Renishaw, (Gloucestershire, United Kingdom). To ensure the reproducibility, three specimens were analyzed for each composition. The deconvoluted peaks, then, were performed statistic analysis by the use of analysis of variance (ANOVA) to increase confidentiality in spectra analysis. Complete Raman assignments and the detail of ANOVA can be found in Appendix A.

## **Chapter 4 Mechanical behavior of polymer nanocomposites**

Impact strength and elastic modulus are two critical properties in many engineering design applications. Most structural designs rely heavily on material stiffness to provide the desired properties to the structure. Lightweight, ease of processing, and low cost are the reasons why polymeric materials are potential candidates in numerous applications. Polymeric materials are hardly used as-is particularly in high-end applications such as mechanical bearing, capacitors, and aircraft windshields because of their poor mechanical behavior. The addition of nanoparticles into polymer matrix has been reported to alter the mechanical behavior of neat polymer.<sup>[1, 2, 3, 4]</sup> For example, with the incorporation of nano-CaCO<sub>3</sub> into polypropylene, the elastic modulus was increased by 85%.<sup>[5]</sup> Such improvements were related to the nanometer scale of the fillers which increase the interacting surface between polymer matrix and the particles. The studies showed that properties of polymer composites are altered not only by the size of the fillers but also particle geometry.<sup>[6, 7, 8]</sup> With the variation of aspect ratio of zirconium phosphate in epoxy matrix, the higher aspect ratio of the fillers deflected crack more efficiently which provide to better property enhancement.<sup>[8]</sup>

In this Chapter, tensile and impact behavior of poly(methyl methacrylate) with the addition of nanoparticles are discussed. Effects of size, shape, and volume fraction of nanoparticles are as well determined.

#### **4.1 Tensile properties of PMMA/metal oxide nanocomposites**

Young's modulus in amorphous polymers is a composite of the very high stiffness of the polymer backbone combined with a geometric factor associated with the degree of orientation and entanglement of the molecular chain. Nanoparticles of inorganic materials have radically different chemistry from polymers and consequently, uncompatibilized systems often result when they are mixed due to poor bonding at the interface. In such systems a reduction in tensile modulus is often observed. However, in some systems, coupling agents are used to link the chemistry of the polymer to the chemistry of the filler. Silane based coupling agents used in fiber glass reinforced polyester composites are a good example.

Proper dispersion of nanoparticles in polymer matrices is a key for optimization of composite properties. If reinforcement particles are aggregated in clumps, good properties will not result. In this work, I sought to avoid particle agglomeration by obtaining nanoparticles predispersed in a suitable medium. A limited number of commercially available nanoparticles are available. By combining the requirements of suitable oxide nanoparticles of appropriate size and a dispersion vehicle of suitable compatibility with PMMA, zinc and aluminum oxide nanoparticles predispersed in PGMEA were used. Naturally, some amount of PGMEA is present in all the composites prepared from these predispersed nanoparticles and the PGMEA could have a significant effect itself in altering the properties of the composite, e.g. as a plasticizer to reduce stiffness. To determine the extent of any effect caused by PGMEA, the mechanical

behavior of PMMA/PGMEA composites at various volume fractions of PGMEA was first examined. Result in Figure 4.1 shows that PGMEA, at the 0.7 volume percent level, has a slight, barely significant, effect on tensile modulus of the neat PMMA, and no measureable effect on the impact resistance.

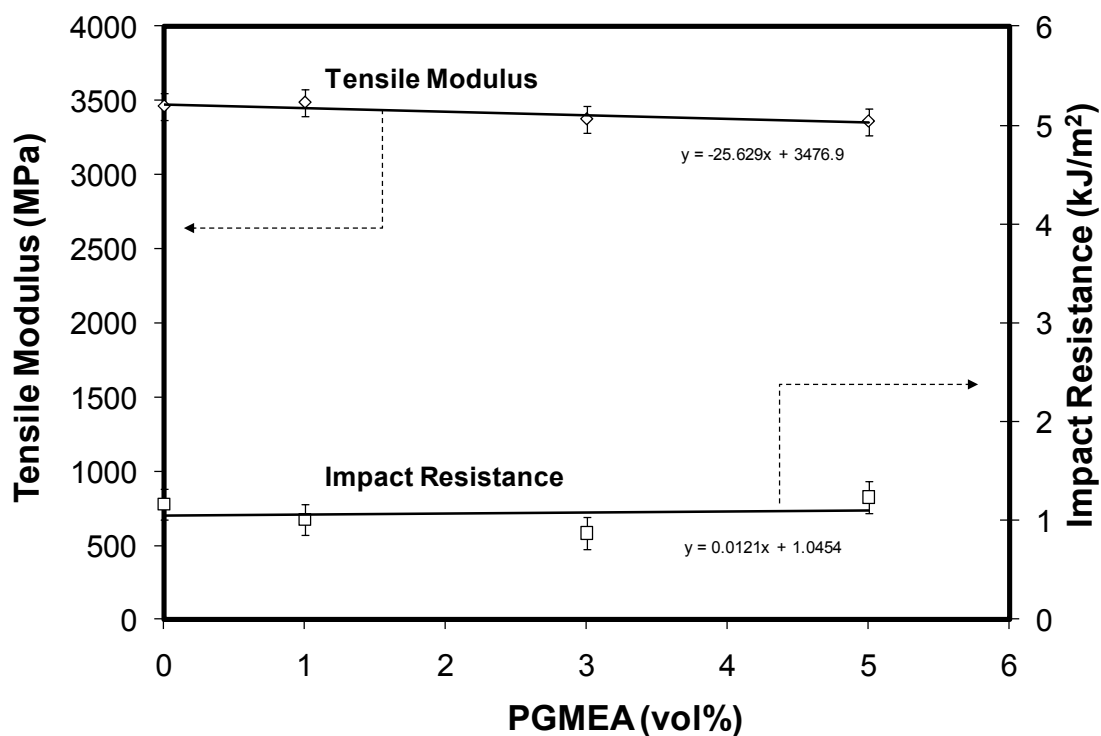


**Figure 4.1** Tensile modulus and impact resistance of PMMA/PGMEA at various volume fractions of PGMEA.

The tensile modulus of polymer nanocomposites is illustrated in Figure 4.2 and 4.3 for systems composed with  $\text{Al}_2\text{O}_3$  and  $\text{ZnO}$ , respectively. Differences in behavior between PMMA/dry nanoparticles and PMMA/FG-nanoparticles were observed. The first system in which dry  $\text{Al}_2\text{O}_3$  powder was dispersed in PMMA syrup, quite good results were obtained. The modulus increases slightly, although not significantly, as the volume fraction of  $\text{Al}_2\text{O}_3$  increases. Besides the good dispersion of nanoparticles (Figure 4.8), load transfer through interfacial adhesion might also contribute to this improvement. The interfacial interaction will be detailed in Chapter 6. In all systems composed with FG-nanoparticles, tensile modulus of the composites is lower compared to the neat PMMA. At 1.0 v/o of FG- $\text{Al}_2\text{O}_3$  addition, the tensile modulus decreases by -25.85% and -15.43% with the particle size of 20 nm and 45 nm, respectively. A similar trend is also observed in the PMMA/FG- $\text{ZnO}$  systems with the modulus reduction of -28.49%, -25.73%, and -19.36% for 20, 35, and 70 nm, respectively. The non-bonded interface or weak interfacial interactions between nanoparticle surface and polymer chain enhances total free volume in the composite systems. As a result, the reduction of tensile modulus is expected.



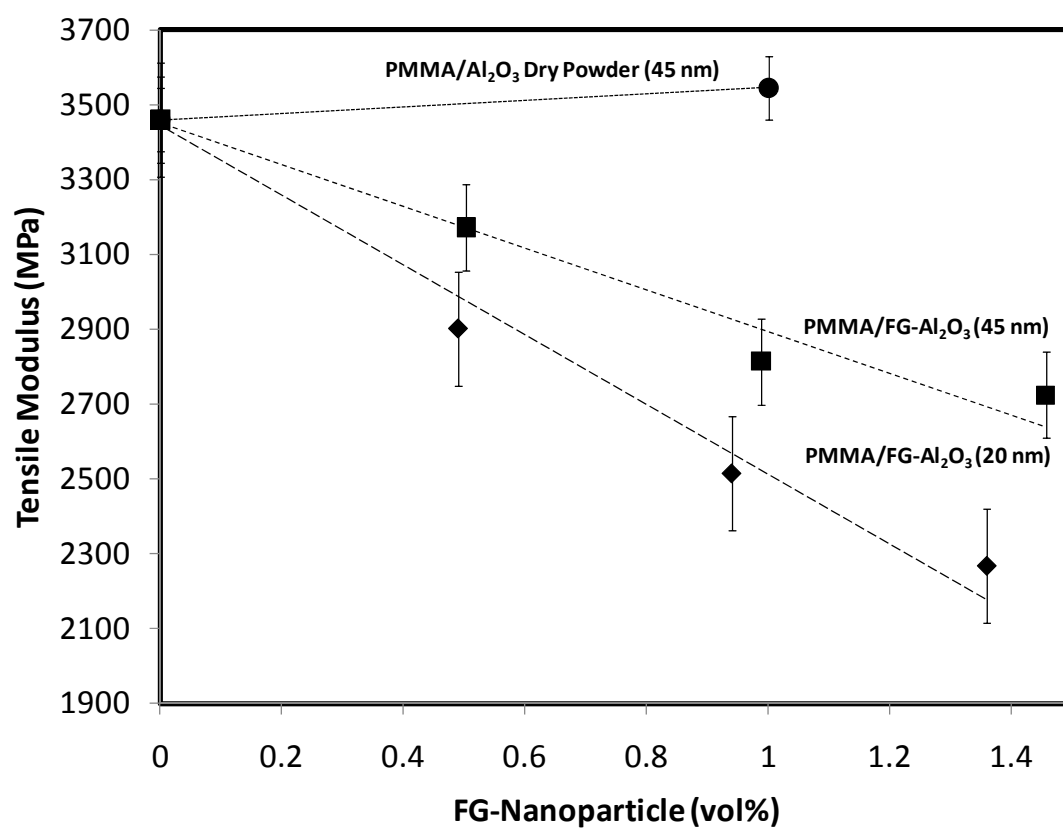


**Figure 4.2** Tensile modulus of PMMA/aluminum oxide nanocomposites at various particle size, shape, and volume fractions.

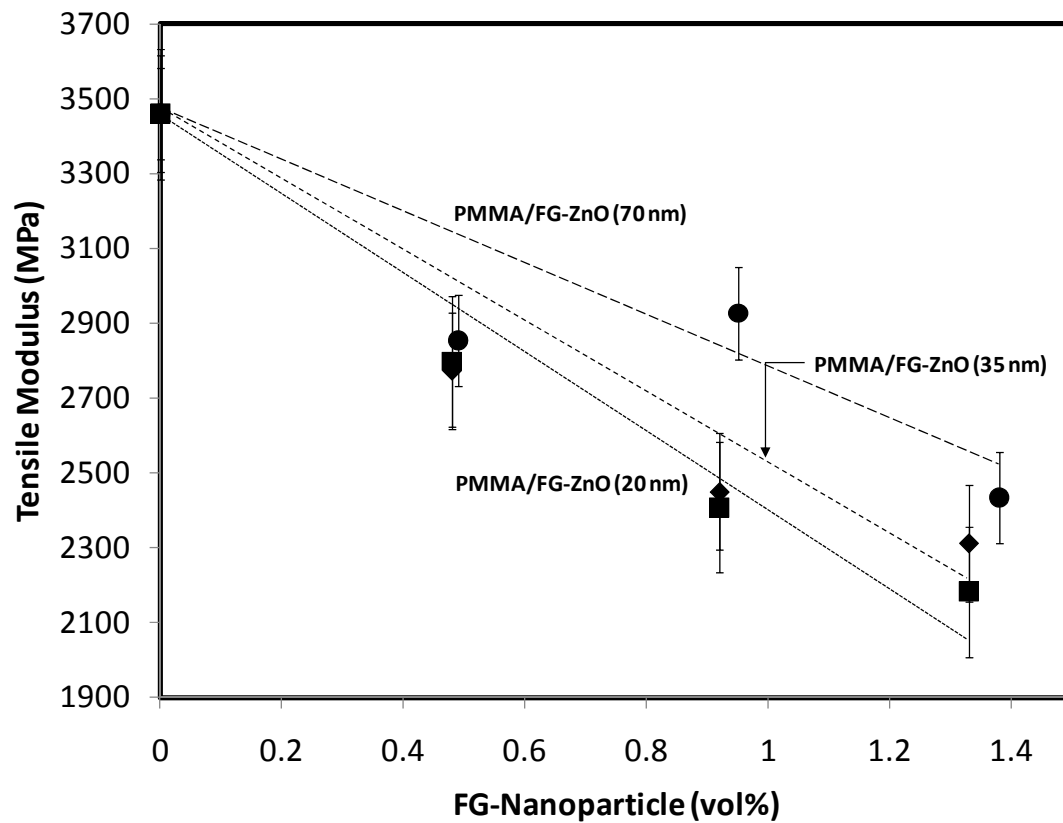


**Figure 4.3** Tensile modulus of PMMA/zinc oxide nanocomposites at various particle size, shape, and volume fractions.

The comparison between the effect of PGMEA molecules and FG-nanoparticles on tensile modulus of the composites was shown in the Figure 4.4. The result reveals that the addition of PGMEA decreases the modulus of composites by some extent. However, the main contribution of the tensile reduction is obviously caused by the nanoparticles.

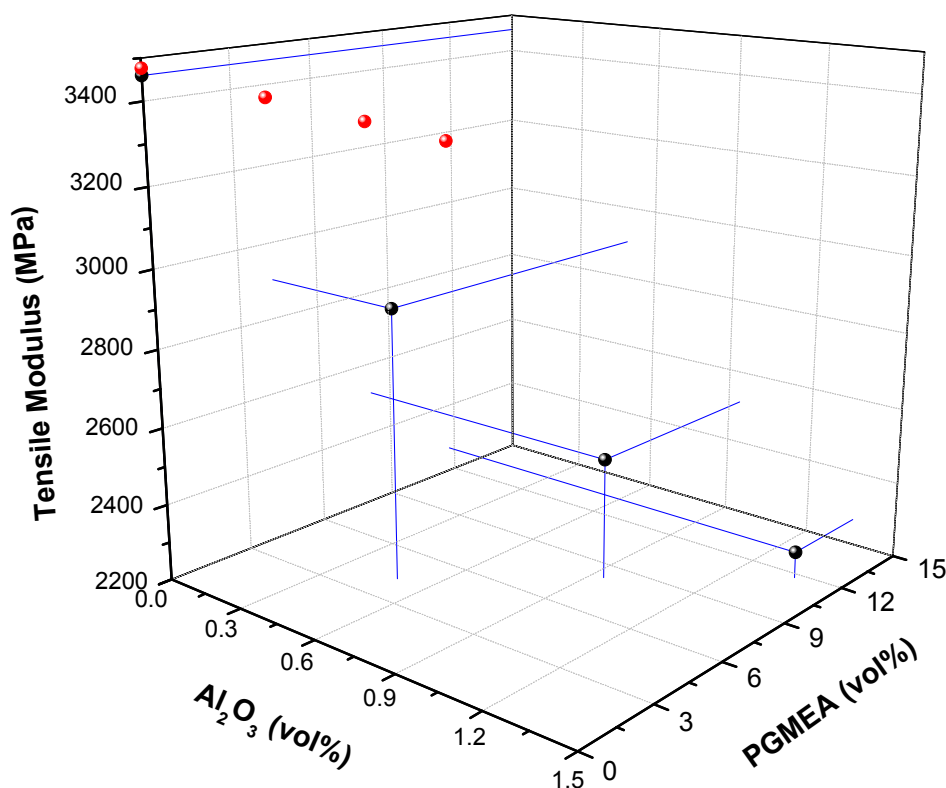


**Figure 4.4** Comparison of tensile modulus in PMMA/PGMEA composites (red dot) and PMMA/ $\text{Al}_2\text{O}_3$  (20 nm) nanocomposites (black dot).

As materials become softer evidenced by the drop in tensile modulus in filled-PMMA nanocomposites (Figure 4.2 and 4.3), the materials will have the higher ability to absorb and dissipate energy throughout the composites. The area under load-

displacement curve of tensile testing relates to amount of work use to break the material which equivalent to the total energy that material absorbs during deformation. The example of load-displacement curve is illustrated in Figure 4.5. The higher displacement of PMMA/FG- $\text{Al}_2\text{O}_3$  (0.5 v/o, 20 nm) is equivalent to the increment of approximately 386 %strain over the neat PMMA.

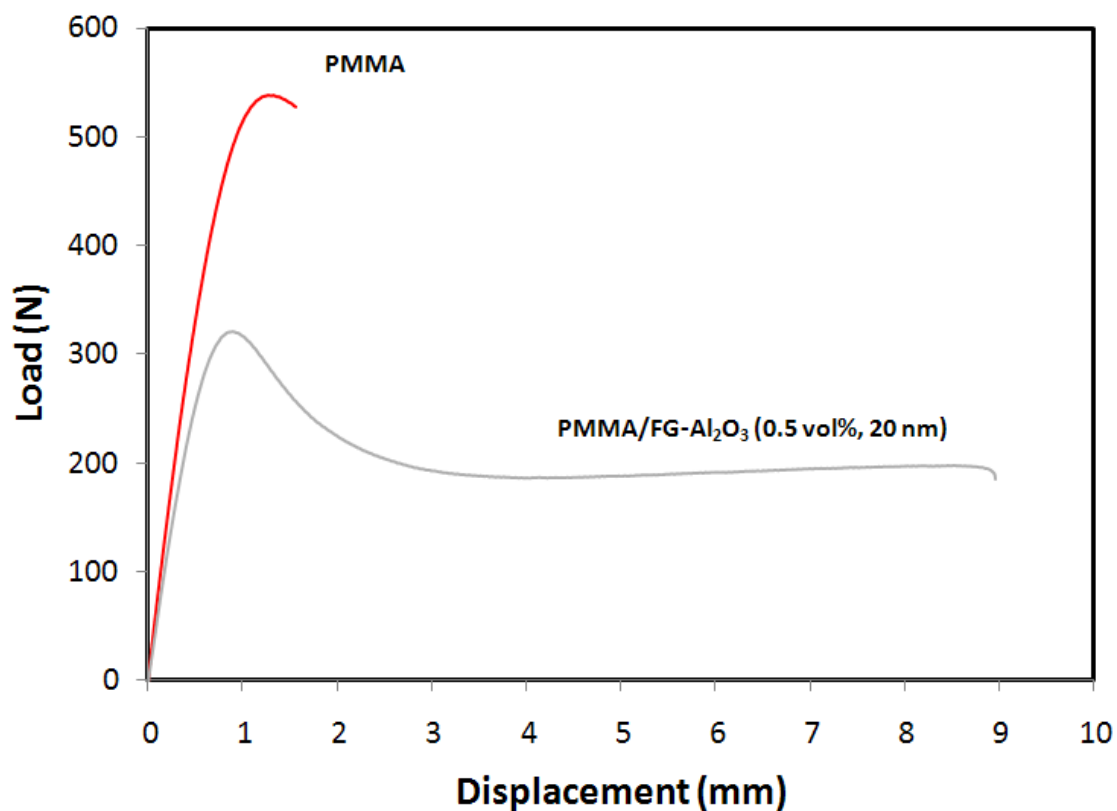


**Figure 4.5** Load-displacement curve comparison: PMMA (red) and PMMA/FG- $\text{Al}_2\text{O}_3$  (0.5 vol%, 20 nm) (grey).

A typical technique to determine toughness of material is the area integration which is defined as work of fracture (WOF). Figures 4.6 and 4.7 show work of fracture of

PMMA/ $\text{Al}_2\text{O}_3$  and PMMA/ $\text{ZnO}$  nanocomposites, respectively. Toughness of material increases with the addition of FG-nanoparticles and highest improvement is observed at 0.5 volume fraction of the nanoparticles. Nevertheless, with further addition of FG-nanoparticles, polymer nanocomposites become softer which consequently reduce over toughness of the composites.

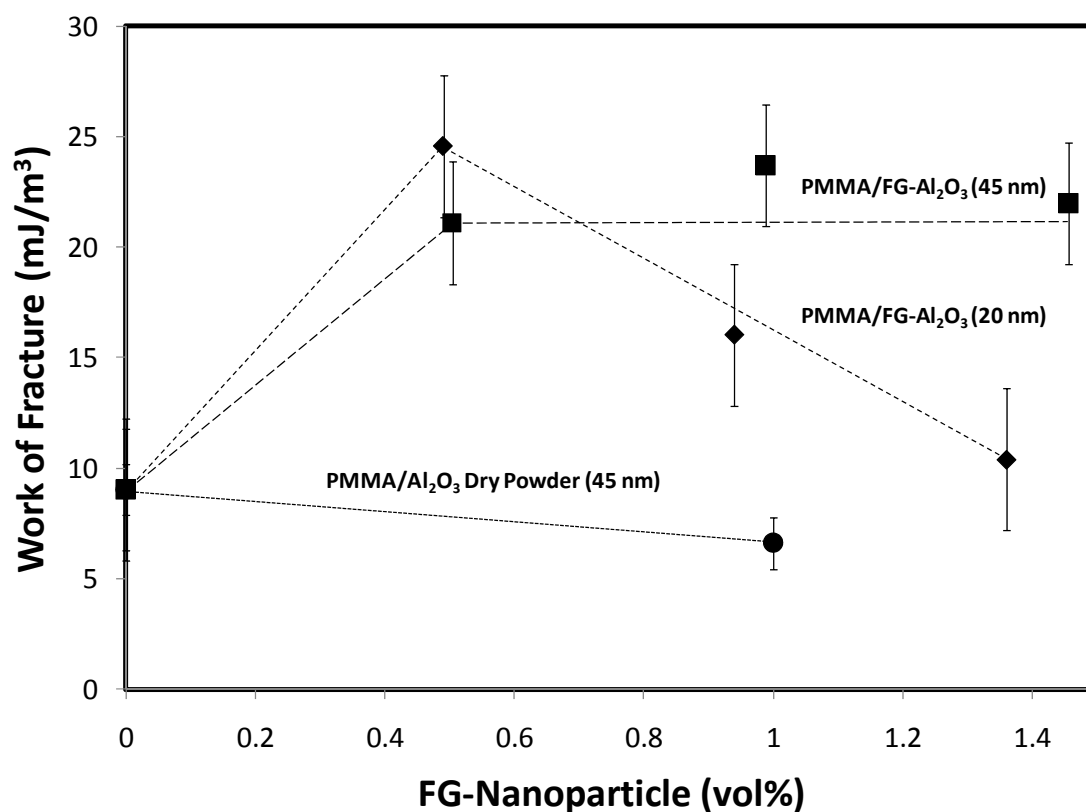


**Figure 4.6** Work of fracture of PMMA/ $\text{Al}_2\text{O}_3$  nanocomposites at various particle size, shape, and volume fractions.

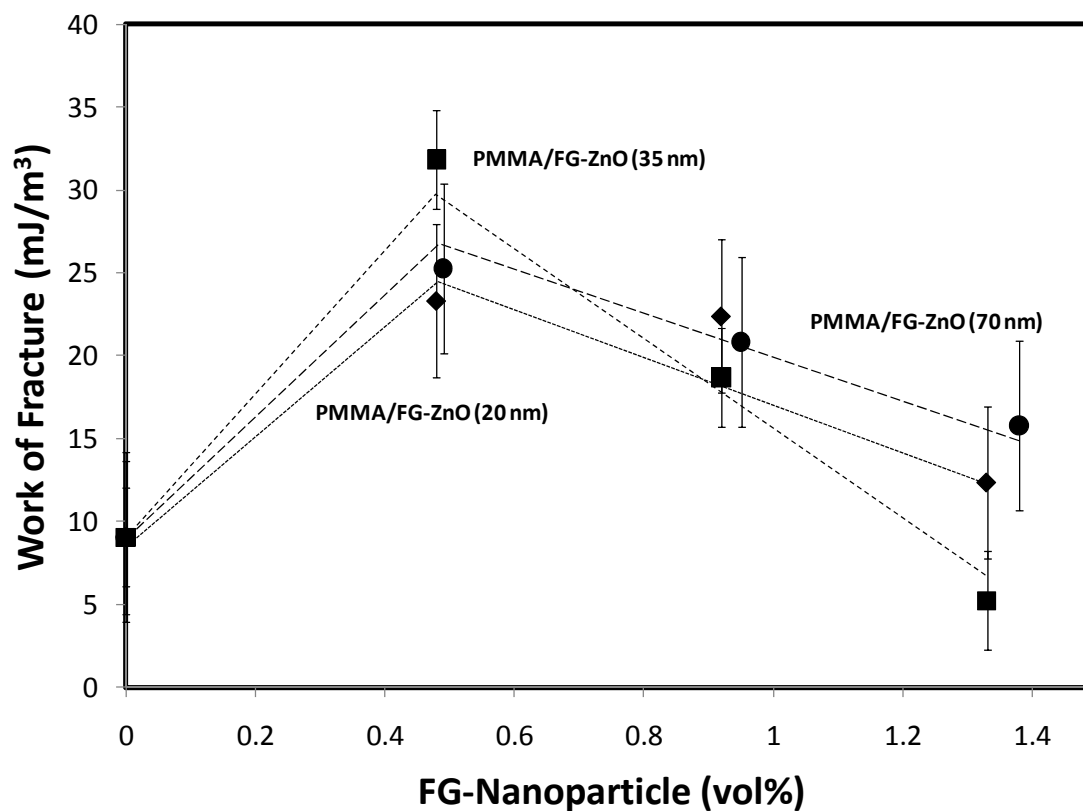


**Figure 4.7** Work of fracture of PMMA/ZnO nanocomposites at various particle size, shape, and volume fractions.

## 4.2 Impact resistance

Impact resistance is a complicated property that does not relate to a single aspect of molecular structure or composite morphology. The simplest view of toughness is just the area under a load/displacement curve as discussed above. In a more engineering sense, however, the instrumented impact method is appropriate since the method characterizes the material under the much higher strain rates characteristic of real applications. Failure at these strain rates, which often exceed the polymer relaxation time and thus produce an

almost brittle type of fracture, is comprised of a variety of mechanisms that include crack deflection, crack multiplications, yielding and some localized ductility. Hence, it is hard to predict impact behavior of the systems tested. However, based on literature results, the hope was that the present nanocomposites would exhibit increased toughness and energy of fracture.

Similar to the tensile modulus, impact resistance is also influenced by the addition of PGMEA, as displayed in Figure 4.1. The effect of nanoparticle on the impact resistance is illustrated in the Figure 4.8 and 4.9 for FG/ $\text{Al}_2\text{O}_3$  and FG/ $\text{ZnO}$ , respectively. Only systems containing FG- $\text{ZnO}$  at 1.0 vol% show enhancement in impact resistance. A major contributor to the zinc oxide particle effect is the acicular shape of the zinc oxide particle, a physical feature that promotes the crack deflection and introduces a high pull-out energy failure mechanism during impact. Such pullout mechanisms are documented and common in fiber reinforced composites. The mechanisms are reflected in fracture surface (Figure 4.13) and will be further discussed in the following section. Interestingly, the smallest particle size (20 nm) provides higher impact improvement, as would be expected from the perspective of particle physics. At 1.0 vol% of FG- $\text{ZnO}$  addition, the impact resistance increases 324%, 298%, and 292% as the particle size increase from 20 nm to 35 nm and 70 nm.

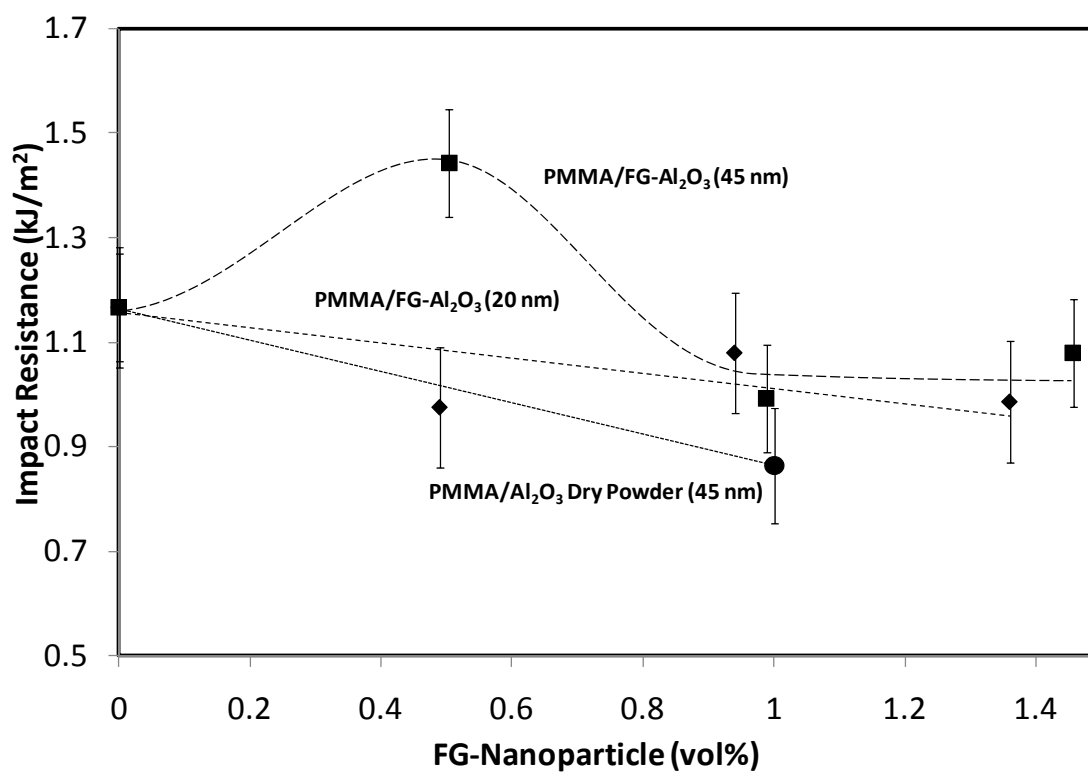


**Figure 4.8** Impact resistance of PMMA/Al<sub>2</sub>O<sub>3</sub> nanocomposites at various particle size, shape, and volume fractions.



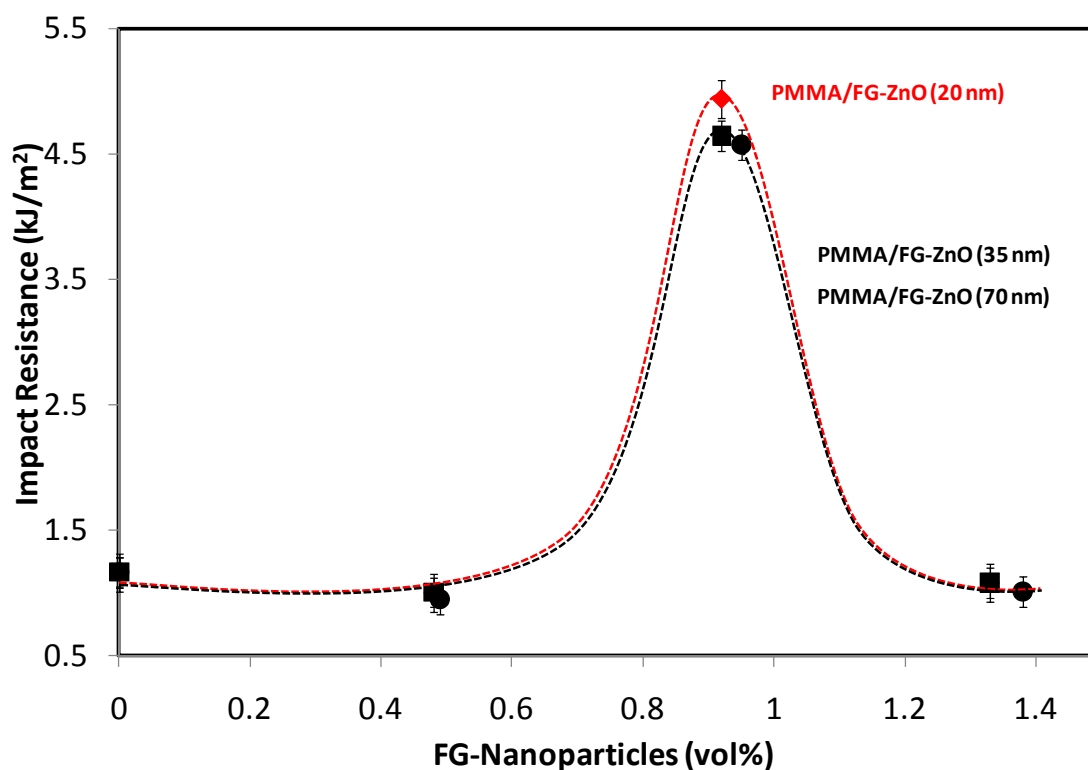


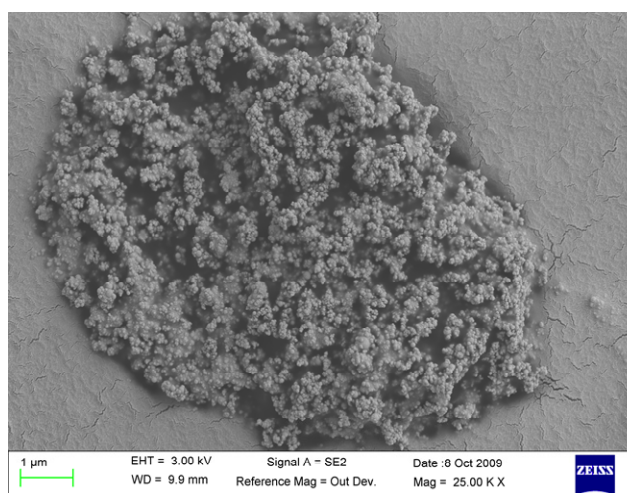
**Figure 4.9** Impact resistance of PMMA/ZnO nanocomposites at various particle size, shape, and volume fractions.

### 4.3 Image analysis

#### 4.3.1 Nanoparticle dispersion

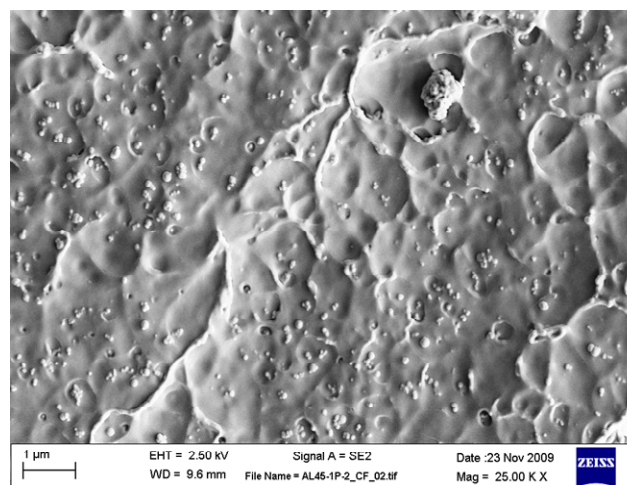
FESEM was used to determine the degree of particle dispersion in polymer nanocomposites on the cold-fractured surfaces. According to Powers et al.<sup>[9]</sup>, the degree of dispersibility of nanoparticle in a medium refers to the relative number of individual particles in comparison to agglomerates. The aggregation of particles is caused not only by the attractive inter-particle forces but also the grafted molecule on the particle surfaces.

In addition, the dispersibility of particles also depends strongly on dispersing and processing techniques.<sup>[10]</sup> In this work, an ultrasonicator was used to disperse nanoparticles in PMMA syrup with the total energy of 420 kJ (detail in Chapter 3). The viscosity of the syrup was thought to somewhat help lowering the precipitation rate of nanoparticles. Figure 4.10 shows the result from ultrasonication of PMMA/dry- $\text{Al}_2\text{O}_3$  (45 nm). The dry aluminum oxide was chosen in the comparison to eliminate the effect of grafted species. The micrographs show a good particle dispersion of nanoparticles throughout polymer matrix although a slight higher particle re-agglomeration at higher particle loading as illustrated in Figure 4.2.



**Dry aluminum oxide powder**

↓  
**Ultra-sonication**  
**(420 kJ)**



**Dispersed dry-Al<sub>2</sub>O<sub>3</sub> in PMMA**

**Figure 4.10** Dispersion of dry-Al<sub>2</sub>O<sub>3</sub> (1 v/o) in PMMA by Ultra-sonication technique.

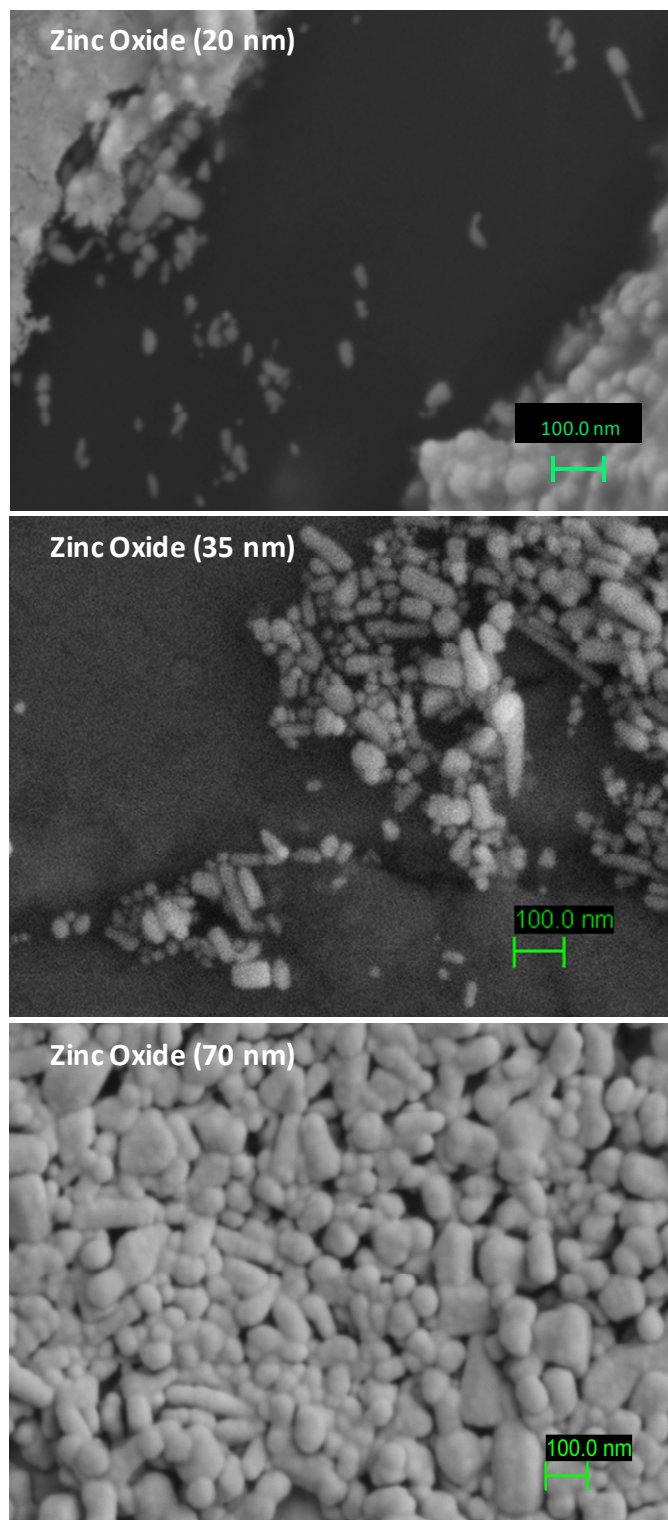


**Figure 4.11** Pre-dispersed zinc oxide nanoparticle in PGMEA.

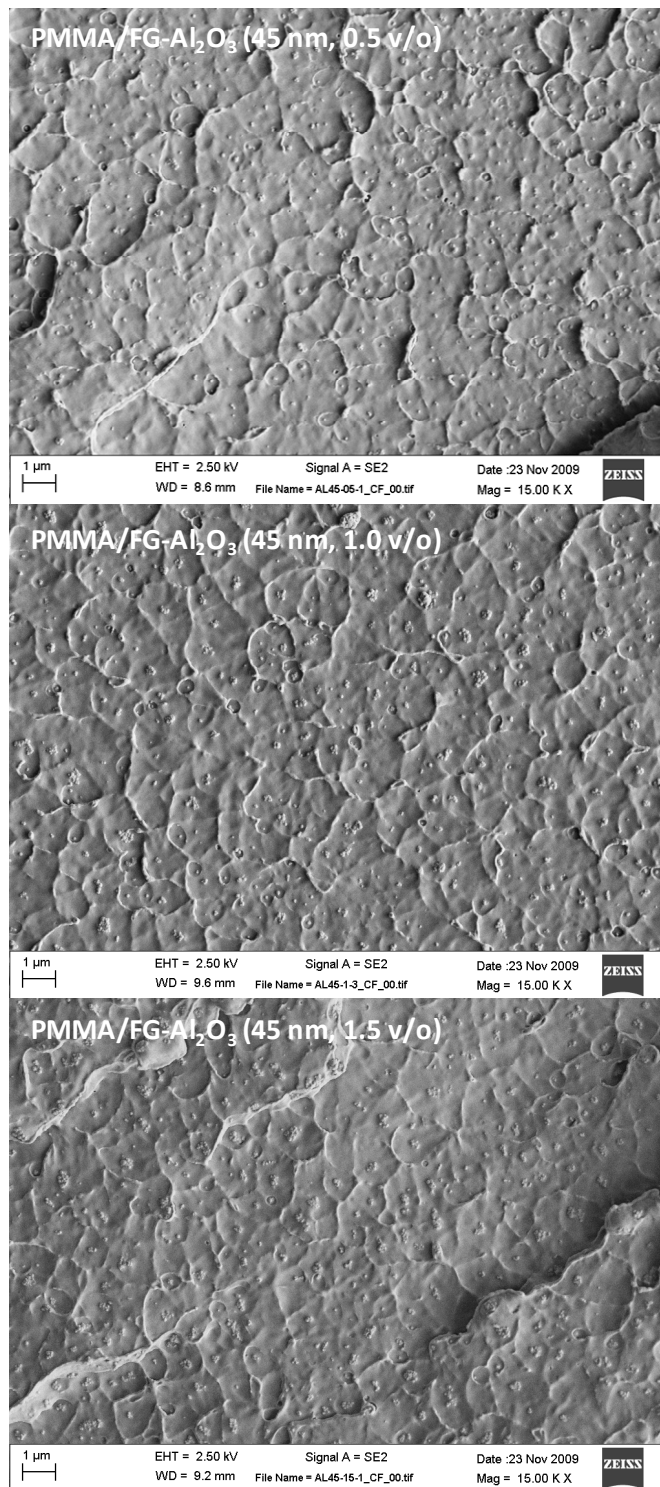


**Figure 4.12** Nanoparticle dispersion as a function of particle volume fraction.

#### **4.3.2 Fractured surface of polymer nanocomposites**

Failure mechanism of material can be evidenced by the micrograph of the fractured surface. Nanoparticle-filled materials are expected to undergo debonding and crack deflection under impact resistance. The fractured surface under impact testing, shown in Figure 4.13, supports the result in the previous section. The intense debonding and crack deflection around zinc oxide particles responsible for improvement in impact behavior of materials. Likewise, the enhancement of work of fracture by the de-bonding mechanism and cavitation is confirmed by the micrograph shown in Figure 4.14.

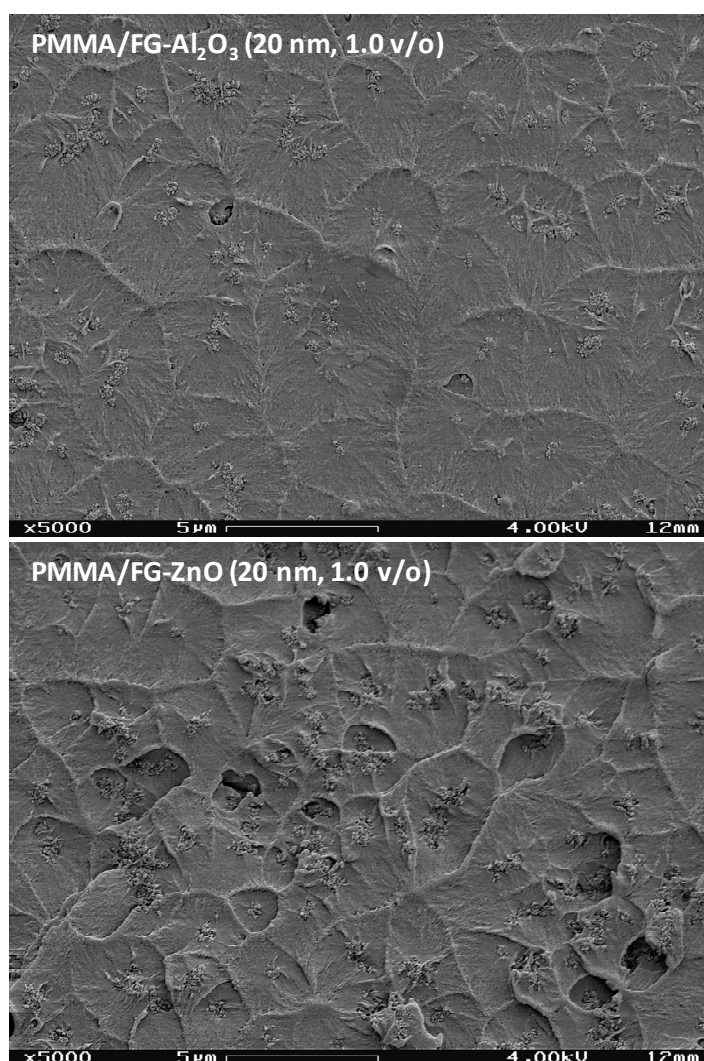


**Figure 4.13** Fracture surface of Impact testing at 1 v/o of nanoparticles.



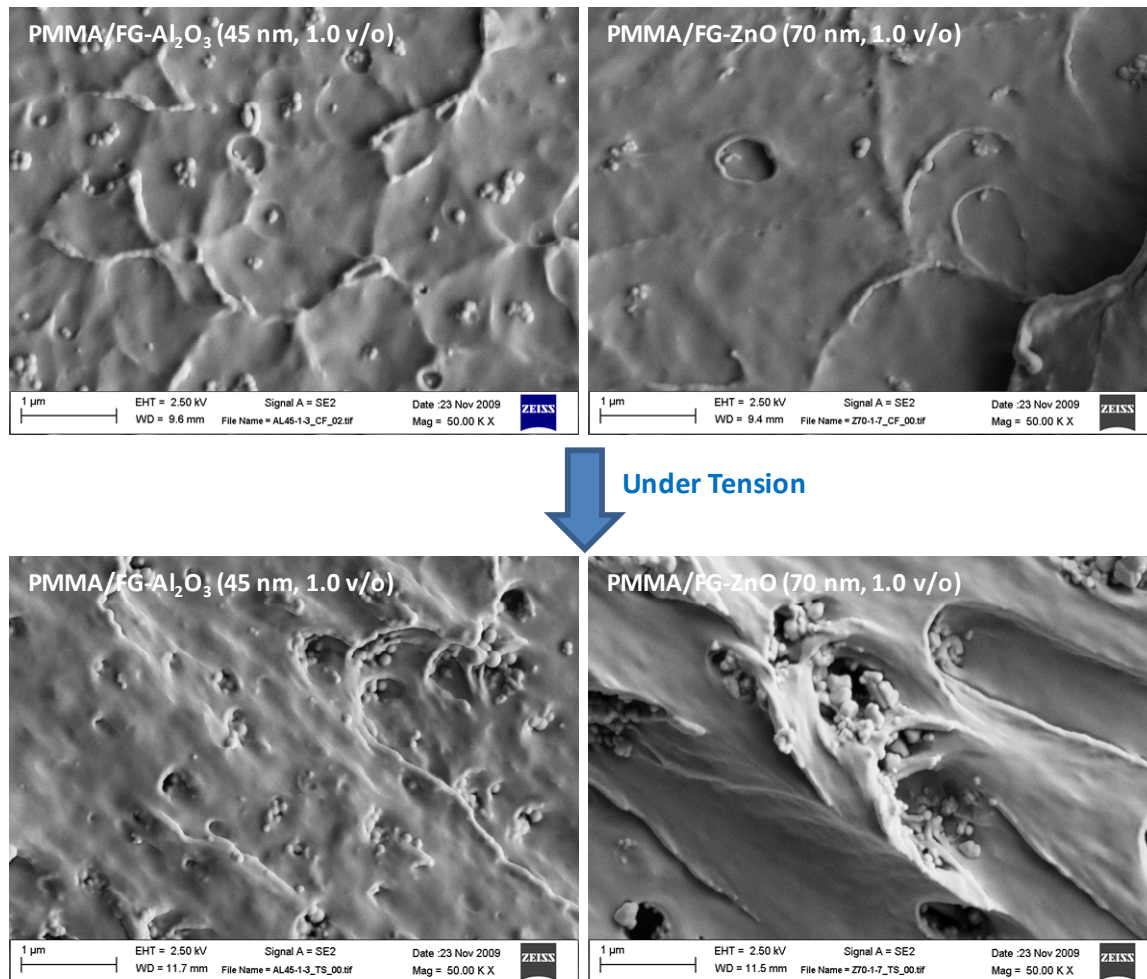


**Figure 4.14** Debonding and cavitation around nanoparticles under tension.

### 4.3.3 Material responses: time-temperature dependence

With variation of speed, polymeric materials at specific temperature and molecular weight may act as either liquid or solid.<sup>[11]</sup> At low temperature, polymer requires more time for the molecule to move because free volume is decreased and chain mobility is limited which leads to large relaxation time of the material under stress. As temperature increases, the polymer chain is swollen raising the total free volume in material.



Consequently, polymer molecules are able to move with ease resulting in small relaxation time.

The addition of nanoparticle behaves in the similar fashion as raising the temperature by increase the total free volume of the composite systems especially at the polymer/particle interface. Such behavior should be equivalent to the reduction in glass transition of the polymer nanocomposites which will be discussed in the Chapter 5. The fracture was done at two temperatures, one at the sub-zero temperature under liquid nitrogen and another at room temperature. As shown in Figure 4.16, at the constant temperature (downward direction in the same column), the fracture surfaces of the systems with nanoparticles added shows better respond to the applied force. Clearly the addition of the nanoparticles greatly alters the glass-like fracture of the neat PMMA, although only a minimal change from the brittle fracture behavior of the neat PMMA is evident in the cold fracture surface of the composites. As the temperature is increased to room temperature (22 C) and the deformation rate of the test is altered (tensile versus impact), the role of the nanoparticles in generating micro-deformations and ductility becomes more evident. Two different testing rates were performed, impact testing (3.5 m/s) and tensile testing (1 mm/min or  $1.67 \times 10^{-5}$  m/s), to reveal the viscoelastic response behavior of the polymer composites. The fractured surfaces clearly show that at slow testing rates the material exhibits more viscous response to the applied force since longer response times exist. The fracture surfaces show a much more feature-rich morphology, greater work of fracture and ductility, and hence greater toughness. As a result, in

PMMA nanocomposites, the de-bonding and cavitation mechanisms around nanoparticles are clearly shown.

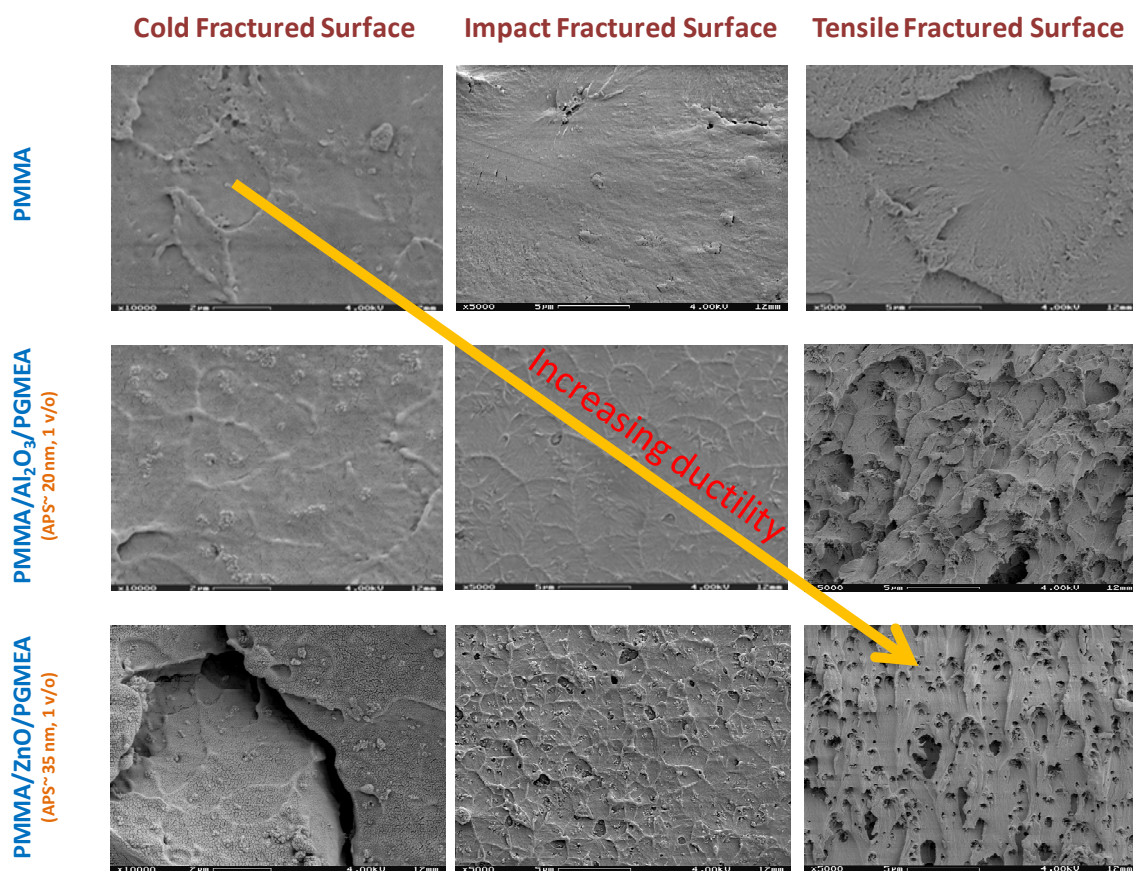


**Figure 4.15** Fracture surfaces of PMMA and PMMA nanocomposites.

## Summary

Mechanical behaviors of PMMA were altered by the incorporation of nanoparticles. No improvement in tensile modulus was observed. Tensile modulus was decreased when nanoparticles were introduced into PMMA and the reductions were increased when particle size get smaller. The particle geometry has a significant effect on impact resistance. Acicular shape of zinc oxide provides crack deflection and pull-out mechanisms in the composite system particularly in smaller particle size. The enhancement of impact resistance was 292%, 298%, and 324% as the particle size decreased from 70 nm to 35 nm and 20 nm.

From the micrographs, the promising dispersion of nanoparticles was achieved although slightly higher particle re-agglomeration was obtained as the volume fraction of nanoparticles increased. With the variation of loading time and temperature, the polymer molecules undergo difference molecular relaxation process. In the case of fast deformation rate and/or low temperature, the polymer chain mobility is limited. On the contrary, when the test is performed at room temperature, the material results in higher molecular respond to the applied force. Mobility of polymer was improved in both cases with the addition of nanoparticles.

## References

1. Y. Kojima, A. Usuki, M. Kawasumi, A. Okada, Y. Fukushima, T. Kurauchi and O. Kamigaito, Mechanical properties of nylon 6-clay hybrid, *J. Mater. Res.* 8 (1993), 1185-1189.
2. A. Usuki, Y. Kojima, M. Kawasumi, A. Okada, Y. Fukushima, T. Kurauchi and O. Kamigaito, Synthesis of nylon 6-clay hybrid, *J. Mater. Res.* 8 (1993), 1179-1184.
3. W. Viratyaporn and R. Lehman, Impact resistance and Raman characterization of  $\text{Al}_2\text{O}_3/\text{ZnO}$  poly(methyl methacrylate) nanocomposites, ANTEC, 2009.
4. B. J. Ash, J. Stone, D. F. Rogers, L. S. Schadler, R. W. Siegel, B. C. Benicewicz and T. Apple, Investigation into the thermal and mechanical behavior of PMMA/alumina nanocomposites, *Mat. Res. Soc. Symp. Proc.* 661 (2001), KK2.10.11.
5. C.-M. Chan, J. Wu, J.-X. Li and Y.-K. Cheung, Polypropylene/calcium carbonate nanocomposites, *Polymer* 43 (2002), 2981-2992.
6. R. P. Singh, M. Zhang and D. Chan, Toughening of a brittle thermosetting polymer: Effects of reinforcement particle size and volume fraction, *J. Mater. Sci.* 37 (2002), 781-788.
7. X. L. Ji, J. K. Jing, W. Jiang and B. Z. Jiang, Tensile modulus of polymer nanocomposites, *Polymer Engineering and Science* 42 (2002), 983-993.
8. W.-J. Boo, L. Sun, G. L. Warren, E. Moghbelli, H. Pham, A. Clearfield and H.-J. Sue, Effect of nanoplatelet aspect ratio on mechanical properties of epoxy nanocomposites, *Polymer* 48 (2007), 1075-1082.
9. K. W. Powers, S. C. Brown, V. B. Krishna, S. C. Wasdo, B. M. Moudgil and S. M. Roberts, Research strategies for safety evaluation of nanomaterials. Part vi. Characterization of nanoscale particles for toxicological evaluation, *Toxicol. Sci.* 90 (2006), 296-303.
10. J. Jordan, K. I. Jacob, R. Tannenbaum, M. A. Sharaf and I. Jasiuk, Experimental trends in polymer nanocomposites—a review, *Mater. Sci. Eng. A* 393 (2005), 1-11.
11. T. A. Osswald and G. Menges, *Materials science of polymer for engineers*, Hanser, Munich, 2003.

## **Chapter 5 Thermal behavior of polymer/particulate nanocomposites**

The ability to withstand a wide range of temperatures is an important engineering property for materials. Nanoparticles have been shown to improve thermal behavior in various polymer nanocomposite systems. Glass transition temperature is associated with free volume and molecular motion in polymers. Since the molecular motion of polymers is strongly affected by nanoparticles it stands to reason that the glass transition of polymer nanocomposites will be different from the glass transition of the neat polymer. In this Chapter, the thermal behavior, including glass transition and thermal degradation temperatures, of PMMA nanocomposites are examined. For thermal degradation analysis, the variations of particle size and chemistry were studied. Two types of particle chemistry were selected, i.e. aluminum oxide ( $\text{Al}_2\text{O}_3$ ) and zinc oxide ( $\text{ZnO}$ ). In the aluminum oxide part of the study, the investigation toward the effect of dry and pre-dispersed powders to assess the effect of the dispersing medium was performed. In the case of zinc oxide nanoparticles, two particle sizes were chosen to study the effect of particle dimension. The effect of nanoparticle to the glass transition temperature is also discussed.

### **5.1 Thermal Gravimetric Analysis (TGA)**

#### **5.1.1 Pre-dispersed nanoparticles**

Dispersion is a critically important parameter in nearly all types of composite materials. In nanocomposites, the high ratio of surface forces to inertial forces of the

nanoscale particles tends to encourage aggregation and agglomeration. To minimize these issues in the present composites, the nanoparticles used in this study were pre-dispersed in propylene glycol methyl ether acetate (PGMEA or PMA) to stabilize the nanoparticles and to prevent them from re-agglomerating. The polar PGMEA molecules are anticipated to chemisorb with the hydroxyl groups on the metal oxide surface, thus maintaining dispersion by a principally steric hindrance mechanism. To determine the effects of particle size and chemistry, four pre-dispersed nanoparticles were selected:  $\text{Al}_2\text{O}_3$  (20 and 45 nm) and  $\text{ZnO}$  (20 and 35 nm). Figure 5.1 for various types of stabilized nanoparticles. The weight loss curve contains two distinct regions, labeled as region I and II. Region I is associated with the loss of excess (i.e. non-bonded) PGMEA molecules while the chemisorbed molecules are more tightly bond and are not evolved until higher temperatures are reached, region II. Since the PGMEA is bonded to the nanoparticles, albeit via weak secondary bonds, the particles are subsequently referred as functionalized and use the nomenclature FG-nanoparticles henceforth. An interesting aspect of this graph is the quantitative weight loss through Region II, which corresponds to the quantity of bonded PGMEA. These values are detailed in Table 5.1 ranging from 2% to 4% depending on the particle size and chemistry of the nanoparticles. Naturally, the final weight of all specimens in the TGA trace corresponded to the inorganic content of the dispersion as formulated and this value was used as a confirming check on the performance of the TGA analysis.

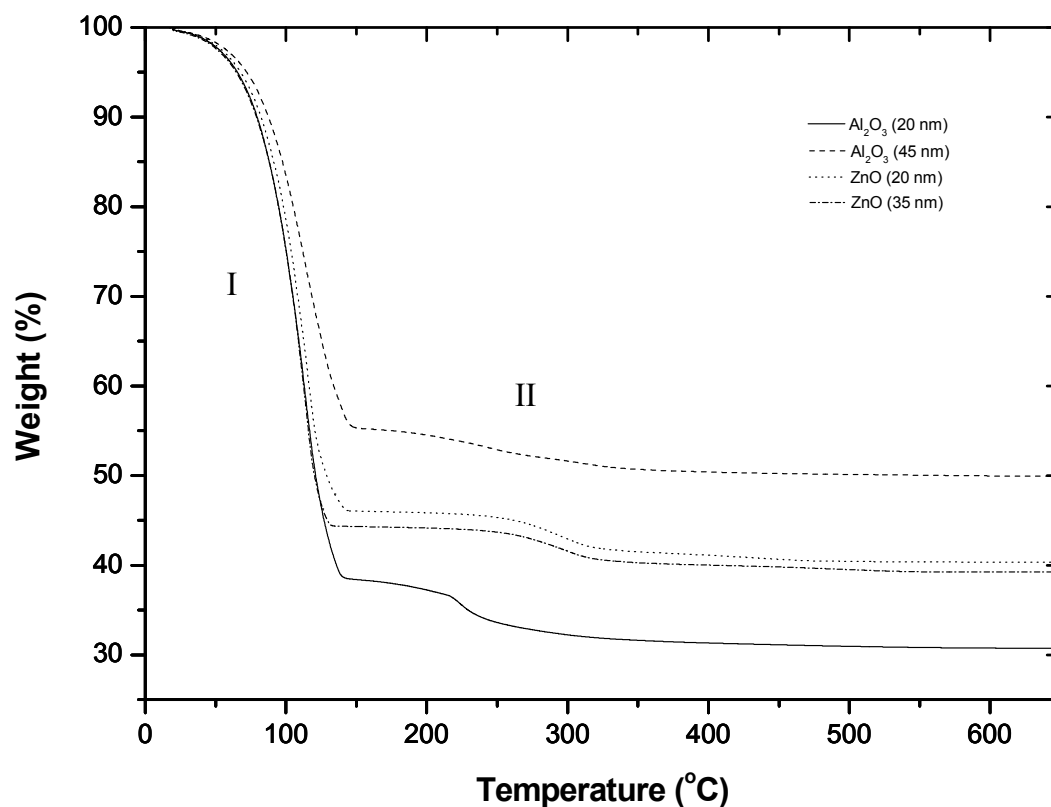


**Figure 5.1** TGA curve of various nanoparticles: I is the reduction of the excess PGMEA and II is the decomposition of the chemisorb molecules.

**Table 5.1** Weight Percent of PGMEA on Nanoparticle Surface (Region II).

	20 nm	35 nm	45 nm
Aluminum Oxide ( $\text{Al}_2\text{O}_3$ )	3.3	-	2.0
Zinc Oxide (ZnO)	3.6	3.1	-

The secondary bonding interaction between the PGMEA and the oxide particles was found to depend on the size of the particle and the specific oxide type. Smaller particles of both  $\text{Al}_2\text{O}_3$  and  $\text{ZnO}$  have adsorbed higher amounts of PGMEA, as expected from the higher surface area and as illustrated in the Figures 5.1 and 5.2. Most interesting from this study, however, is the profile of the derivative weight loss curve that illustrates the temperature of maximum weight loss rate and the shape of the area under this curve, a behavior that is determined jointly by the particle size and oxide nature. Both aluminum oxide nanoparticles showed peak derivative loss rates in the temperature range 223-240 °C, whereas the zinc oxide nanoparticles bonded more tightly with the PGMEA and both  $\text{ZnO}$  particle samples produced peak derivative loss values near 300 °C. A correlation of the area under the derivative weight loss curves with particle size shows that the integrated area is principally a function of the particle size with a secondary effect of oxide. Ionic potential is a determining factor for electron density at the metal oxide surfaces (detail discussed in Chapter 2). The lower ionic potential ( $q/r$ ) of  $\text{ZnO}$  (~2.7) compared to  $\text{Al}_2\text{O}_3$  (~5.6) arises from the high proton concentration at the oxide surface leading to increased interaction with both carbonyl and carboxylate ionic groups. This greater secondary bonding of  $\text{ZnO}$  particles is reflected in the insert in Figure 5.2 that illustrates the greater area under the derivative curve for these particles after the effect of particle size is factored.



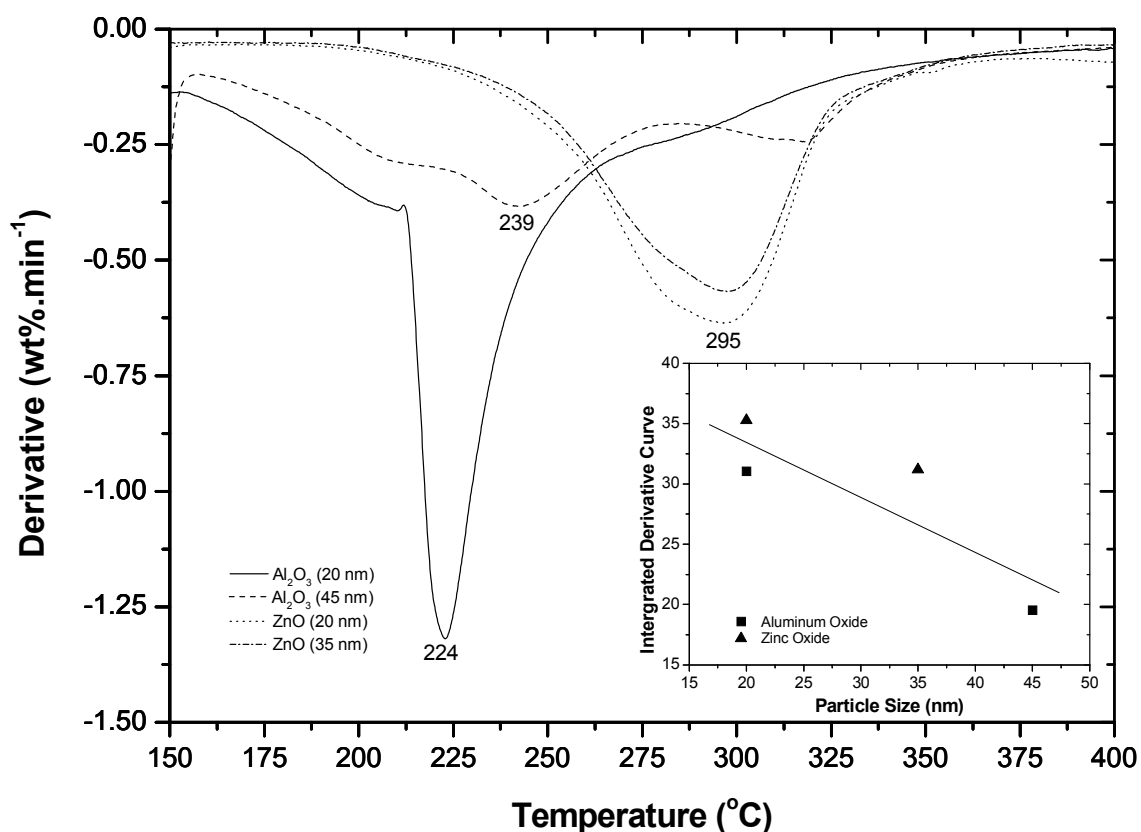


**Figure 5.2** DTG curve of chemisorb molecules (region II) of various nanoparticles and the area under region II (inserted).

### 5.1.2 Polymer-inorganic nanocomposites

Neat poly(methyl methacrylate) is known to have poor thermal behavior. A study of thermal degradation temperature of PMMA by TGA showed that the polymer degrades in three steps at 180°C, 250°C, and 350°C.<sup>[1]</sup> The degradation mechanisms are given as the scission of H-H linkage, the scission of C-C bond in the  $\beta$ -position to the unsaturated vinylidene end group, and the random scission of polymer main chain, respectively. In our work, the degradation temperature of the neat AIBN-initiated-PMMA was observed

to have two steps, as shown in the Figure 5.3, with the maximum weight loss rates at about 265°C and 330°C for the first and second steps, respectively. Due to the low stability of H-H linkage, the scission takes place below 200 °C. Thus, the first step is associated with the scission initiated by the double bond end group resulting from the disproportionation process. The second step consists of many overlapping peaks as a result of bond strength fluctuations along the polymer chain. MMA polymerized in the presence of some oxygen will form occasional peroxide linkages.<sup>[2]</sup> Similarly, when PMMA decomposes in the presence of oxygen, radicals produced from the scission of H-H linkage can react with the oxygen and form peroxide radical which is more stable than the tertiary carbon radical.<sup>[3]</sup> Correspondingly, in this work, the PMMA specimens were polymerized in a sealed mold, but not in oxygen-free environment, such that the ambient oxygen molecules are available to react with the propagating radical and form peroxide in the polymer chain. The multiple peaks of the second polymerization step likely results from the competition between random scission of main chain carbons, combination of propagating radical with ambient oxygen, and the decomposition of peroxide linkages. The PMMA was completely decomposed at about 405°C. The absence of the significant H-H scission, which normally occurs below 200°C, may result from decreased stability of the propagating radical which shifts the termination process towards disproportionation.

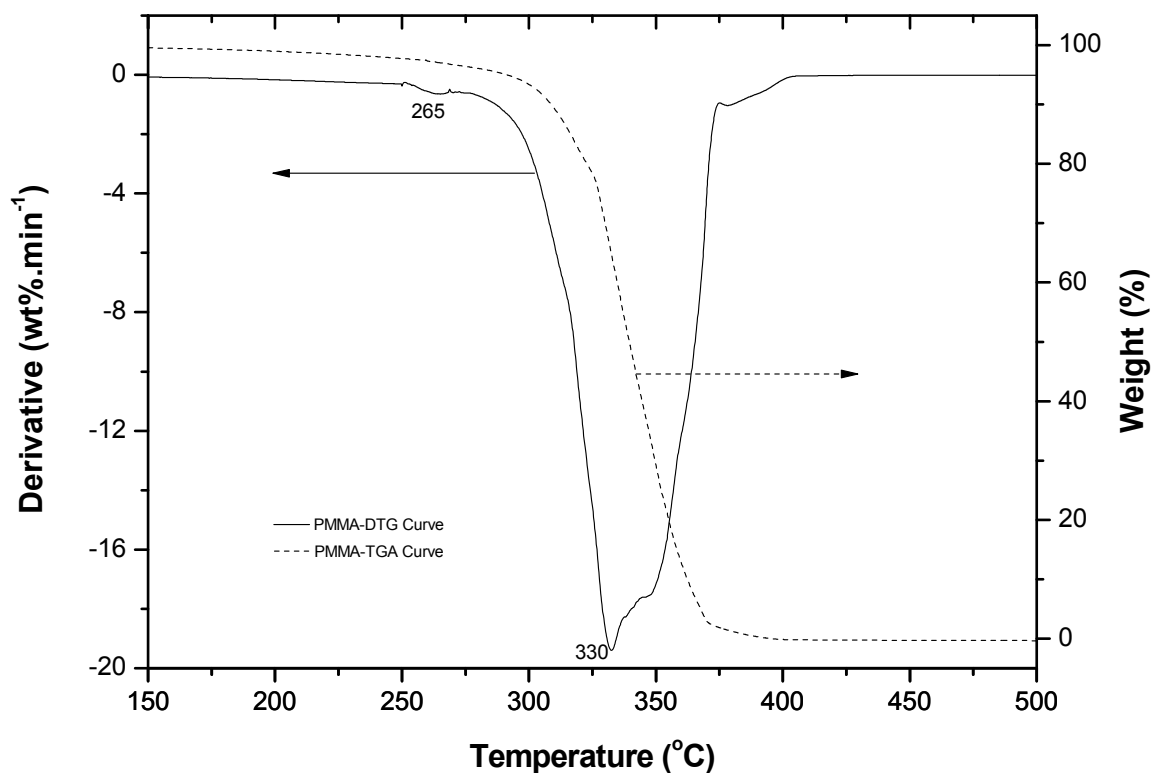


**Figure 5.3** DTG and TGA curves of neat PMMA.

The thermal stability of PMMA is improved by the addition of nanoparticles. PMMA nanocomposites having relative concentration of 1 vol% was chosen for thermal analysis study (45 nm of  $\text{Al}_2\text{O}_3$  and 20 and 35 nm of ZnO). PMMA/ $\text{Al}_2\text{O}_3$  (dry and wet, 45 nm) nanocomposites were used to investigate effect of PGMEA to thermal stability of PMMA nanocomposites (Figure 5.4). Dry refers to aluminum oxide particles dispersed directly in the MMA prior to polymerization. Wet refers to aluminum oxide particle pre-dispersed in PGMEA prior to addition to MMA and polymerization. In the system containing pre-dispersed nanoparticles, weight loss commences near 145°C, approximately the boiling point of PGMEA (~146 °C), whereas when dry powders (e.g.

the PMMA/Al<sub>2</sub>O<sub>3</sub> system) are used the measureable weight loss commences around 212°C. The early weight loss associated with the PGMEA containing systems is a very small effect and is not readily apparent in the figures, but was examined closely during data analysis as we searched vainly for indications of H-H decomposition below 200°C. The degradation of vinylidene end groups most likely occurs in the same temperature range as in neat PMMA, but effects related to the adsorbed polymer complexes (PGMEA/PMMA) and/or the nanoparticles themselves obscure the characteristic shape of the vinylidene decomposition curve. This early degradation caused by PGMEA was also observed in all pre-dispersed nanoparticle/PMMA systems (Figures 5.3 – 5.5). Another interesting observation is that there are small peaks prior to the main degradation peak observed in PMMA/FG-Al<sub>2</sub>O<sub>3</sub> systems which are not carried on to the PMMA/FG-ZnO systems. Further investigation for this still needed, however, it seems to relate to the type of the oxides.

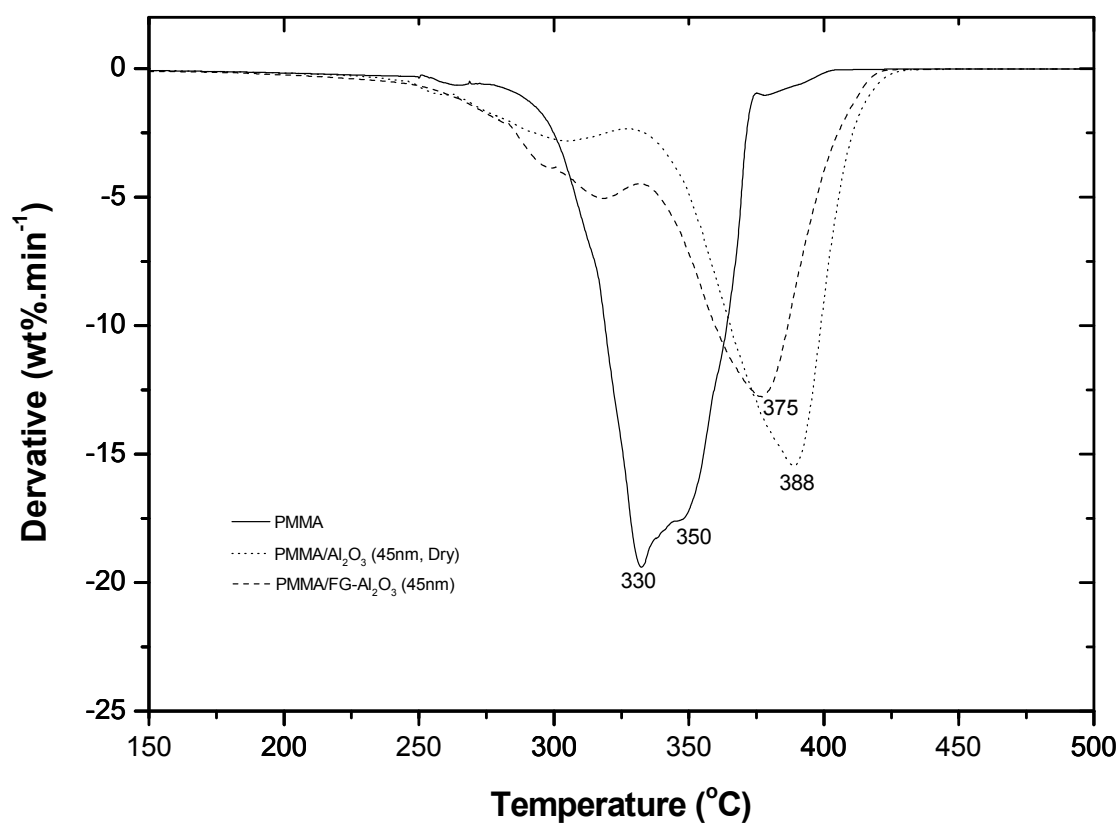


**Figure 5.4** DTG curve on the effect of aluminum oxide nanoparticles and small molecules of PGMEA on the thermal stability of PMMA.

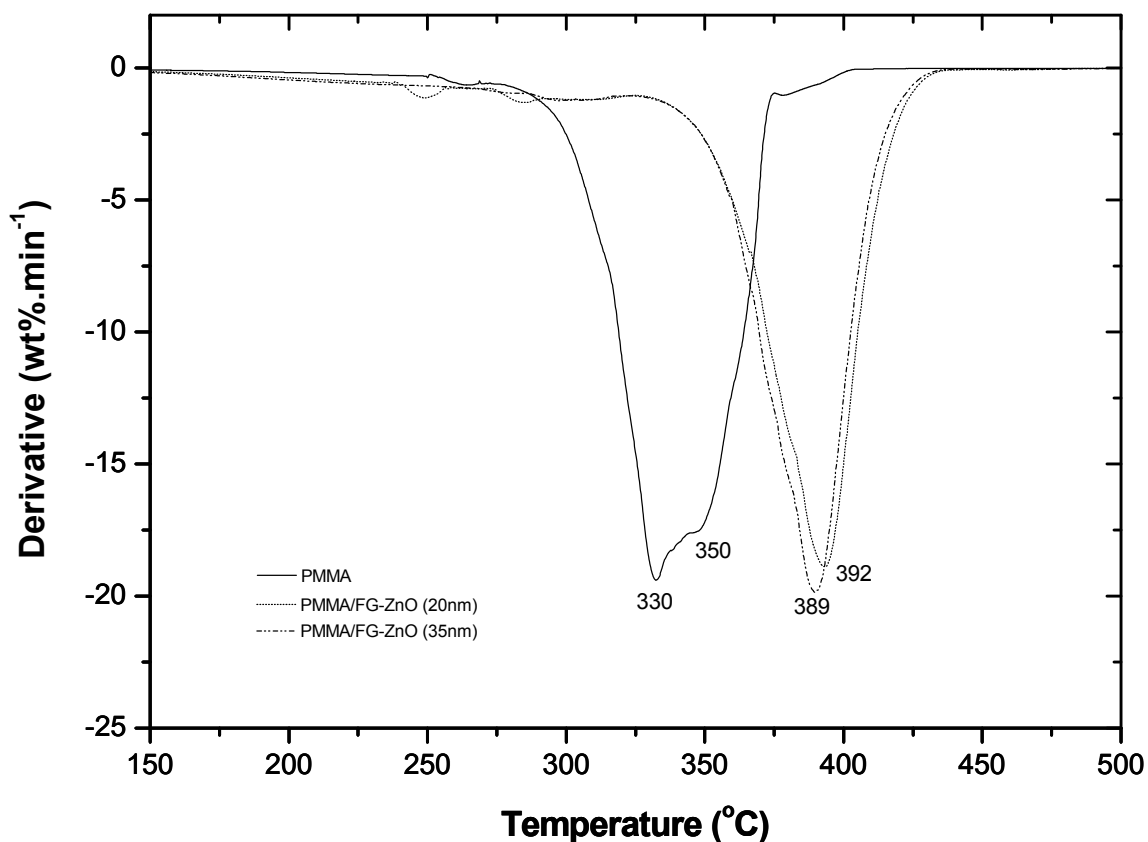


**Figure 5.5** DTG curve on the effect of zinc oxide nanoparticles on the thermal stability of PMMA.

The vast bulk of the decomposition of PMMA and PMMA nanocomposites occurs as the main chain begins to depolymerize above 300 °C, as has been exhaustively discussed in the literature for neat PMMA and various composites. The incorporation of nanoparticles in PMMA clearly raises these decomposition temperatures as shown in the present work. The effect is largest for the zinc oxide nanoparticle composites that presented decomposition peaks (Figure 6) at 392° and 389° for zinc oxide particles sizes of 20 and 35 nm respectively. This represents a 60 °C increase over neat PMMA.

Aluminum oxide particles were somewhat less effective, although element type and particle size are partially confounded in this study, as evidenced by maximum degradation peaks at 388 and 375 respectively for 45 nm alumina particles incorporated “dry” and “wet” respectively. The greater effectiveness of zinc oxide nanoparticles in improving the thermal stability of PMMA seems to result from the higher surface proton density for zinc oxide ( $ZPC = 9.2$  for  $ZnO$  <sup>[4, 5]</sup>,  $7.5$  for  $Al_2O_3$  <sup>[6, 7]</sup>) compared to alumina as well as the smaller particle size of the zinc oxide.

Two mechanisms are commonly used to explain the increase in the thermal degradation temperature of the polymer nanocomposites. Both mechanisms involve interruption of the physical and/or chemical environment of the polymer. The first mechanism is comprised simply of steric hindrance of polymer chain motion that reduces thermally induced strain on the polymer backbone and also reduces the number of chain-scission-promoting encounters with neighboring moieties.<sup>[8]</sup> The second mechanism, which is not well documented in the literature, addresses the chemical inducing and inhibiting effects of nanoparticle oxide surfaces. The localization of charge arising from the carbonyl dipole and similar surface moieties may be effective in promoting bond scission, particularly as the charge destabilizes polymer units and promotes various scissions including the vinylidene decomposition discussed above. Countering this mechanism is the tendency for nanoparticles to act as defect getters during the fabrication of the composites<sup>[9]</sup>, terminating chains for example at H-H linkages and thus stabilizing the composite against thermal degradation during subsequent heating.

To determine whether the improvement in thermal stability is caused by chain restriction, the glass transition temperature of the composites was examined. Glass transition temperature ( $T_g$ ) is directly related to the polymer chain mobility. Thus, if added nanoparticles obstruct polymer chain motion,  $T_g$  will increase (or relative constant) and vice versa.<sup>[10]</sup> However, in this study, PMMA was not only modified by nanoparticles but also small molecules of the dispersing agent (PGMEA). PGMEA can interfere with the polymer chain and cause free space in the polymer matrix. Consequently, higher mobility of polymer chain is normally observed thus lowering the  $T_g$  of the neat PMMA (Figure 5.6). Therefore, to examine the true effect of nanoparticles, the glass transition temperature of polymer nanocomposites was compared to the PMMA/PGMEA composite at certain v/o of PGMEA instead. The results from MDSC showed that nanoparticles slightly reduced  $T_g$  by  $\sim 1.15\%$  in both PMMA/FG-ZnO (20 nm and 35 nm) systems. Such a small reduction of  $T_g$  suggests that interfacial interactions between nanoparticle and polymer matrix do not substantially constrain the intrinsic chain mobility of the PMMA nor do they alter the  $T_g$ -reducing effect of the PGMEA additive. This passive role of the nanoparticles with regard to  $T_g$  changes suggest that the polymer chain does not bond tightly to the nanoparticle surface as would be expected if the chains assumed the flatten configuration. This result is further supported by the spectroscopic results discussed in Chapter 6.



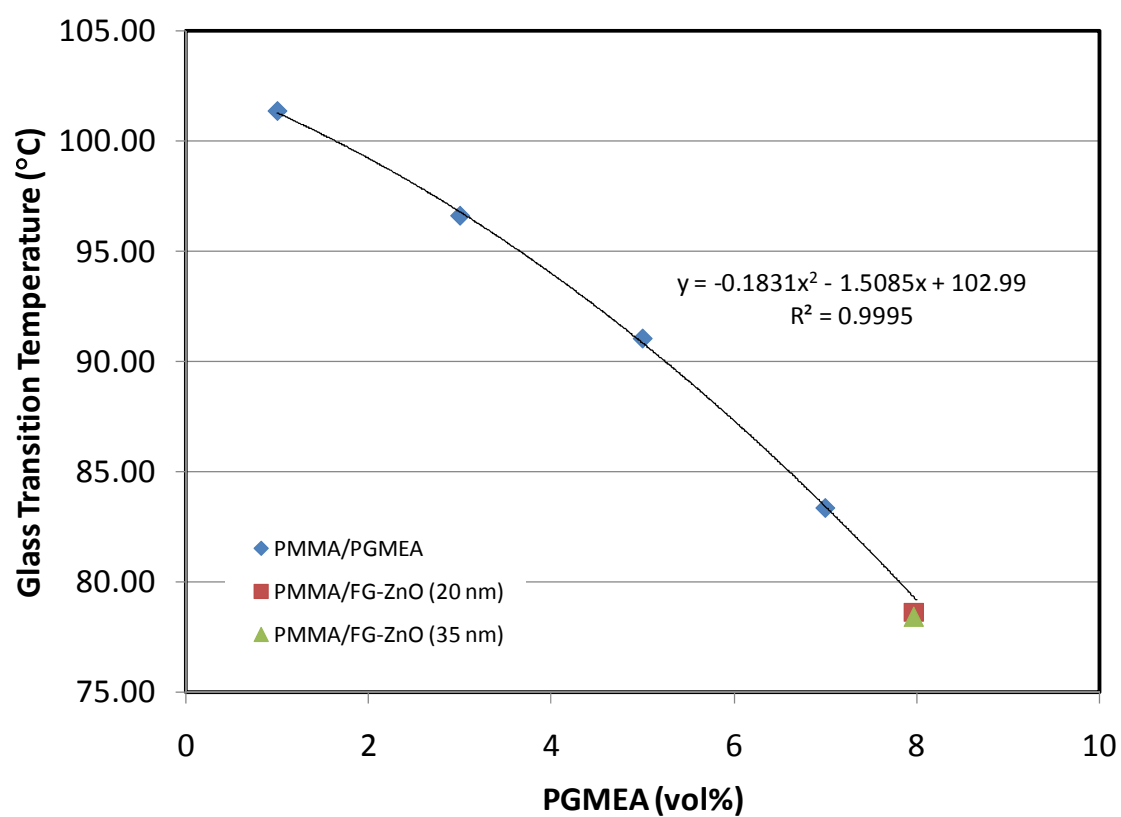


**Figure 5.6** Glass transition temperature of PMMA/FG-ZnO nanocomposites and PMMA/PGMEA at various PGMEA volume fractions.

## Summary

The polar molecule of PGMEA is confirmed to attach to the aluminum oxide and zinc oxide surfaces by the weight loss at about 223-240 °C for FG-Al<sub>2</sub>O<sub>3</sub> and 300 °C for FG-ZnO. The higher degradation temperature of PGMEA on zinc oxide surface is associated with the high proton concentration on the surface of zinc oxide. This trend was further observed in the PMMA nanocomposite systems. The thermal stability of the PMMA was improved by the addition of both the zinc oxide and aluminum oxide nanoparticles. H-H and vinylidene scission mechanisms contributed minimally to the overall breakdown of the composites. The vast majority of the decomposition occurred due to random main chain scission in the temperature range of 330 – 392 °C. Approximately a 62 °C increase in peak decomposition was noted for 20 nm zinc oxide composites. The small reduction of  $T_g$  in PMMA nanocomposites suggested that interactions between polymer and nanoparticles is to some extent exist and associated with the chain restriction concept. Therefore, the mechanism for this increased thermal stability appears to arise from two mechanisms, steric restriction of chain motion and radical deactivation by nanoparticles.

## References

1. C. Dong and X. Ni, The photopolymerization and characterization of methyl methacrylate initiated by nanosized titanium dioxide, *Journal of Macromolecular Science Part A—Pure and Applied Chemistry A41* (2004), 547-563.
2. G. Boven, M. L. C. M. Oosterling, G. Challa and A. J. Schouten, Grafting kinetics of poly(methyl methacrylate) on microparticulate silica, *Polymer* 31 (1990).
3. J. D. Peterson, S. Vyazovkin and C. A. Wight, Kinetic study of stabilizing effect of oxygen on thermal degradation of poly(methyl methacrylate), *Journal of physical chemistry. B* 103 (1999), 8087-8092.
4. O. A. Fouad, A. A. Ismail, Z. I. Zaki and R. M. Mohamed, Zinc oxide thin films prepared by thermal evaporation deposition and its photocatalytic activity, *Applied Catalysis B: Environmental* 62 (2006), 144-149.
5. M. Mrowetz and E. Selli, Photocatalytic degradation of formic and benzoic acids and hydrogen peroxide evolution in TiO<sub>2</sub> and ZnO water suspensions, *Journal of Photochemistry and Photobiology A: Chemistry* 180 (2006).
6. J. M. Dominguez, J. L. Hernandez and G. Sandoval, Surface and catalytic properties of Al<sub>2</sub>O<sub>3</sub>–ZrO<sub>2</sub> solid solutions prepared by sol–gel methods, *Applied Catalysis A: General* 197 (2000), 119-130.
7. B. Xing, Natural organic material characteristics affect the environmental behavior of manufactured nanoparticles, *Assessment of the Biological Effects of Nanomaterials Symposium*, 2009.
8. A. Laachachia, M. Cocheza, M. Ferriola, J. M. Lopez-Cuestab and E. Leroy, Influence of TiO<sub>2</sub> and Fe<sub>2</sub>O<sub>3</sub> fillers on the thermal properties of poly(methyl methacrylate) (pmma), *Materials Letters* 59 (2005), 36-39.
9. M. M. Demir, M. Memesa, P. Castignolles and G. Wegner, PMMA/zinc oxide nanocomposites prepared by in-situ bulk polymerization, *Macromol. Rapid Commun.* 27 (2006), 763-770.
10. L. Schadler, "Polymer-based and polymer-filled nanocomposites," *Nanocomposite science and technology*, Wiley, 2003, pp. 77-153.

## Chapter 6 PMMA/particulate nanocomposites: Spectroscopic analysis

Interfacial interactions specifically and the interphase region in general of polymer nanocomposites is an important material behavior that controls the final properties of the material. Complete understanding of the relationship between fillers, the polymer matrix, and the interphase, will enable us to predict, engineer, and control the properties to match with certain applications. In this work, our polymer nanocomposite systems consisted of three components: polymer matrix (PMMA), nanoparticles ( $\text{Al}_2\text{O}_3$  and  $\text{ZnO}$ ), and a dispersing agent (PGMEA) for the nanoparticles. Results from thermal analysis (Chapter 5) revealed that nanoparticles retard the degradation process of both PMMA and PGMEA which could be related to the interaction between them. Even though the functional groups of both PMMA and PGMEA are similar, the long length and flexibility of PMMA polymer chain provides it with a unique interacting configuration that will affect the polymer chain conformation not only at the interface but also in the surrounding region.

In this Chapter, infrared and Raman spectroscopy were used to further analyze the interaction between PGMEA/nanoparticles and PMMA/nanoparticles as well as the configuration and conformation effect of PMMA in polymer nanocomposites.

### 6.1 Interfacial interactions

Changes in wavenumber and intensity/area of infrared and Raman band are respectively associated to the changes in bonding environment and quantity of the particular molecular species. The vibrational frequency of a molecule ( $\nu_m$ ) is a function

of bond strength and atomic mass. In the simple case of a molecule consisting of two atoms, let  $m_1$  and  $m_2$  be the mass of atom 1 and 2 respectively, then, the vibrational frequency based on simple harmonic approximation is given by

$$\nu_m = \frac{1}{2\pi} \sqrt{\frac{k}{\mu}} \quad (6.1)$$

where  $k$  is force constant which is related to the bond strength and  $\mu$  is the reduced mass which is calculated from

$$\mu = \frac{m_1 m_2}{m_1 + m_2} \quad (6.2)$$

Therefore, the frequency will increase, which corresponds to the shift toward higher wavenumber, in the case of the stronger bond and lighter atom.<sup>[1]</sup>

Generally, surface of metal oxides are covered with hydroxyl groups (-OH) as a result of the interaction between the metal oxide and surrounding chemical moieties, which can vary in type but are often of alcohol or OH character. Regardless of how they originate, the pure O-H stretching, without any secondary bonding between the neighboring atoms, produces an absorption band near  $3675 \text{ cm}^{-1}$ . Additionally, the hydroxyl group can interact with the other hydroxyl groups via secondary bonding, an effect that shifts and broadens the O-H stretching peak towards lower frequencies. As compared to the ATR-FTIR of PGMEA and metal oxide, the spectra of absorbed PGMEA indicate that the interactions of between metal oxide and PGMEA exist. Figures 6.1 and 6.2 represent the spectra for FG- $\text{Al}_2\text{O}_3$  and FG-ZnO, respectively. A typical

interaction between surface hydroxyl and polar substance is acid-base interaction via secondary bonding<sup>[2,3]</sup> which is expected to occur at the high electron density sites (ester and ether) of the PGMEA molecule. Such interaction is evidenced by the shift of the hydroxyl group absorption band and the related counter interactions, which are carbonyl (from 1734  $\text{cm}^{-1}$  to 1731  $\text{cm}^{-1}$ ) and ether (1113  $\text{cm}^{-1}$  to 1103 $\text{cm}^{-1}$ ) vibrations, to lower frequency, as shown in Figure 6.2 and 6.3. When such interaction occurs, the bonds within the molecules are altered: some are weakened and some are restricted in terms of their motion. For example, the C-H stretching peak (2800 – 3050  $\text{cm}^{-1}$  region) changes its shape and intensity as PGMEA molecule is bound onto the particle surface. The localization of electrons toward the binding site can weaken and consequently lower the frequency of the neighboring bonds. The disappearance of C-H stretching of  $-\text{O}-\text{CH}_3$  (ether) peaks at around 2800  $\text{cm}^{-1}$  can be explained by the following rationale. When an ether group hydrogen bonds to the nanoparticle surface, the electrons in surrounding methyl groups (see Scheme I below) are drawn towards the oxygen, which produces a partial positive charge in the group. Furthermore, the shift of electrons from the bonded hydrogen makes the hydrogen atom more positive and prone to the protonation reaction and loss its characteristic as  $-\text{O}-\text{CH}_3$ , as expressed in Scheme I. Interestingly, when spectra are examined for bound PGMEA on  $\text{Al}_2\text{O}_3$  compared to ZnO, the C-H stretching peaks show different behavior, the relative peak intensities in this region are nearly reversed. This could be explained by the higher interacting site available on the zinc oxide surface discussed in Chapter 5 and the stronger electron donating group at the ether site as compared to carbonyl group. The higher possibility that ether groups interact with

particle surface lead to higher possibility of the hydrogen at the  $-O-CH_3$  involve in the protonating reaction. Besides these three peaks, there are some other peaks in the spectrum that were as well effected as PGMEA bound onto metal oxide surface including bending vibration of  $CH_3$  ( $1370\text{ cm}^{-1}$ ) and asymmetric stretching of ester  $C-O-C$  ( $1235\text{ cm}^{-1}$ ). The reduction in peak intensity of these two peaks could be explained by the restriction of that particular vibrational mode.

Ester compound can undergo hydrolysis reaction upon the interaction with surface hydroxyl group and form carboxylate ( $-COO^-$ ) end groups. Three binding configurations between carboxylate group and metal oxide surface have been suggested – unidentate, bridging bidentate, and chelating bidentate.<sup>[4, 5, 6, 7]</sup> Each structure can be distinguished by the wavenumber differences between symmetric and asymmetric stretching of the carboxylate anion. The vibrational frequency of asymmetric stretching in the case of unidentate configuration is higher than that of bidentate one and in the reverse fashion for symmetric stretching. Consequently, the extent of frequency differences ( $\Delta\nu_{a-s}$ ) are higher in unidentate configuration than bidentate one, as listed in Table 6.1.<sup>[4, 7]</sup> Bidentate species were reported to behave in form of either as bridging or chelating structure where the  $\Delta\nu_{a-s}$  is smaller in the chelate one.

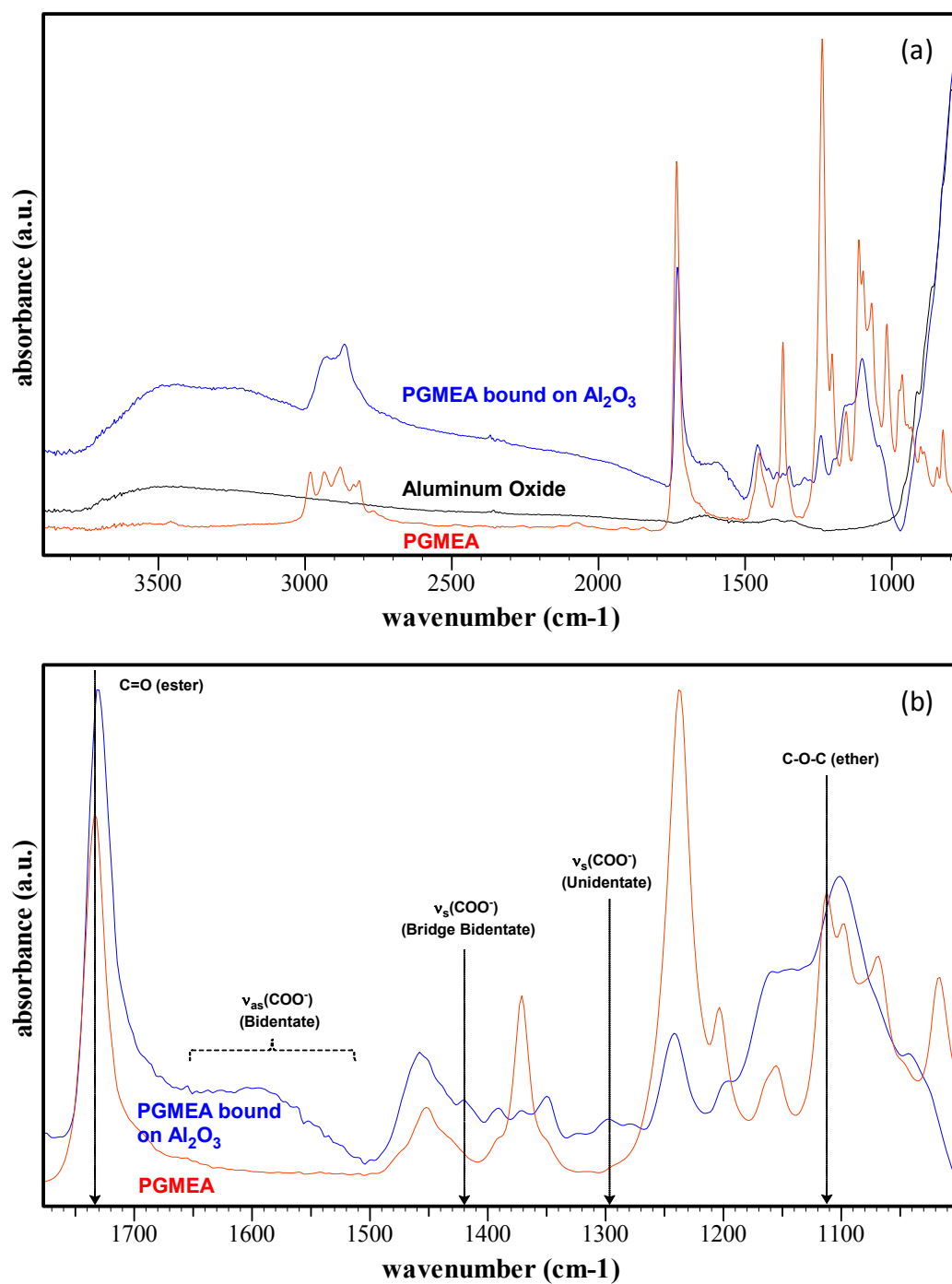
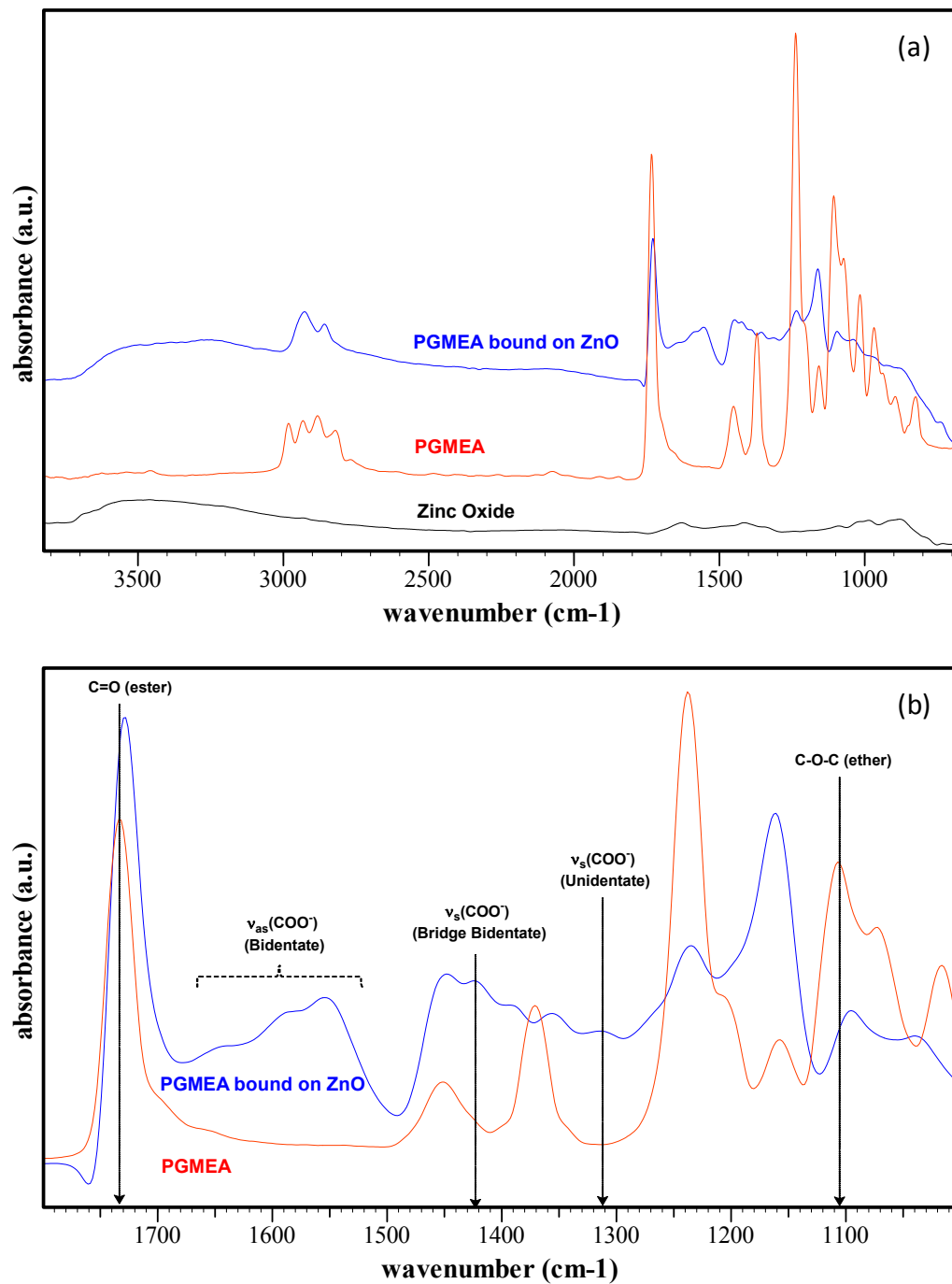
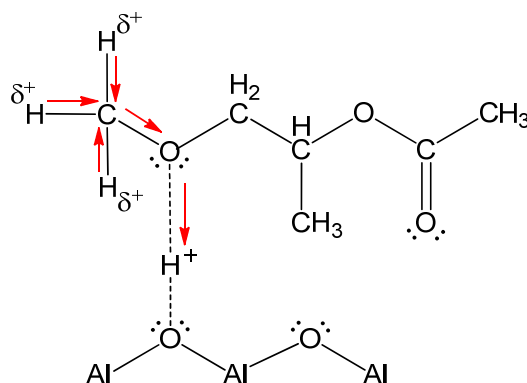


Figure 6.1 ATR-FTIR spectra of PGMEA, bound PGMEA, and aluminum oxide.





**Figure 6.2** ATR-FTIR spectra of PGMEA, bound PGMEA, and zinc oxide.



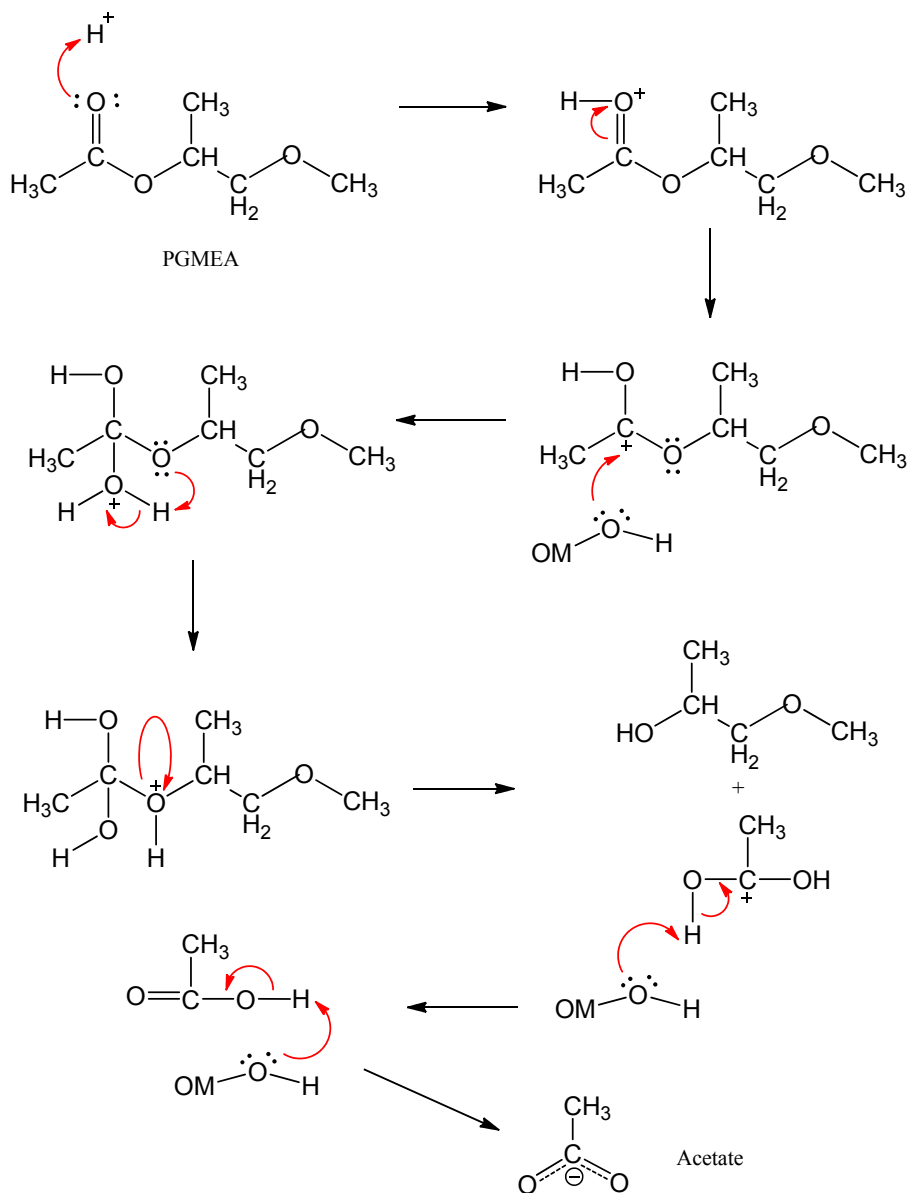
**Scheme I** Localization of electron at the ether group.

**Table 6.1** Vibrational frequency of carboxylate complex.<sup>[4]</sup>

	Unidentate	Bridging bidentate	Chelating bidentate
$\nu_a(\text{COO}^-)$	1720	1580	1550
$\nu_s(\text{COO}^-)$	1295	1432	1463
$\Delta\nu_{a-s}$	425	148	87

The vibrational frequency of the complex structure particularly a broad peak at  $1500 - 1600 \text{ cm}^{-1}$  (Figures 6.1 and 6.2) indicates that hydrolysis reaction of PGMEA occurred in the system. The hydrolysis mechanism (de-esterification) of PGMEA is expressed in Scheme II. Only two types of complex structure are detected which are unidentate and bridging bidentate structure. Although the  $\text{COO}^-$  asymmetric stretching of unidentate ( $\sim 1720 \text{ cm}^{-1}$ ) is not visible due to the location of the expected  $\text{COO}^-$

asymmetric stretching (it could also simply be overpowered by the large C=O stretching peak), the small peak at  $1295\text{ cm}^{-1}$  belonging to the symmetric one is clearly observed. The chemical structures of the bound PGMEA on metal oxide surface are illustrated in Figure 6.3.



**Scheme II** Hydrolysis reaction of PGMEA with surface hydroxyl of metal oxide.

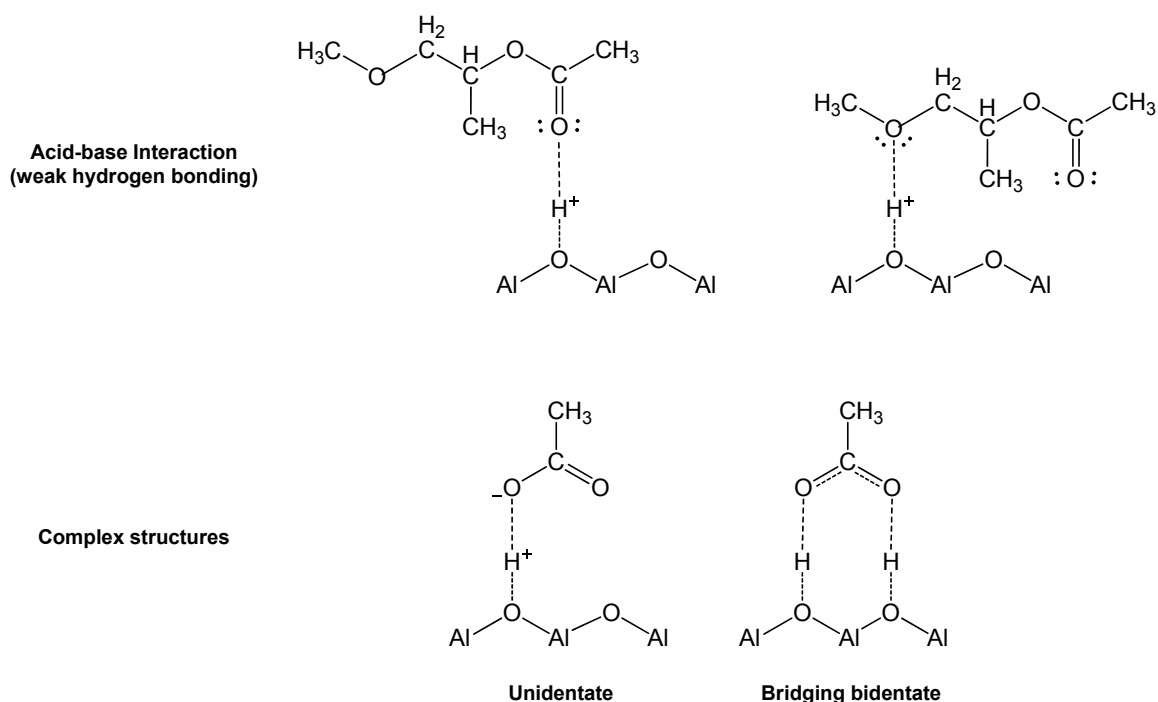
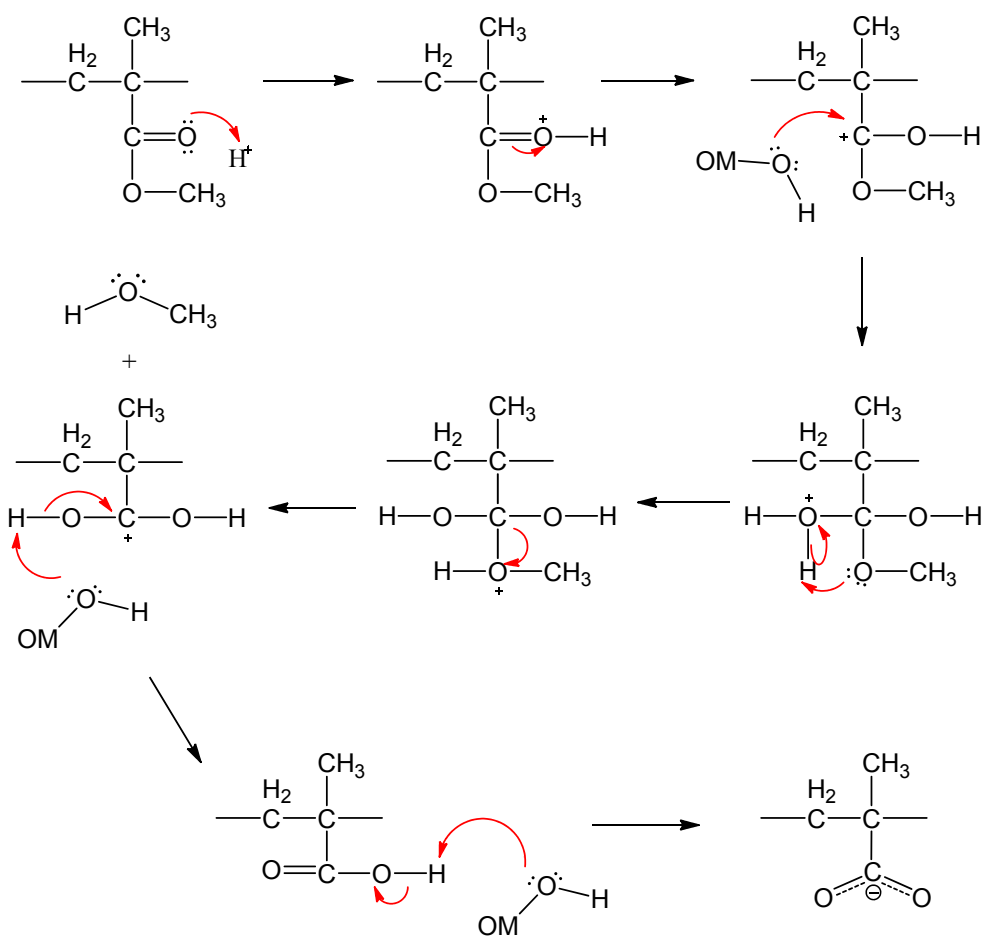


**Figure 6.3** Interfacial interactions between PGMEA and aluminum oxide.

Since PMMA nanocomposites were analyzed in totality, i.e. without isolating the nanoparticles with just the surface bound species, it is no surprise that no peak shift as an indication of hydrogen bonding was observed. Nevertheless, the carbonyl groups of PMMA are expected to interact with the metal oxide nanoparticles in the same fashion as the PGMEA molecule. Additionally, the ratio of  $-\text{OCH}_3$  to  $\alpha\text{-CH}_3$  resolved in the Raman spectrum indicates the reduction of  $-\text{OCH}_3$  group with the addition of nanoparticles, as shown in Figure 6.4. This reduction is associated to the hydrolysis reaction of PMMA occur in the system according to the mechanism expressed in Scheme III. Consequently, PMMA is thought to interact with metal oxide the same way the PGMEA does and the chemical structures are shown in Figure 6.5.



**Scheme II.** Hydrolysis reaction of PMMA with metal oxide surface.

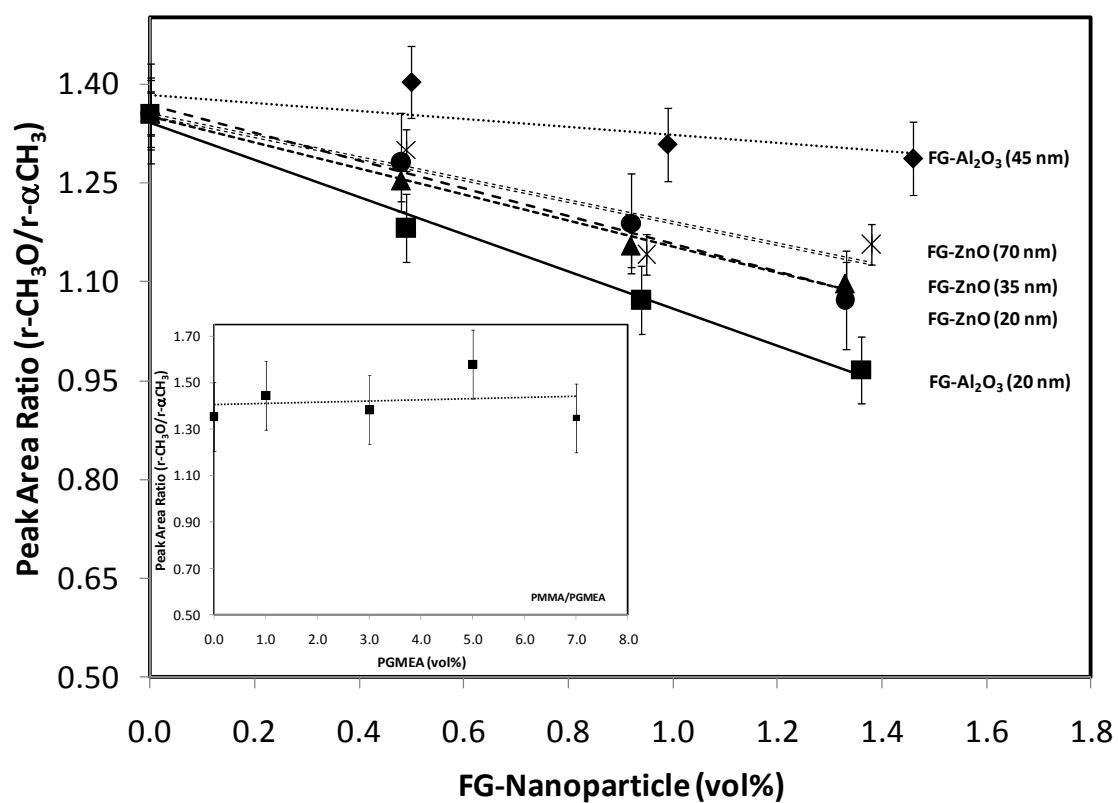


**Figure 6.4** Effect of nanoparticles on hydrolysis reaction of PMMA. The extent of hydrolysis reaction in the absence of nanoparticles shown as inserted.

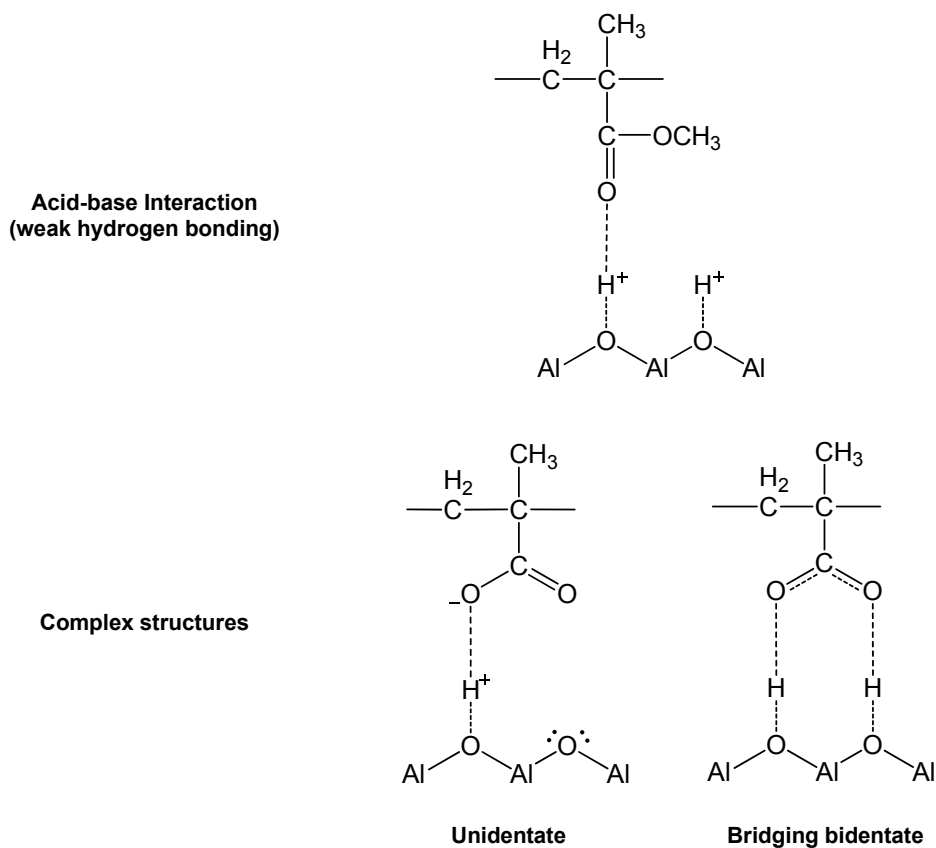


**Figure 6.5** Interfacial interactions between PMMA and aluminum oxide nanoparticles.

## 6.2 Extent of polymerization

Polymerization reaction of poly(methyl methacrylate) is an highly exothermic reaction, particularly in bulk free radical polymerization. During polymerization, due to limitation of molecular diffusion and insufficiency of heat dissipation, polymerization rate will suddenly increase and cause rapid solidification which can trap unpolymerized monomers and propagating radicals inside the polymer chain. This auto-acceleration process is also known as gel or Trommsdorf effect.<sup>[8, 9]</sup> As the viscosity becomes higher, the polymerization process can no longer proceed. The amount of unreacted monomer is

dependent on the polymerization condition, as shown in Figure 6.6.<sup>[9]</sup> The unreacted monomers lead to undesired properties and side effects in the final products which cannot be accepted in various applications. Nevertheless, a hundred percent conversion of methyl methacrylate monomer was also reported.<sup>[10]</sup>

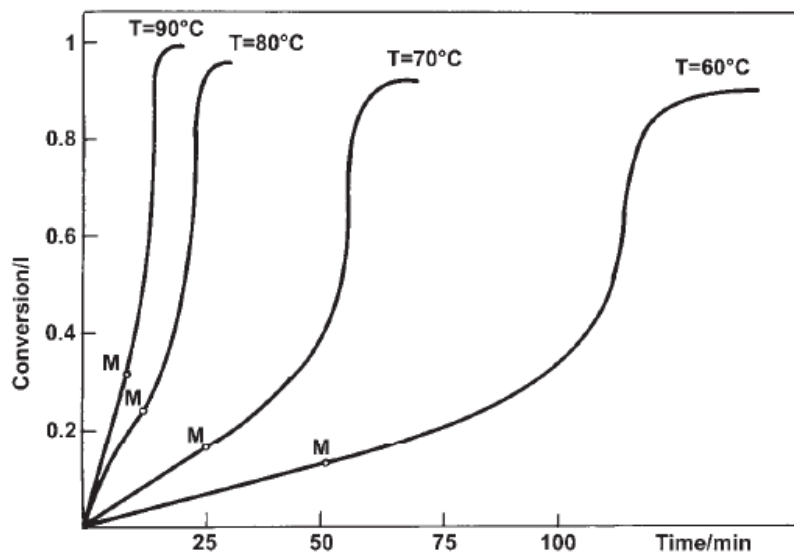


**Figure 6.6** Conversion vs. time curves of MMA polymerization (1 mass% AIBN).<sup>[9]</sup>

Raman spectroscopy is suitable for analysis of polarized molecules; therefore, one interesting application that has been performed is to investigate the percent conversion of monomer in polymerization process.<sup>[11, 12, 13]</sup> Methyl methacrylate monomer has unsaturated double bond which will open upon polymerization to form long polymer chain, while the carbonyl group remains unchanged. Thus, the mass percent of unpolymerized monomer can be calculated from the intensity ratio of  $I_{C=C}/I_{C=O}$ .<sup>[12]</sup> The vibrational frequencies of C=C and C=O are  $1640\text{ cm}^{-1}$  and  $1730\text{ cm}^{-1}$ , respectively. To eliminate the effect from broadening of the peak, the ratio was calculated from area under



the peak. The monomer content decreases linearly as a function of the polymerization time (Figure 6.7). Clearly, the finishing step taken place in the oven (95°C for 1 h) helps improve the degree of polymerization and the finished product of PMMA had the residue monomer only about 7.4%. In other words, radical bulk polymerization of PMMA with 1 wt% AIBN achieves up to 93% monomer conversion.

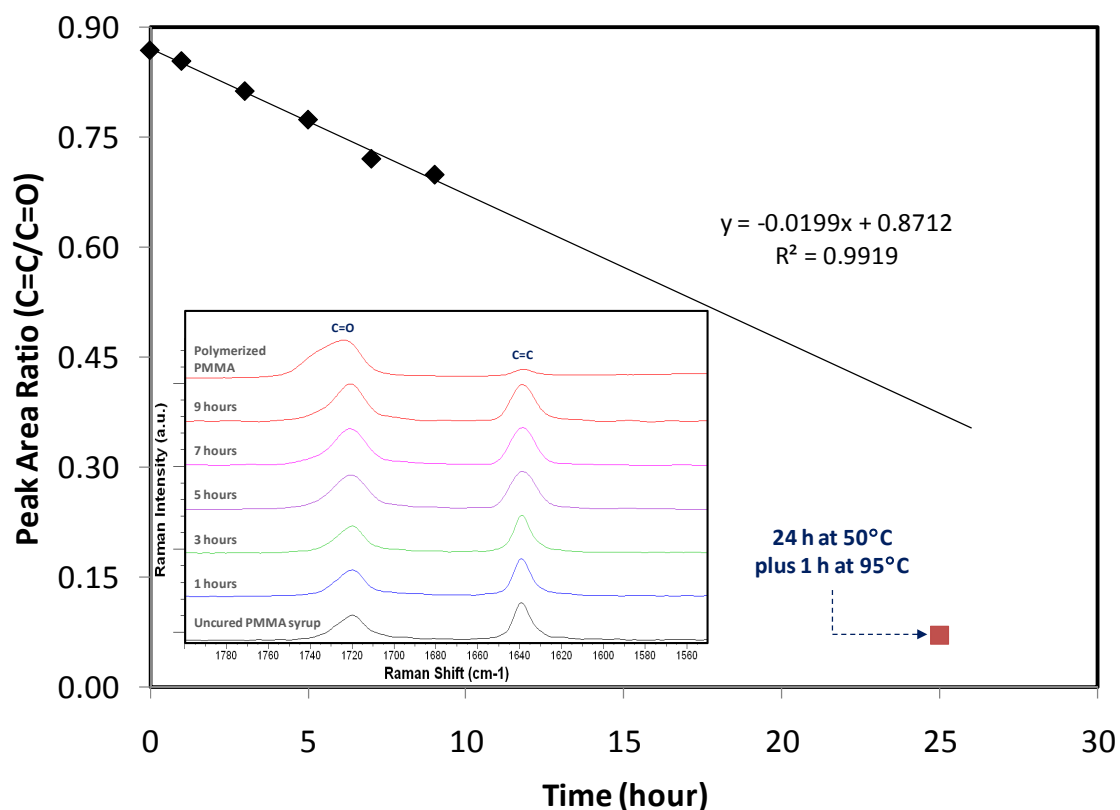


**Figure 6.7** Raman intensity ratio and Raman spectra (inserted) as a function of polymerization time.

With the incorporation of PGMEA, monomer conversion increases with increasing PGMEA content (Figure 6.8). The C=C stretching peak at 1640  $\text{cm}^{-1}$  has nearly vanished

when the concentration of PGMEA approaches 5 v/o. The reason for this effect is not clear at this time.

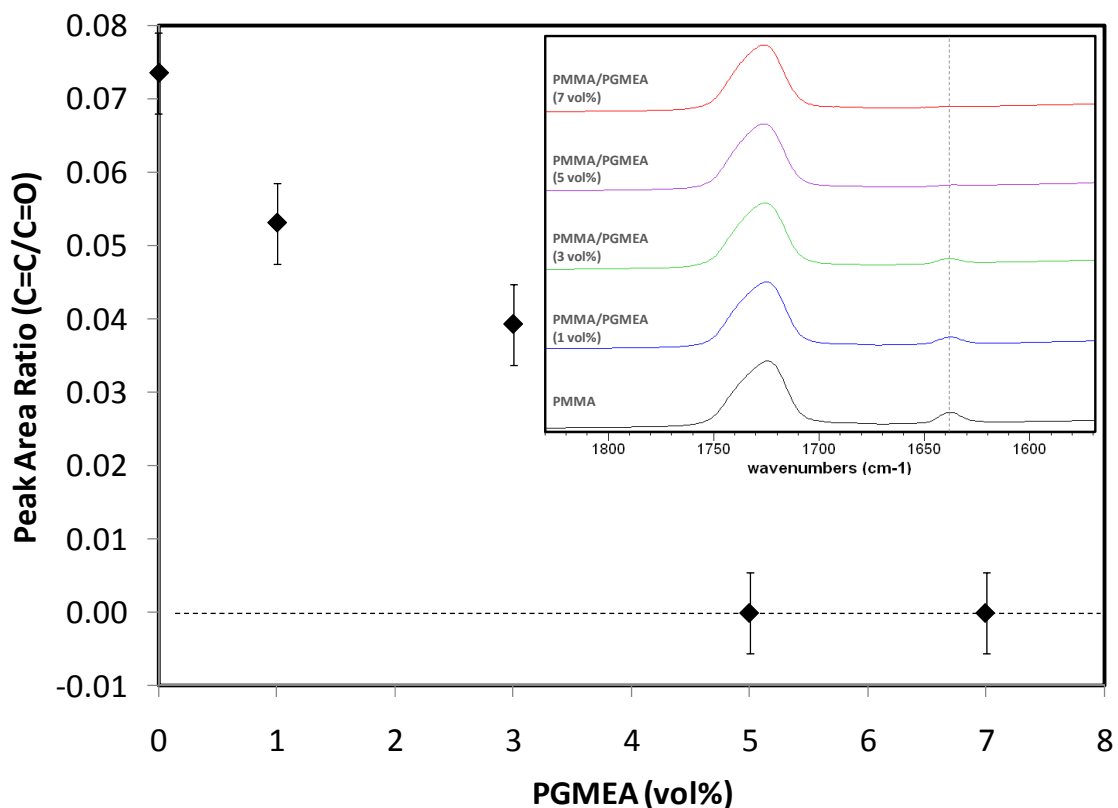


**Figure 6.8** Effect of PGMEA additions on the C=C to C=O Raman intensity ratio in bulk PMMA in the absence of nanoparticles.

Nanoparticles are incorporated into polymer matrices in two ways – during polymerization process (*in situ*) and after the polymer is polymerized (*ex situ*). In the case of *in situ* polymerization of polymer nanocomposites, the added nanoparticles were reported to affect the degree of polymerization to some extent.<sup>[14]</sup> The presence of silver nanoparticles during suspension polymerization slightly lowered rate of polymerization

and degree of polymerization as compared to the neat PMMA system as a result of radical absorption by silver nanoparticles.<sup>[14]</sup> The *in situ* polymerization of polymer nanocomposites in this work revealed that the existence of nanoparticle during polymerization had an influence on the degree of polymerization of PMMA, as shown in Figure 6.9. The higher degree of polymerization is related to the higher monomer conversion. In the system composed with dry aluminum oxide (1.0 v/o), the relative residue content of MMA monomer is approximately 75% higher than the neat PMMA. However, the monomer residue was significantly decreased with the presence of PGMEA. By comparison at 1.0 v/o of aluminum oxide particle, degree of polymerization increase by 15% from 0.8 to 0.92, 38% reduction of residue monomer, with the presence of PGMEA. The reason for the observed phenomenon can be linked to the surface coverage of metal oxide particles. In the PMMA/dry aluminum oxide system, the particle surface is directly exposed to the radical species and consequently the radicals are readily absorbed, whereas in the FG-aluminum oxide the majority of particle surface is covered by PGMEA and therefore the probability of radical absorption is reduced. Moreover, the excess PGMEA also lowers the viscosity of the system which facilitates the diffusion of radicals.

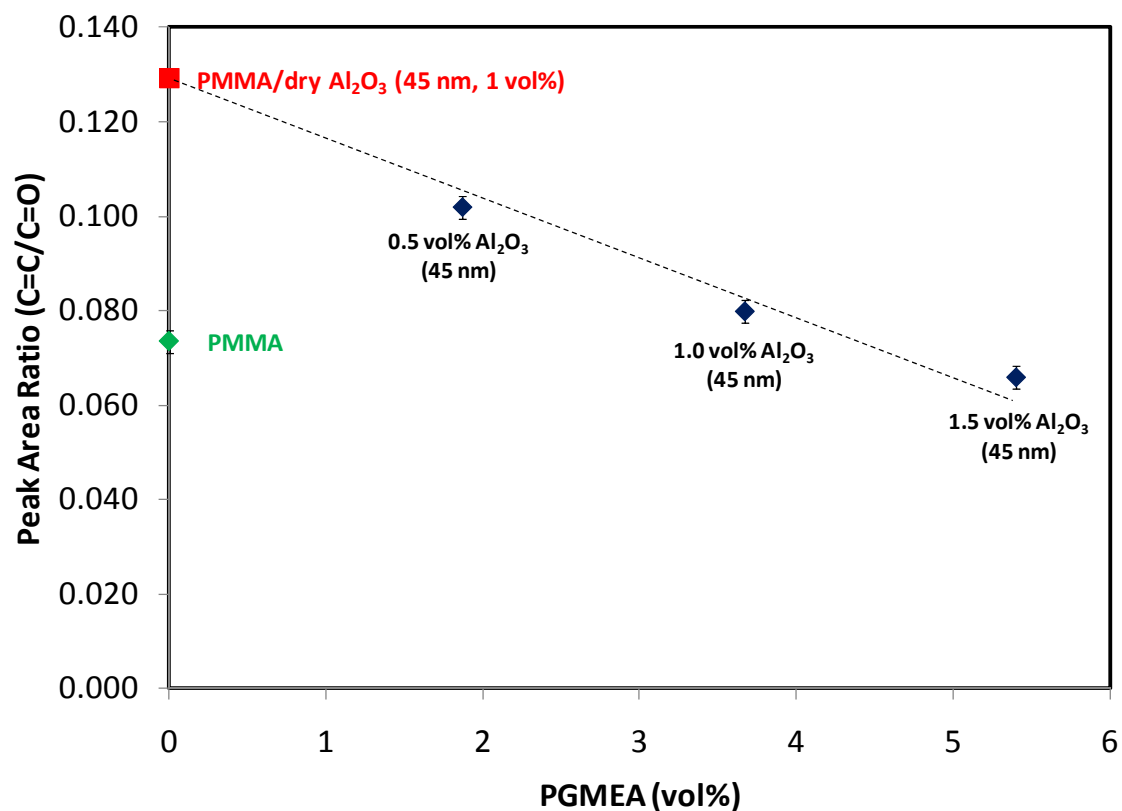


**Figure 6.9** Effect of dry nanoparticle and FG-nanoparticle additions on the C=C to C=O Raman intensity ratio in bulk PMMA.

### 6.3 Effect of polymer microstructure

Poly(methyl methacrylate) is categorized as a vinylidene polymer where one pendent group is methyl ( $-\text{CH}_3$ ) and another is methacrylate ( $-\text{COOCH}_3$ ). The arrangement of the pendent group results in three different tacticities: isotactic, syndiotactic and atactic. The first two are considered to be ordered structures, while the last one is random. Isotactic regularity is associated with the chain that has all the pendent groups located on the same side along polymer chain, whereas the alternating

arrangement is referred as syndiotactic. An atactic polymer possesses a random arrangement of the pendent groups.

According to colloidal chemistry theory, to neutralize surface charges, close proximity of a counter ion or other charge carrying group is required. This can also be applied to the interaction between polymer chain and nanoparticles. Isotactic regularity of poly(methyl methacrylate) was reported to provide a more lengthened morphology than syndiotactic.<sup>[15]</sup> This flatten morphology of i-PMMA have been suggested to provide better surface coverage on the metal oxide surface.<sup>[3, 16]</sup> In many studies, however, polymers were absorbed from dilute solution either by mixing the particle into the dilute solution of polymer<sup>[3, 17]</sup> or by spin-coating of polymer solution on the metal oxide surface<sup>[18, 16]</sup>. Thus, besides strongly flatten structure of isotactic PMMA, the driving force for such specific adsorption was also related to polymer/solvent compatibility. s-PMMA was claimed to provide better interaction and accessibility to the solvent molecule as a result of a looser structure (higher monomer unit per turn) due to alternative position of the pendent groups.<sup>[17, 19]</sup> Consequently, the isotactic chains were segregated out and become available for interaction with the particle surface.

Raman peak intensities in the 500 – 1100  $\text{cm}^{-1}$  range are thought to be tacticity dependent.<sup>[20]</sup> The peaks at 953  $\text{cm}^{-1}$  and 967  $\text{cm}^{-1}$  are associated with rocking vibration of  $\alpha\text{-CH}_3$  for isotactic and syndiotactic PMMA, respectively.<sup>[21]</sup> The ratio of peak area 967/953 is plotted in Figure 6.10. The result demonstrates that the syndiotacticity of PMMA increases with the addition of FG-nanoparticles. In addition, change in polymer

chain regularity also particle size and volume fraction dependence. To investigate how much effect the PGMEA has on the polymer chain regularity, PMMA/PGMEA at various volume fractions of PGMEA were analyzed and the 967/953 peak ratio was plotted as a function of PGMEA content, shown as inserted graph in Figure 6.10. The result shows that PGMEA somewhat effect on the tacticity of PMMA as expected from the polymer tacticity/solvent compatibility aspect found in the literatures. Thus, the majority of the change in polymer chain regularity in PMMA nanocomposites was associated with the presence of nanoparticles during polymerization. This can be explain in term higher curvature of s-PMMA as demonstrated by Vacatello based on four monomer segments<sup>[15]</sup> and the ability to form loop and tail as interact with particle surface<sup>[22]</sup>. As the nanoparticles were pre-dispersed in PGMEA and the interactions between PGMEA and both aluminum oxide and zinc oxide were confirm by both TGA and FT-IR, the majority of the particle surfaces were thought to be covered. The question came up, of course, whether PMMA can replace the adsorbed PGMEA molecule on the metal oxide surface. Hydrogen bonding has the bond energy of 4 – 170 kJ/mol which depends on the electron donor/accepter combination,<sup>[23]</sup> while polymerization energy of PMMA is 54 kJ/mol<sup>[24]</sup>. Thus, it is possible to destroy the existing hydrogen bond and form a new one with the PMMA chain.

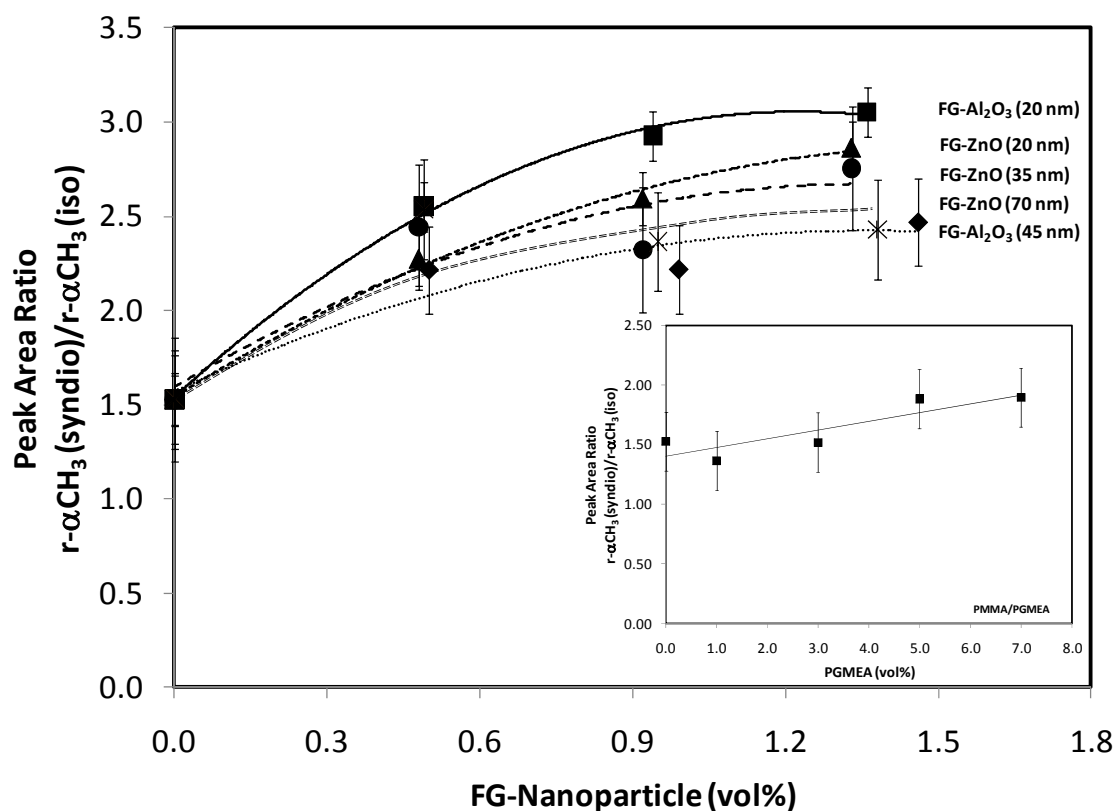


**Figure 6.10** Effect of nanoparticle additions on polymer tacticity determined by the ratio of rocking vibration of  $\alpha\text{-CH}_3$  for syndiotactic to isotactic PMMA. The effect of PGMEA on the polymer tacticity shown as inserted.

## Summary

The interfacial interaction was analyzed. Both acid-base interaction and complex structures of absorbed species (PGME and PMMA) were confirmed to form at the metal oxide surface. The hydrogen bonding results in the red shift of the carbonyl stretching and ether stretching peaks. Both unidentate and bidentate complex structures were identified in the infrared spectrum.

Raman spectroscopy was used to investigate the degree of polymerization of polymer. High rates of monomer conversion (93%) were obtained by simple free radical bulk polymerization. The monomer conversion increases with the addition of PGMEA and no monomer residue was observed when volume fraction of PGMEA reaches 5.0 percent. However, the percent conversion was decreased when aluminum oxide was introduced into the system. This can be explained by the radical adsorption of metal oxide surface. On the other hand, when nanoparticles were added along with PGMEA, the percent conversion was increased by 15% at 1.0 v/o of nanoparticles.

The small scale of nanoparticles affects the microstructure of PMMA both in the interfacial region and surrounding area. The syndiotactic sequence of PMMA increased with the addition of nanoparticles in all composite systems. The favoring of the syndiotactic conformation appears to be driven by the lower free energy of the syndiotactic conformation in association with the nanoparticle surface as well as with the chemisorbed solvent molecules. Both closer association of dipole groups and a higher



concentration of such groups at the particle surface contribute to this reduction in free energy and hence stability of the configuration.

## References

1. D. I. Bower and W. F. Maddams, *The vibrational spectroscopy of polymers*, Cambridge, 1992.
2. S. Kulkeratiyut, S. Kulkeratiyut and F. D. Blum, Bound carbonyls in PMMA adsorbed on silica using transmission FTIR, *Journal of Polymer Science: Part B: Polymer Physics* 44 (2006), 2071–2078.
3. Y. Grohens, J. Schultz and R. E. Prud'homme, Pmma conformational changes on  $\gamma$ -alumina powder: Influence of the polymer tacticity on the configuration of the adsorbed layer, *Int. J. Adhesion and Adhesives* 17 (1997), 163-167.
4. W. tao, F. fei and W. yue-chuan, Structure and thermal properties of titanium dioxidepolyacrylate nanocomposites, *Polymer Bulletin* 56 (2006), 413–426.
5. S. M. Khaled, A. S. Rizkalla and P. A. Charpentier, Development of a new generation of bone cement using nanotechnology, *Aiche Annual Meeting*, 2008.
6. X.-W. Du, Y.-S. Fu, J. Sun, X. Han and J. Liu, Complete UV emission of ZnO nanoparticles in a PMMA matrix, *Semicond. Sci. Technol.* 21 (2006), 1202-1206.
7. M. Nara, H. Torii and M. Tasumi, Correlation between the vibrational frequencies of the carboxylate group and the types of its coordination to a metal ion: An ab initio molecular orbital study, *The Journal of Physical Chemistry* 100 (1996), no. 51, 19812-19817.
8. W. L. Rasmussen, "Novel carbozole based methacrylates, acrylates, and dimethacrylates to produce high refractive index polymers," *Virginia Polytechnic Institute and State University*, 2001.
9. R. Radicevic, D. M. Stoiljkovic and J. Budinski-Simendic, Characteristic events in free radical polymerization of lower n-alkyl methacrylates, *Journal of Thermal Analysis and Calorimetry* 62 (2000), 237-249.
10. F. Pallikari-Viras, X. Li and T. A. King, Thermal analysis of PMMA/gel silica glass composites, *J. Sol-Gel Sci. and Tech.* 7 (1996), 203-209.
11. M. A. Galin, L. Turkish and E. Chowchuvech, Detection, removal, and effect of unpolymerized methylmethacrylate in intraocular lenses., *Am J Ophthalmol.* 84 (1977), 153-159.
12. F. Pallikari, G. Chondrokoukis, M. Rebelakis and Y. Kotsalas, Raman spectroscopy: A technique for estimating extent of polymerization in PMMA, *Materials Research Innovations* 4 (2001), no. 2, 89-92.

13. Z. Kantarci, S. Aksoy and N. Hasirci, Estimation of monomer content in polymethyl methacrylate contact lens materials by Raman spectroscopy., *Int J Artif Organs*. 20 (1997), 407-411.
14. J.-H. Yeum and Y. Deng, Synthesis of high molecular weight poly(methyl methacrylate) microspheres by suspension polymerization in the presence of silver nanoparticles, *Colloid Polym Sci* 283 (2005), 1172–1179.
15. M. Vacatello and P. J. Flory, Conformational statistics of poly(methyl methacrylate), *Macromolecules* 19 (1986), 405-415.
16. Y. Grohens, M. Brogly, C. Labbe and J. Schultz, Chain flattening of spin-cast PMMA on aluminum mirrors: Influence of polymer tacticity, *Eur. Polym. J.* 33 (1997), 691-697.
17. P. Carriere, Y. Grohens, J. Spevacek and J. Schultz, Stereospecificity in the adsorption of tactic PMMA on silica, *Langmuir* 16 (2000), 5051-5053.
18. K. Konstadinidis, B. Thakkar, A. Chakraborty, L. W. Potts, R. Tannenbaum and M. Tirrell, Segment level chemistry and chain conformation in the reactive adsorption of poly(methyl methacrylate) on aluminum oxide surfaces, *Langmuir* 8 (1992), 1307-1317.
19. J. Spevacek and B. Schneider, Aggregation of stereoregular poly(methyl methacrylates), *Adv. Colloid Interface Sci.* 27 (1987), 81-150.
20. A. Bertoluzza, C. Fagnano, A. Tinti, M. A. Morelli, M. R. Tosi, G. Maggi and P. G. Marchetti, Raman and infrared spectroscopic study of the molecular characterization of the biocompatibility of prosthetic biomaterials, *J. Raman. Spectrosc.* 25 (1994), 109-114.
21. A. Jain, R. M. Misra, P. Tandon and V. D. Gupta, Vibrational dynamics and heat capacity of syndiotactic poly(methyl methacrylate), *J. Macromol. Sci., Part B: Phys.* 45 (2006), 263-284.
22. Y. Grohens, M. Brogly, C. Labbe and J. Schultz, Interfacial conformation energies of stereoregular poly(methyl methacrylate) by infra-red reflection absorption spectroscopy, *Polymer* 38 (1997), 5913-5920.
23. Y. He, B. Zhu and Y. Inoue, Hydrogen bonds in polymer blends, *Prog. Polym. Sci.* 29 (2004), 1021–1051.
24. S. Aydin, E. Bozdogan, E. Sunbuloglu, H. Unalan, M. Hanci, O. Aydingoz and C. Kunday, In vitro investigation of heat transfer in calf spinal cord during polymethylmethacrylate application for vertebral body reconstruction, *Eur Spine J* 15 (2006), 341-346.

## Chapter 7 Summary and Conclusion

Poly(methyl methacrylate)/particulate nanocomposites were synthesized via in situ bulk polymerization. Enhancements in both mechanical and thermal properties were observed. Toughness of PMMA was improved without significantly sacrificing other mechanical properties. The greatest improvement in impact resistance was observed only at a single optimum nanoparticle loading in PMMZ/FG-ZnO systems, which appeared to be related to the geometric shape of the nanoparticles. The high surface area and elongated shape of small zinc oxide particles creates energy-absorbing fracture mechanisms that are responsible for the higher impact resistance. This thesis produced nanocomposites with impact resistance approximately three times that of the neat polymer at reinforcement concentrations of only one volume percent of zinc oxide predispersed in PGMEA. In particular the improvement in impact resistance over the neat PMMA polymer was 292%, 298%, and 324% for zinc oxide particle sizes of 70 nm, 35 nm, and 20 nm respectively.

The weight loss of PGMEA at about 223-240 °C for FG-Al<sub>2</sub>O<sub>3</sub> and 300 °C for FG-ZnO confirms the affinity between the PGMEA and nanoparticles. The higher adsorption of PGMEA on zinc oxide surface was driven by the higher proton concentration available on the surface. The thermal stability of the PMMA was substantially improved (~50 °C) by the addition of both the zinc oxide and aluminum oxide nanoparticles. H-H and vinylidene scission mechanisms were virtually inactivated by the addition of nanoparticles to PMMA. The vast majority of the decomposition occurred due to random

main chain scission in the temperature range of 330 – 392 °C. Approximately a 62 °C increase in peak decomposition was noted for 20 nm zinc oxide composites. The chain immobilization and the radical deactivation mechanisms by nanoparticles are responsible for the thermal stability enhancement.

FTIR and Raman spectroscopy are useful tools to elucidate the nature of absorbed surface moieties and characterize the way these surface groups influence the tacticity and extent of polymerization of the surrounding polymer. Both acid-base and complex interactions of bound PGMEA were observed by FTIR. The shift of FTIR bands of O-H, C=O, and C-O-C to lower wavenumber are associated to the acid-base interaction via weak hydrogen bonding between PGMEA molecules and metal oxide nanoparticles. The new bands observed in the 1290 – 1700  $\text{cm}^{-1}$  relate to complex dipole structures. PMMA interact with the nanoparticles in the same way the PGMEA does due to the similar types of the functional group. Furthermore, the extent of polymerization, calculated by the Raman ratio of C=C/C=O, increases and decreases respectively with the PGMEA and nanoparticle additions. The incremental of free volume in the presence of PGMEA and the ability to absorb the active radicals of metal oxide are correspondingly responsible for such effect. Additionally, the syndiotactic sequence increases in the PMMA nanocomposites to accommodate the existence of both nanoparticles in the system and provide better accessibility for polymer/particle interaction. The scientific understanding of the dipole interaction between various polymer-related oxy-complexes and the nanoparticles surfaces has been substantially increased by this segment of the thesis.

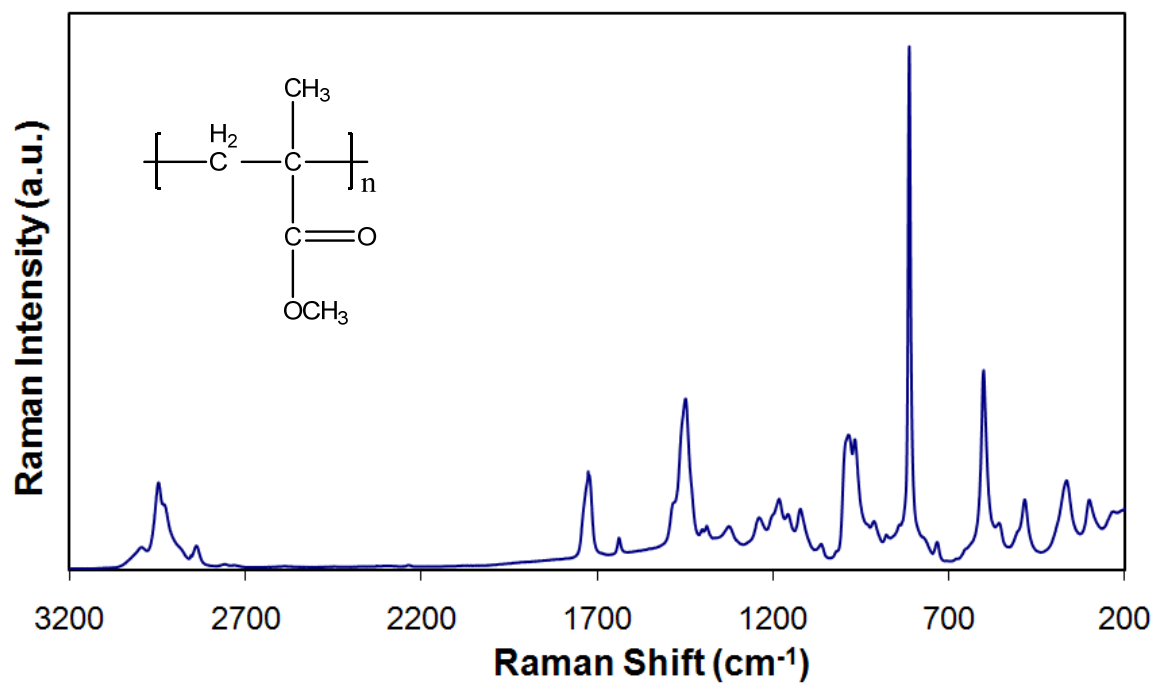
## Chapter 8 Future work

1. Characterization of the bound interface was a major thrust of this thesis. Future investigators should expand on this work to determine how engineering of the bound interface will affect and enhance composite properties.
2. Thermal stability of PMMA is an important property. This work showed that oxide type is important and that the decomposition sequence is more complicated than previously thought. Further elucidation of these mechanisms is needed.
3. Impact behavior has been shown in this thesis to depend strongly on particle acicularity and perhaps on oxide type. More work is required in this direction to develop highly impact resistant composites.
4. Overall, I only studied two nanoparticle chemistries: ZnO and Al<sub>2</sub>O<sub>3</sub>. Similar work should be conducted on a variety of oxide and non-oxide materials.
5. Processing techniques have an influence on properties of polymer nanocomposites. In this work, the composites were synthesized by free radical bulk polymerization. Future investigators should study the same composite systems prepared by another synthesis technique such as emulsion polymerization.
6. Polymer physic is tightly related to the final properties of the polymer nanocomposites. The analysis of molecular weight and polydispersity index of polymer with the addition of nanoparticles will provide better understanding in the polymer nanocomposite systems.

7. This study showed that the addition of nanoparticles affected the stereo regularity of polymer chains. NMR is another good technique to elucidate the regularity of polymer chain and should be part of a further study.

## Appendix A - Raman spectroscopic analysis

### A.1 Raman assignment



**Scheme A.1** Raman spectrum of poly(methyl methacrylate).

### Vibrational frequency of syndiotactic and syndiotactic PMMA.<sup>1, 2</sup>

Raman shift (cm <sup>-1</sup> )		Assignment
isotactic	syndiotactic	
951	967	α-CH <sub>3</sub> rocking vibration
996	988	-OCH <sub>3</sub> rocking vibration

<sup>1</sup> A. Jain et al., J. Macromol. Sci., Part B: Phys. 45 (2006), 263-284.

<sup>2</sup> J.M. O'Reilly et al., Macromol., 14 (1981), 602-608.



**Raman band assignments of PMMA.**<sup>[3,4,5,6,7]</sup>

Raman Shift (cm <sup>-1</sup> )	Assignment
3035	–OCH <sub>3</sub> asymmetric stretching
3003	–OCH <sub>3</sub> symmetric stretching
2955	–CH <sub>3</sub> symmetric stretching
2934	–CH <sub>3</sub> asymmetric stretching
2903	–CH <sub>2</sub> asymmetric stretching
2846	–CH <sub>2</sub> symmetric stretching
1739	Free C=O stretching
1706	Bound C=O stretching
1640	C=C stretching
1485	-CH <sub>3</sub> asymmetric bending
1452	-CH <sub>2</sub> - deformation
1402	-CH <sub>2</sub> - wagging of –C=CH <sub>2</sub>
1391	-CH <sub>3</sub> symmetric bending
1324	-CH <sub>2</sub> wagging
1180-1250	C-C degenerate stretching of CC <sub>4</sub>
1031-950	C-C main chain stretching
988, 997	-OCH <sub>3</sub> rocking vibration
955, 968	α-CH <sub>3</sub> rocking
814	C-C symmetric stretching of CC <sub>4</sub>
720	-CH <sub>2</sub> rocking
549, 599	O-C=O in-plane bending in hydrogen bonding
300, 365, 484	C-C skeletal deformation of CC <sub>4</sub>

3 F. Pallikari et al., Materials Research Innovations 4 (2001), 89-92.

4 A. Jain et al., J. Macromol. Sci., Part B: Phys. 45 (2006), 263-284.

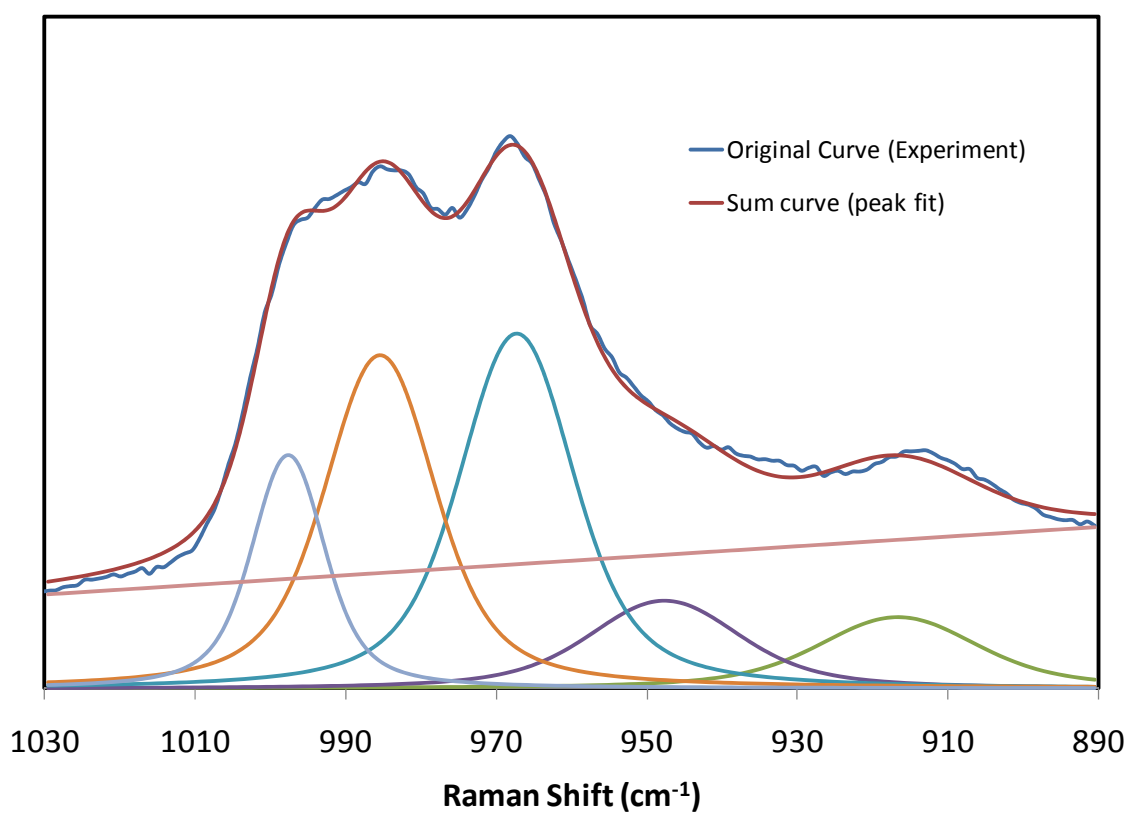
5 V. L. Furer et al., J. Appl. Spectros. 50 (1989), 179-183.

6 R. Yanzhi et al., Vibrational Spectroscopy 23 (2000), 207-218.

7 H. G. M. Edwards et al., Vibrational Spectroscopy 41 (2006), 160-169.

## A.2 Statistical analysis

Peaks in the range of  $890 - 1030 \text{ cm}^{-1}$  are deconvoluted by use of peak fit function in Wire 2 software provided by Renishaw, as shown in Figure A.2. Then, deconvoluted data was performed analysis of variance (ANOVA) to determine the significant of peak variation.



**Scheme A.2** Peak deconvolution.

*Variance between groups ( $S_B^2$ )*

$$S_B^2 = \frac{SS_B}{df_B} = \frac{\sum_{i=1}^k n_i (\bar{X}_i - \bar{X})^2}{k - 1}$$

where  $SS_B$  is the sum of square between,  $df_B$  is degree of freedom between,  $n_i$  is size of group  $i$ ,  $\bar{X}_i$  is mean of group  $i$ , and  $\bar{X}$  is grand mean. The variance between groups is also known as mean square between ( $MS_B$ ).

### ***Variance within group ( $S_w^2$ )***

The variance within group is also known as mean square within ( $MS_w$ ) and can be determined as follow.

$$S_w^2 = \frac{SS_w}{df_w} = \frac{\sum_{i=1}^k (n_i - 1) S_i^2}{N - k}$$

where  $SS_w$  is the sum of square within,  $df_w$  is degree of freedom within,  $S_i$  is standard deviation of group  $i$ , and  $N$  is total number of samples.

### ***ANOVA Table***

The variation is considered to be significant if the F-value is greater than F-critical which is determined from the F-statistic table.

Source of Variation	Sum of Square (SS)	Degree of Freedom (df)	Mean of Square (MS)	F-Value
Between	$SS_B$	$df_B = k - 1$	$S_B^2 = \frac{SS_B}{df_B}$	$F = \frac{S_B^2}{S_w^2}$
Within	$SS_w$	$df_w = N - k$	$S_w^2 = \frac{SS_w}{df_w}$	

## Curriculum Vita

Wantinee Viratyaporn

### Education

**PhD – Materials Science & Engineering – concentration in polymeric materials**  
(January 2010)

Rutgers, the State University of New Jersey, New Brunswick, NJ

**M.S.– Materials Science & Engineering – concentration in polymeric materials**  
(January 2008)

Rutgers, the State University of New Jersey, New Brunswick, NJ

**B.E. – Petrochemical and Polymeric Materials** (March 2004)  
Silpakorn University, Thailand

### Publications/Presentations

1. W. Viratyaporn and R. Lehman, “Effect of Metal Oxide Nanoparticles on The Mechanical Properties and Tacticity of Poly(Methyl Methacrylate),” Proceeding of MRS (2009).
2. W. Viratyaporn and R. Lehman, “Impact Resistance and Raman Characterization of Al<sub>2</sub>O<sub>3</sub>/ZnO Poly(Methyl Methacrylate) Nanocomposites,” Proceedings of SPE ANTEC (2009).
3. X. Luo, R. Ou, D. E. Eberly, A. Singhal, W. Viratyaporn and P.T. Mather, “A Thermoplastic/Thermoset Blend Exhibiting Thermal Mending and Reversible Adhesion,” ACS Applied Materials and Interfaces 1 (3) 612-620 (2009).
4. W. Viratyaporn, R. Lehman, J. Joshi, “Impact Resistance of Selected Immiscible Polymer Blends,” Proceedings of SPE ANTEC (2007).
5. W. Viratyaporn, N. Twu, R. Lehman, “Fiber Reinforced Multiphase Polymer Composites by In-situ Fiber Alignment,” Proceedings of MRS Fall Meeting (2007).
6. W. Viratyaporn, R. Lehman, J. Joshi, “Effect of Composition and Processing on the Impact Behavior of Certain Immiscible Polymer Blends,” J. App. Polym. Sci., (2007) – submitted.
7. W. Viratyaporn and R. Lehman, “Effect of Nanoparticles on the Thermal Stability of Poly(methyl methacrylate)-inorganic Nanocomposites Prepared by in-situ Bulk Polymerization,” To be submitted.